

SELF-ASSEMBLY OF THE S-LAYER PROTEIN OF  
*SPOROSARCINA UREA* ATCC 13881

Dissertation

zur Erlangung des akademischen Grades

Doctor rerum naturalium

(Dr. rer. nat.)

vorgelegt der

Fakultät Mathematik und Naturwissenschaften

der Technischen Universität Dresden

von

**Melinda Varga**

(M.Sc. Mol. Bioeng.)

geboren am 27.01.1982 in Cluj, Rumänien

Gutachter: Prof. Dr. Gerhard Rödel  
Prof. Dr. Wolfgang Pompe

Eingereicht am 29.10.2010

Verteidigt am 24.01.2011

*To my parents...*

*„Ever tried. Ever failed.  
No matter. Try again.  
Fail again. Fail better. “*

*Samuel Beckett*

# CONTENTS

<b>List of figures and tables</b>	<b>6</b>
<b>Abbreviations</b>	<b>8</b>
<b>1 Introduction</b>	<b>9</b>
1.1 Molecular self-assembly and self-assembling systems	10
1.2 Protein crystallization	11
1.2.1 Driving force of protein crystallization- thermodynamical aspects	11
1.2.2 Protein crystal nucleation	12
1.2.3 Protein crystal growth	16
1.3 Surface layer proteins (S-layers)	17
1.3.1 Structure of S-layers	17
1.3.2 Properties of S-layers	19
1.3.3 Genetics of S-layers	22
1.3.4 Functions of S-layers	23
1.3.5 Genetic engineering of S-layers	24
1.3.6 Applications of S-layers	25
1.3.7 The S-layer of <i>Sporosarcina ureae</i> ATCC 13881 (SslA)	28
1.4 Molecular biotemplating	33
1.5 Aims of the thesis	35
<b>2 <i>The native S-layer protein of Sporosarcina ureae ATCC 13881</i></b>	<b>37</b>
2.1 Topographical characterization	38
2.2 Self-assembly of the S-layer of <i>S. ureae</i> ATCC 13881	39
2.2.1 Growth stages in the self-assembly process	40
2.2.2 Factors that influence the self-assembly process	42
2.2.3 Kinetic studies on the self-assembly process	57
2.3 Functionalization of the SslA protein template with gold nanoparticles	62
2.4 Conclusions and outlook	67

<b>3</b>	<b>The recombinant S-layer of <i>S. ureae</i> ATCC 13881</b>	<b>69</b>
3.1	Characterization of the recombinant SslA	70
3.1.1	Cloning	70
3.1.2	Heterologous expression in <i>E. coli</i> , isolation and purification	71
3.1.3	Self-assembly	74
3.2	Tailoring the recombinant SslA - towards elucidation of SslA protein domain responsible for self-assembly	80
3.2.1	Mutagenesis and molecular characterization of SslA truncation derivatives	81
3.2.2	Heterologous expression in <i>E. coli</i> , isolation and purification	83
3.2.3	Self-assembly	87
3.2.4	Factors that influence the self-assembly process	96
3.2.5	Kinetic studies on the self-assembly process	105
3.3	Conclusions and outlook	107
<b>4</b>	<b>The SslA-streptavidin fusion protein</b>	<b>110</b>
4.1	Design of the SslA-streptavidin fusion protein	111
4.2	Chimeric gene expression, isolation and purification	114
4.3	Self-assembly of the chimeric S-layer protein	116
4.3.1	<i>In vitro</i> recrystallization in solution	116
4.3.2	<i>In vitro</i> recrystallization on silicon wafer	119
4.4	Determination of biotin binding ability	121
4.4.1	Interaction of biotinylated quantum dots and SslA <sub>341-925</sub> CN-cstrp monomers	121
4.4.2	Binding of biotinylated quantum dots onto the recrystallized SslA <sub>341-925</sub> CN-cstrp protein template	125
4.5	Relevance of the fusion protein as a bio(nano)template	129
4.6	Conclusions and outlook	131
	<b>Summary</b>	<b>135</b>

<b>Bibliography</b>	<b>137</b>
<b>Appendix</b>	<b>154</b>
<i>A.1 Materials</i>	<i>154</i>
<i>A.2. Methods</i>	<i>158</i>
<b>Publications</b>	<b>175</b>
<b>Acknowledgements</b>	<b>177</b>

# LIST OF FIGURES AND TABLES

Figure 1-1 Static and dynamic self-assembly	10
Figure 1-2 Illustration of the nucleation process.	12
Figure 1-3 Shape of the free energy plot as a function of a growing patch.	14
Figure 1-4 Different S-layer lattice types.	18
Figure 1-5 Structural difference between the two S-layer sides	19
Figure 1-6 <i>In vitro</i> recrystallization of S-layers.	20
Figure 1-7 The S-layer of <i>S. ureae</i> ATCC 13881	29
Figure 1-8 The outer and inner surface of the S-layer of <i>S. ureae</i> ATCC 13881	30
Figure 1-9 Schematic representation of the SslA protein sequence	31
Figure 1-10 Pt cluster deposition onto the S-layer of <i>S. ureae</i> ATCC 13881	32
Figure 2-1 The S-layer protein of <i>S. ureae</i> ATCC 13881	38
Figure 2-2 Growth stages in the S-layer self-assembly process.	41
Figure 2-3 Influence of initial monomer concentration on the self-assembly.	44
Figure 2-4 Tube formation in case of the S-layer of <i>S. ureae</i> ATCC 13881.	48
Figure 2-5 Influence of Ca <sup>2+</sup> ions on the self-assembly of the S-layer of <i>S. urea</i> ATCC 13881.	50
Figure 2-6 Influence of buffer pH on the self-assembly of the S-layer of <i>S. ureae</i> ATCC 13881.	52
Figure 2-7. Influence of the Si substrate on the self-assembly performed at low pH	54
Figure 2-8 Influence of Si substrate on the self-assembly of SslA	56
Figure 2-9 Influence of protein concentration on the kinetics of SslA self-assembly.	58
Figure 2-10 Influence of temperature on the kinetics of SslA self-assembly	60
Figure 2-11 Functionalization of the S-layer of <i>S. ureae</i> ATCC 13881 with Au nanoparticles.	63
Figure 2-12 Arrangement of Au nanoparticles on the SslA template.	66
Figure 3-1 Heterologous expression of SslA <sub>32-1097</sub> in <i>E. coli</i> and purification	72
Figure 3-2 <i>In vitro</i> recrystallization of SslA <sub>32-1097</sub> in solution	75
Figure 3-3 SslA <sub>32-1097</sub> self-assembly at low versus high initial monomer concentration	76
Figure 3-4 Morphology and lattice structure of SslA <sub>32-1097</sub> <i>in vitro</i> recrystallized on Si wafer	78
Figure 3-5 Creation of SslA truncation derivatives	82
Figure 3-6 Heterologous expression of SslA truncation derivatives in <i>E. coli</i>	84
Figure 3-7 Purification of SslA truncation derivatives	86
Figure 3-8 Self-assembly of the recombinant SslA truncation derivatives in solution	88
Figure 3-9 Self-assembly of the recombinant SslA truncation derivatives on a Si wafer	92
Figure 3-10 Self-assembly of SslA <sub>341-925</sub> CN on a Si wafer	95
Figure 3-11 Influence of initial monomer concentration on the self-assembly of the SslA truncation	

derivatives in solution	98
Figure 3-12 Influence of several factors on self-assembly of SslA <sub>341-925</sub> CN on a Si wafer	102
Figure 3-13 SslA <sub>341-925</sub> CN <i>in vitro</i> recrystallized on different substrates	104
Figure 3-14 Kinetics SslA <sub>341-925</sub> CN self-assembly monitored by DLS	106
Figure 4-1 Strategy to yield SslA <sub>341-925</sub> CN-cstrp fusion protein	113
Figure 4-2 Heterologous expression of SslA <sub>341-925</sub> CN-cstrp in <i>E. coli</i> and purification	114
Figure 4-3 <i>In vitro</i> recrystallization of SslA <sub>341-925</sub> CN-cstrp in solution	117
Figure 4-4 <i>In vitro</i> recrystallization of SslA <sub>341-925</sub> CN-cstrp on a Si wafer	120
Figure 4-5 Electrophoretic mobility shift assay (EMSA) of SslA <sub>341-925</sub> CN-cstrp and biotinylated quantum dots.	123
Figure 4-6 Biotemplating of biotinylated quantum dots on the chimeric protein template	126
Figure 4-7 Scheme showing the potential application of the SslA-CN-cstrp fusion protein template	130
Figure 4-8 Schematic representation of the hybrid S-layer structure	133
Figure 4-9 Hybrid S-layer structures.	134
Table 1: Summary of the used and created recombinant plasmids	156
Table 2: Summary of primers used in this work	157
Table 3: Summary of strains used in this work	157

## ABBREVIATIONS

AFM	Atomic force microscopy
APTES	Aminopropyltriethoxysilane
bp	Base pairs
C-terminal	Carboxy-terminal
CN-terminal	Amino and carboxy-terminal
DLS	Dynamic light scattering
DNA	Deoxyribonucleic acid
dNTP	Deoxynucleosidetriphosphate
kDa	Kilodalton
N-terminal	Aminoterminal
OD	Optical density
O.N.	Overnight
PCR	Polymerase chain reaction
RNA	Ribonucleic acid
RT	Room temperature
SCWP	Secondary cell wall polymer
SDS	Sodium dodecyl sulfate
SDS-PAGE	SDS polyacrylamide gel electrophoresis
SEM	Scanning electron microscopy
S-layer	Surface layer
SLH-domain	S-layer homology domain
SslA	<i>Sporosarcina ureae</i> S-layer protein A
sslA	<i>Sporosarcina ureae</i> S-layer gene A
TEM	Transmission electron microscopy
V	Volt
v/v	Volume per volume
w/v	Weight per volume



# CHAPTER 1

## 1 INTRODUCTION

Gordon Moore, a senior member of Intel's Board of Directors and one of the company's founders, conceived Moore's Law back in 1965 [1]. The premise stating that the number of transistors per integrated circuit will grow exponentially over time has held true to this day.

In the computing world, having more transistors on a chip means higher speed and possibly more functions. While Moore's Law has driven the industry for more than four decades, the continuation of Moore's Law now requires innovations not only in dimensions and scaling but through integrated circuit materials and structure. Physical limits of atomic structures or power density could be reached by 2020 [2].

To continue the remarkably successful scaling of conventional complementary metal oxide semiconductor (CMOS) technology and possibly produce new paradigms for logic and memory, many researchers have been investigating devices based on nanostructures. Instead of the conventional **“top-down”** manufacturing which uses microfabrication methods where externally-controlled tools are used to cut, mill, and shape materials into the desired shape and order, a new category of devices could emerge by simply assembling small, single molecule components possessing special properties into more complex assemblies. This would constitute the **“bottom-up”** approach, which utilizes the concepts of molecular recognition and **molecular self-assembly**.

Nature provides inspiration for the design and engineering of functional electronic devices at nanoscale. In biological systems, inorganic materials are always in the form of nanometre-scale objects, which are self-assembled into ordered structures for full benefits of their function, that derive from their controlled size, morphology and organization into two- and three-dimensional constructions. Furthermore, biology may provide unique tools for nanofabrication.

## 1.1 MOLECULAR SELF-ASSEMBLY AND SELF-ASSEMBLING SYSTEMS

Self-assembly is the process in which a system's components - be it molecules, polymers, colloids, or macroscopic particles - organize into ordered and/or functional structures or patterns as a consequence of specific, local interactions among the components themselves, without external direction/intervention.

Self-assembly is classified as being either static or dynamic [3] based on the thermodynamic description of the resulting assemblies (Figure 1-1). In **static self-assembly**, the ordered state forms as a system approaches equilibrium, reducing its free energy. The structures that emerge are ordered but static—once made, they cannot be further reconfigured and cannot perform different functions depending on the changes in external parameters.

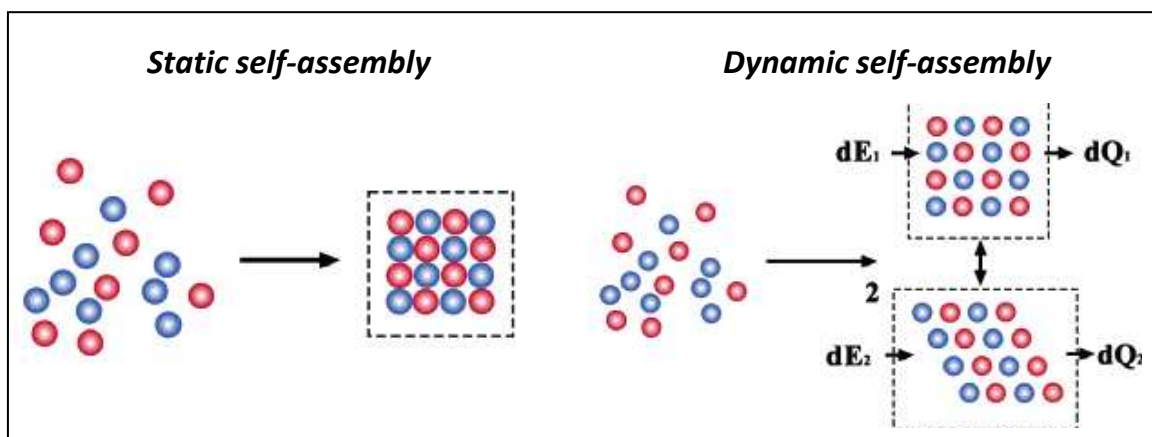


Figure 1-1 Static and dynamic self-assembly [adapted from [3]]

**Dynamic self-assembly** builds structures that change and function outside the confines of thermodynamic equilibrium. A disordered collection of components evolves into an ordered structure through input of energy from an external source; this energy dissipates *e.g.* as heat. The system can realize different configurations dependent on the rate of energy input, and when no energy is driving the system, it “falls apart.” Many examples of dynamic self-assembly are found in living cells: the transcriptional machinery that replicates DNA, fibers comprising the cytoskeleton and motors powering bacteria.

**In nanotechnology**, self-assembly underlies various types of molecular structures (*e.g.* Langmuir-Blodgett films [4], self-assembled monolayers [5, 6, 7], amphiphilic fibers [8, 9] as well as higher-order architectures built from nanoparticles [10, 11, 12,13], nanotubes [14], or nanorods [15]).

**In molecular sciences**, self-assembly provides the basis for crystallization of organic [16, 17] and inorganic [18, 19] molecules and is at the heart of supramolecular chemistry [20, 21] where the “instructions” of how to assemble larger entities are “coded” in the structural motifs of individual molecules.

Crystallization is the acme of self-assembly.

## 1.2 PROTEIN CRYSTALLIZATION

Understanding protein crystallization is important for biology for a number of reasons. First, crystals are needed for diffraction studies to elucidate the three-dimensional structures of proteins. Secondly, crystalline proteins occur in normal and diseased tissues [22]. Finally, there is growing interest in using protein crystals in biotechnology, as means of batch purification and enzymatic reactions [23].

Many studies have contributed to the understanding of protein crystallization; however, there is no unified approach that can yet fully explain its mechanism at a molecular level. In the following, specified notions of the factors governing protein crystal nucleation and growth are presented.

### 1.2.1 DRIVING FORCE OF PROTEIN CRYSTALLIZATION- THERMODYNAMICAL ASPECTS

From the perspective of thermodynamics and experimental kinetics, the driving force of crystallization is the difference of the chemical potential ( $\Delta\mu$ ) of the protein molecule in solution and in the crystal:

$$\Delta\mu = -kT \ln(c/s) \quad (1)$$

where  $k$  is the Boltzmann constant,  $T$  the absolute temperature and the  $c/s$  ratio the so called supersaturation. The supersaturation is defined by  $c$ , the protein concentration

in solution and  $s$ , the solubility of the protein meaning the concentration of the protein for which the solution is in dynamic equilibrium with the crystal. If the concentration of the molecules equals the solubility, the crystal neither grows, nor dissolves because on average the same numbers of molecules attach and dissociate from its surface.

Protein crystallization proceeds at very high supersaturations *e.g.* in the range of 3-30 which is larger than required for crystallization of inorganic crystals [24].

Three phases of protein crystallization can be distinguished: nucleation, post-nucleational growth and cessation of growth [25]. Protein nuclei that have reached a critical size will grow into crystal lattices. Growing ceases after a certain size and researchers are attributing it to the lattice defects and impurities [26, 27].

### 1.2.2 PROTEIN CRYSTAL NUCLEATION

During nucleation ordered nuclei are formed as a result of matter fluctuations. If these are formed in the volume of ideally pure solutions, *e.g.* containing only the protein and solvent molecules, the process is called **homogeneous nucleation**. If monomers nucleate on the surface of seeds added to the solution or on substrates that provide active centres for nucleation, it is referred as **heterogeneous nucleation** (Figure 1-2).

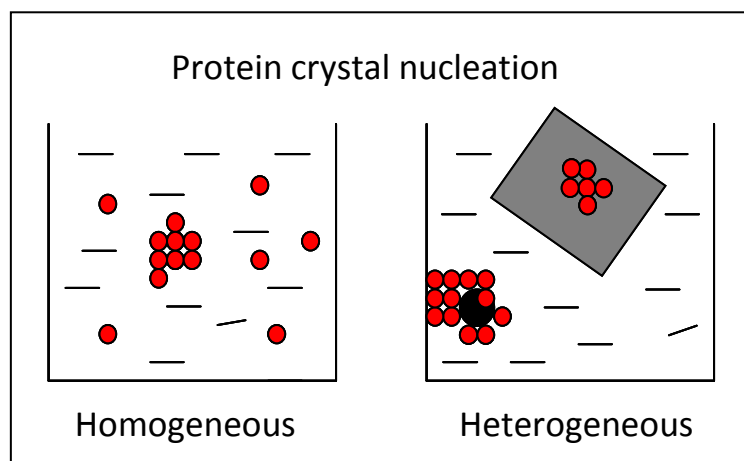


Figure 1-2 Illustration of the nucleation process.

The creation of a nucleus implies the formation of an **interface** between the monomers at the boundaries of the new phase. The importance of the interface is that energy of a monomer in the interfacial region is much higher than in the bulk of the cluster. Clusters grow larger in order to reduce their interfacial area per element and increase the bulk fraction of the cluster.

The work to form a nucleus of  $j=1, 2, 3, \dots$  molecules can be found by thermodynamic considerations since it is defined as the difference between the free energy of the system in its final and initial states, *e.g.* before and after the cluster formation.

The **free energy change ( $\Delta G_j$ )** on formation of the cluster can be estimated by considering the number of monomers in the cluster and their free energy in the homologous phase and their free energy in the new phase defined by the presence of an interface. The change in standard free energy  $\Delta G_j$  for the aggregation of  $j$  monomers can be expressed as [27]:

$$\Delta G_j = \nu_j G_B + \beta j^\gamma G_S \quad (2)$$

where  $\nu$  is the volume of growth unit,  $G_B$  represents the **bulk free energy gain** resulting from the energy release during bond formation at the new interface and is proportional to the volume of the crystal,  $G_S$  is the free energy per unit area of the surface (effective excess energy of the cluster [28]) and corresponds to the unsatisfied bonds present on the surface of the crystal whereas  $\beta$  and  $\gamma$  coefficients depend on the shape of the nuclei.

Under crystallization conditions  $G_B$  is negative as it corresponds to the favourable interactions formed in the crystal and  $G_S$  is positive as it results from unsatisfied bonds.

In the initial phase of nucleation, the positive surface term prevails. The addition of new monomers to the cluster causes an increase in the free energy. As the volume grows faster than the surface, the favourable volume term starts to dominate the free energy expression when the nuclei exceed a certain critical size ( $a_c$ ). The free energy of the nuclei with the critical size is called the **activation free energy of nucleation**. From

this point stable growth of the cluster occurs. Every cluster below this size can be dissolved because the interactions are not enough to hold the molecules in the cluster. The shape of the free energy versus size of the nuclei curve is shown in Figure 1-3:

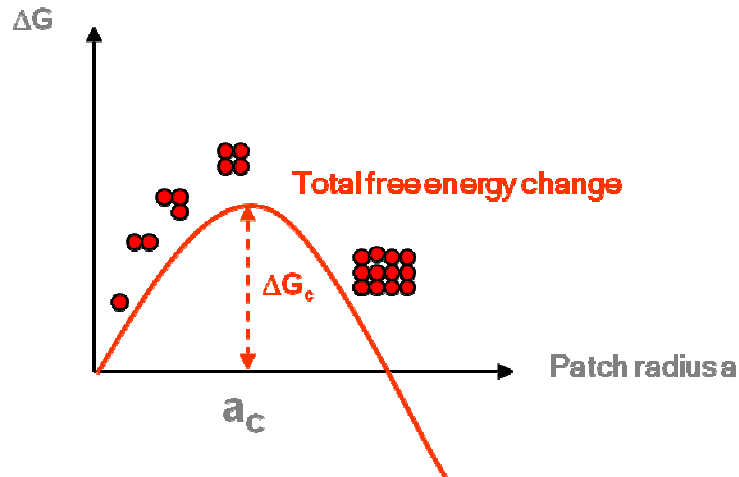
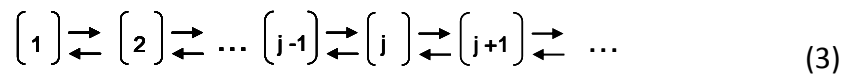


**Figure 1-3 Shape of the free energy plot as a function of a growing patch.**

Ordered nuclei that have reached a critical size ( $a_c$ ) can overcome the nucleation barrier ( $\Delta G_c$ ) and grow up to a crystal.

### 1.2.2.1 NUCLEATION MECHANISM (KINETICS)

Among researchers it is generally agreed that nucleation occurs by the Szilard mechanism of successive attachments and detachments of single monomers to and from the clusters of various size  $j=1, 2, 3, \dots$ . Accordingly, the chain reaction can be described as [28]:



where  $(j)$  refers to a cluster of  $j$  molecules. Thus the nucleation kinetics are governed by the attachment frequencies  $f(j)$  ( $s^{-1}$ ) and  $g(j)$  ( $s^{-1}$ ) of monomer attachment to and detachment from an  $j$ -sized cluster, respectively.

In both homogeneous and heterogeneous nucleation process, the monomer

attachment usually occurs by diffusion of the monomers in the volume of the solution towards the nucleus or by transfer of solute across the nucleation/solution interface.

### 1.2.2.2 NUCLEATION RATE

The nucleation rate  $J$  [28] giving the number of supernuclei generated in the system per unit time and per unit volume or area is an important kinetic characteristic of the nucleation process.

At constant temperature and supersaturation the monomer attachment and detachment frequencies are time independent and nucleation can proceed in the stationary regime. The process is then characterized by the stationary nucleation rate  $J$ , which is the frequency of transformation of the nuclei (the  $j^*$  sized cluster) into the supernuclei (the  $j^*+1$  sized cluster). Therefore, if  $Z(j)$  is the time independent stationary concentration of  $j$  sized clusters,  $J$  is the difference between the rate  $f(j^*)Z(j^*)$  of all  $j^* \rightarrow j^*+1$  transitions per unit volume area of the system and the rate  $g(j^*+1)Z(j^*+1)$  of all  $j^*+1 \rightarrow j^*$  ones:

$$J = f(j^*)Z(j^*) - g(j^*+1)Z(j^*+1) \quad (4)$$

Knowing  $J$  is necessary for the comprehensive description of other processes involving nucleation, such as, for instance, mass crystallization and nucleation-mediated crystal growth.

### 1.2.2.3 INDUCTION TIME

It is defined as the time required until the detection of the first portions of a new crystalline phase that nucleates and grows in the supersaturated solution. After the initial moment of supersaturating the solution, a certain time may elapse until the first stable crystals appear. This time is experimentally observable and attributed to

the “ability” of the solution to remain supersaturated, *i.e.* in metastable equilibrium [28]. The appearance of the very first supernucleus brings the solution out of metastable phase.

### 1.2.3 PROTEIN CRYSTAL GROWTH

During the crystal growth, protein monomers are transported from the bulk phase of the solution to the cluster surface where they become incorporated. In order to be incorporated into the existing crystal structure, they must acquire the proper conformation and orientation at a certain site of the crystal as a consequence of the 3D symmetry. Hence, the process of growth implies the volume transport, rearrangement and integration of protein molecules [29]. When the volume transport is much faster than the surface integration, amorphous aggregation is kinetically more favourable above crystallization [30] because the first coming molecule does not have enough time to find its optimal orientation before the next molecule arrives. Indeed, if surface integration is a rapid process, the adsorbed molecules have enough time to rearrange before the arrival of additional molecules resulting in crystalline phase formation.

Protein crystals grow typically under high supersaturations, usually several magnitudes higher than inorganic crystals do [31]. Despite the higher supersaturation, protein crystals grow very slowly, fact demonstrated by the growth rate which is at least 2-3 magnitudes lower than for inorganic molecules. The difference is attributed to the difficulties in the proper spatial orientation (forming the defined interface) of the big biomolecules when entering the crystal lattice site (so called kink sites).

In conclusion, protein solutions under crystallization conditions are very complex systems and most probably will continue to be a subject of future research.



### 1.3 SURFACE LAYER PROTEINS (S-LAYERS)

It is now generally accepted that in the course of evolution life on this planet has divided into three domains: archaea, bacteria and eucarya [32, 33]. Both archaea and bacteria are prokaryotes resembling extremely small unicellular form of life.

Most of the prokaryotes possess a supramolecular layered cell-wall structure outside the cytoplasmic membrane. The cell wall and the cytoplasmic membrane constitute the prokaryotic cell envelope complex which regulates the molecular exchange between the cell and its environment.

One of the most commonly observed surface structures on the prokaryotic cell envelopes are crystalline arrays of proteinaceous subunits, termed **Surface Layers** (S-layer). In archaea, S-layers bind directly to the cytoplasmic membrane, in Gram-negative bacteria to lipopolysaccharides of the outer membrane and in Gram-positive bacteria to the cell wall.

For the first time, a surface layer structure was described in 1953 by Houwink on the cell wall of *Spirillum* sp [34]. Since then, S-layers have been identified in hundreds of different bacterial and archaeal strains [35] and have been a widely used subject for various research studies. The wealth of information accumulated on the S-layers led to a broad spectrum of applications [36, 37, 38].

#### 1.3.1 STRUCTURE OF S-LAYERS

High resolution electron microscopic studies and atomic force microscopy in combination with computer image enhancement procedures have provided structural information about S-layers.

S-layers are composed of single protein or glycoprotein subunits which after secretion, crystallize into two dimensional lattices. The lattices can have different types of symmetries. Depending on the lattice type, one lattice unit consists of one, two, three, four or six protein monomers rendering therefore oblique ( $p1$ ,  $p2$ ), trimeric ( $p3$ ), square ( $p4$ ) or hexagonal symmetry ( $p6$ ) to the lattice (Figure 1-4). The lattice structure is further characterized by the lattice constants  $a$  and  $b$  as well as by the base angle  $\gamma$ . The centre to centre distance of the units varies from 3.5 - 35 nm.

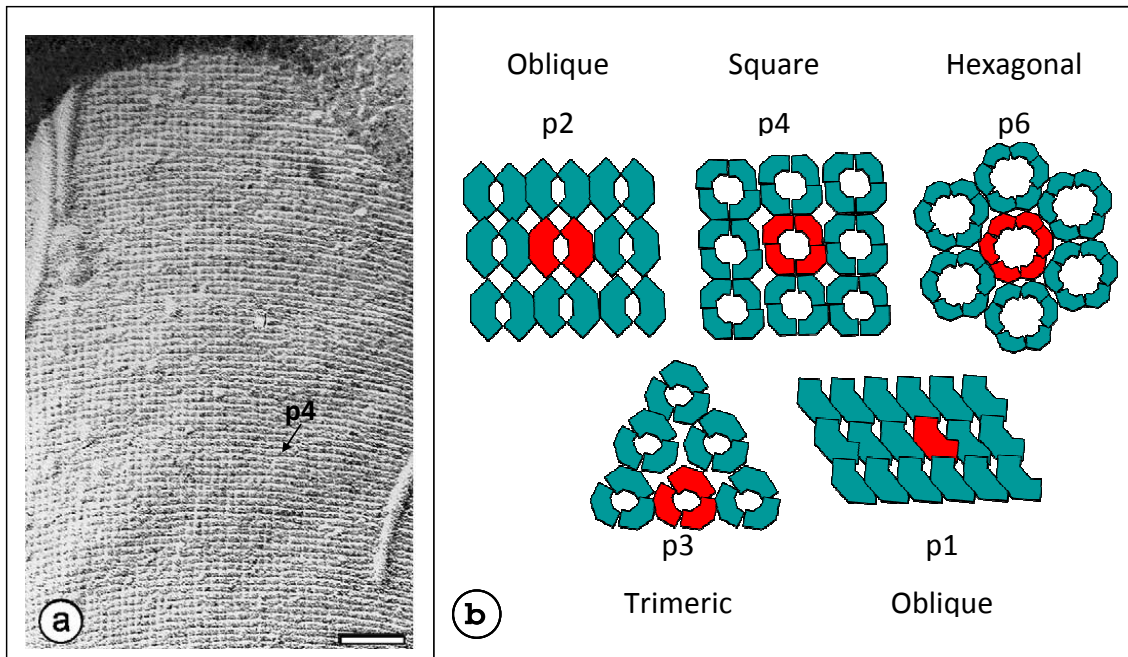


**Figure 1-4 Different S-layer lattice types**

a) TEM of freeze etching preparation of *Desulfotomaculum nigrificans* NCIB 8706 showing an S-layer with square lattice symmetry b) The well ordered S-layer lattices show oblique (p1, p2), square (p4), trimeric (p3) or hexagonal (p6) symmetry. The morphological units are composed of one, two, four, three or six identical subunits (marked in red) [modified from [39, 40].

Since S-layers are monomolecular assemblies of identical subunits, they exhibit pores identical in size and morphology. The pore sizes differ from 2-8 nm and can occupy up to 70% of the surface area.

Most S-layers are 5 to 25 nm thick [41] and they reveal a rather smooth outer surface (facing the environment) and a more corrugated inner surface (which is in contact with the cell membrane) [42].

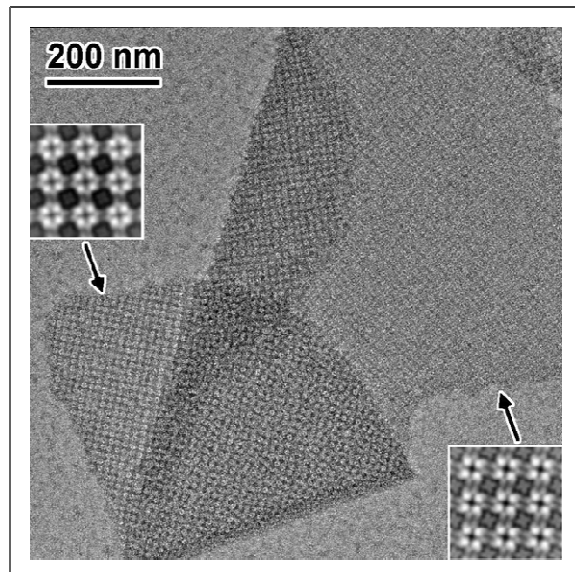


**Figure 1-5 Structural difference between the two S-layer sides**

The TEM micrograph of a partly folded S-layer stained with uranyl acetate. The two different sides of the S-layer exposed have different structure as evidenced by the inserted lattice image reconstructions [adapted from [42]].

S-layers isolated from different *Bacillaceae* revealed significant differences in charge of the inner and outer surface. The outer surface is charge neutral due to an equimolar proportion of exposed amino and carboxyl groups, whereas the inner surface can possess either a net positive or net negative charge.

### 1.3.2 PROPERTIES OF S-LAYERS

S-layers represent a fascinating model of self-assembling a supramolecular structure. *In vivo*, the S-layer monomers after secretion are transported to the cell surface where they crystallize into a regularly ordered protein lattice that covers the whole cell surface.

The isolated S-layer subunits maintain this remarkable intrinsic property of self-assembling into protein lattices. After detachment from the cell surface and disintegration into monomers using high concentrations of chaotropic (*e.g.* guanidium hydrochloride or ureae in case of Gram-positive bacteria) [43, 44] or metal chelating agents (*e.g.* EDTA for Gram-negative bacteria) [45, 46] S-layers are able to *in vitro*

reassemble into regular lattices identical to those observed on intact cells upon removal of the disrupting chemical. Reassembly can occur in solution, on solid surfaces, at air water interface or on liposomes and the self-assembly process may lead to the formation of flat sheets, open ended cylinders or vesicles (Figure 1-6). This special property has been observed for both, native and recombinant S-layer proteins.

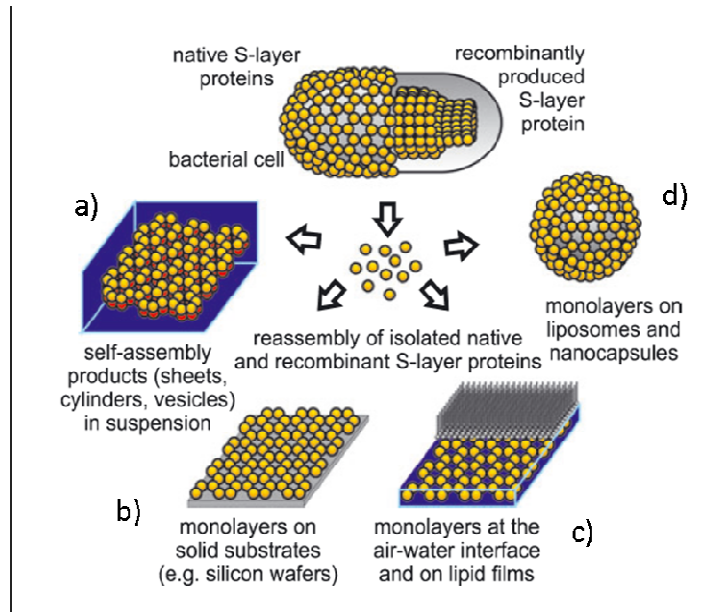


**Figure 1-6 *In vitro* recrystallization of S-layers**

The self-assembly can occur a) in suspension b) on solid substrates c) at the air/water interface or on lipid films and d) on liposomes [adapted from [47]].

The conditions required for extraction and disintegration have shown that S-layers are held together and onto the supporting envelope by noncovalent forces including hydrogen or ionic bonds, hydrophobic or electrostatic interactions [48, 49, 50, 51] and that the bonds holding the subunits together are stronger than those between the crystalline array and the cell envelope layer.

In comparison to the proteins protected by the cell wall, S-layers, resided on the cell surface of prokaryotes, must withstand the harsh physicochemical conditions of the environment and protect the cells. In this sense, the S-layers of *Archea* - as the only wall component [52] - are very resistant to extraction and disintegration, high temperature and ionic concentrations, extreme pH, exogenous proteases, osmotic shock or mechanical stress while allowing cell division and incorporation of the new S-

layer subunits. For example, the S-layer of *Bacillus anthracis* (SbpA) recrystallized on a silicon wafer has preserved its two dimensional crystalline structure even after exposure to 80% ethanol, only losing its regular structure upon low pH treatment, *i.e.* pH 3 and exposure to 70 °C for more than 10 minutes [53].

In most S-layer carrying organisms, the S-layer protein comprises up to 15% of the total cellular protein [54].

S-layer proteins of bacteria of all phylogenetic branches revealed a rather similar overall amino acid composition. Most S-layers are composed of an acidic protein or glycoprotein species with an isoelectric point (pI) between 3 and 6 [55]. Exceptions are the S-layer proteins of *Methanothermobacter ferredoxigenes* with a pI value of 8.4 and *Lactobacilli* (pI > 9.5) [56]. The molecular weight of S-layer proteins varies between 46 (*Lactobacillus spp*) and 169 kDa (*Rickettsia spp*) [56]. A unique feature of S-layers is a low content or complete absence of sulphur containing amino acids and a high proportion (40-60%) of hydrophobic amino acids which seem to be particularly important for the assembly process. Lysine is the predominant basic amino acid, while the arginine, histidine and methionine content is generally low and cysteine was only detected in a few S-layers [57]. According to circular dichroism measurements, approximately 20% of the amino acids are organized in  $\alpha$ -helices and about 40% occur as  $\beta$ -sheets. Post translational modifications of S-layers include removal of the signal peptide, phosphorylation and glycosylation [58, 59, 60].

The N-terminal part of S-layers is highly conserved. By sequence comparison, S-layer-homologous (SLH) motifs have been identified at the N-terminal part of many S-layer proteins [61, 62, 63, 64, 65]. Typically, S-layer proteins possess three repeats of the SLH motifs, each consisting of 50 to 60 amino acids including 10-15 highly conserved residues. SLH motifs function as anchoring sites to the negatively charged secondary cell wall polymer (SCWP) of bacterial cell surface. The recognition mechanism was shown to be of lectin-polysaccharid type [66]. However there are S-layers devoid of SLH domains *e.g.* in case of *B. stearothermophilus* [63] wild type strains and *Lactobacillus* [67]. These S-layers are anchored to the SCWP only via electrostatic interactions.

### 1.3.3 GENETICS OF S-LAYERS

For maintaining a complete S-layer on the surface of a cell growing with a generation time of 20 to 30 minutes, at least 500 copies of a single polypeptide have to be synthesized, translocated to the cell surface and incorporated into the existing lattice per second [68]. This means that promoters preceding S-layer genes must be very strong. Indeed, the promoter of the S-layer gene from *Lactobacillus acidophilus* is two times more efficient than that of the gene encoding lactate dehydrogenase, which is considered one of the strongest promoters in bacteria [69]. In *Bacillus stearothermophilus* ATCC 12980 two promoters (P1 and P2) have been identified for gene expression, which are most probably used during different growth stages. The P2 promoter is located closer to the start codon and is 2.4 times more frequently used in exponentially growing cells than the P1 promoter [70]. The existence of three tandemly arranged promoters has been reported for the expression of the *cwp* operon of *Bacillus brevis* 47, an organism which concomitantly produces two types of S-layer proteins that assemble sequentially into superimposed S-layer lattices [71].

With exception of those from *Campylobacter* and *Caulobacter*, all S-layer proteins are produced with an N-terminal signal peptide which is cleaved off after the translocation through the plasma membrane, suggesting the classical route of secretion [56].

However, environmental factors, such as oxygen limitation can influence the S-layer gene expression. For instance, the S-layer gene *sbsA* was stably expressed by *Bacillus stearothermophilus* PV72/p6 in continuous culture under oxygen limitation [72]. After relieving oxygen limitation, variant formation and expression of a second S-layer gene *sbsB* were induced and SbsA expression decreased suggesting that the S-layer expression is a synchronous process in the whole cell culture.

In comparison to other prokaryotes, mRNAs of the S-layers have been found to have an unusually long half-life time: 10 to 15 minutes for mRNA of *Caulobacter crescentus* [73], 22 minutes for *Aeromonas salmonicida* [74] and 15 minutes for *Lactobacillus acidophilus* [75]. This extended half time might be a consequence of the specific mRNA folding. The mRNAs harbouring an untranslated 5'-region (UTRs) are

able to fold into the stable secondary structures. Secondary structures within the UTRs are supposed to prolong the half-life of mRNAs.

### 1.3.4 FUNCTIONS OF S-LAYERS

In comparison to the amount of data accumulated about the structure, chemistry, genetics and assembly of S-layers, relatively little is known about their function. Since S-layers of Gram-positive and Gram-negative bacteria can be lost in the course of laboratory cultivation, elucidation of functional significance would require experiments that mimic the complex natural habitats of the microorganism bearing the S-layer protein. Most of the functions assumed are hypothetical and have no confirmed experimental prove. Considering that S-layer carrying organisms are ubiquitous in the biosphere, the supramolecular concept of an isoporous, crystalline surface layer could have the potential to fulfill a broad spectrum of functions.

It is now generally recognized that the S-layers as the main part of the bacterial cell envelope might play a role in the protection of the organism against hostile environmental conditions. They are of major importance for cell-cell interaction and cell growth and division and should withstand expansion to keep the shape in archaea [48, 38, 76].

Because S-layers possess pores identical in size and morphology in the 2-8 nm range, they work as precise molecular sieves with sharp cut-off levels for the cells. Depending on the pore size, small molecules such as gases and salts or macromolecules with a molecular weight of 30000 or 40000 Da are rejected or filtrated.

S-layers from *Bacillaceae* were found to function as adhesion sites for cell-associated exoenzymes. For instance, the high molecular weight exoamylase from two *B. stearothermophilus* strains were bound to the S-layer surface without disturbing diffusion of nutrients and metabolites through the S-layer lattice.

Concerning specific functions, the most detailed knowledge exists for S-layers from pathogenic organisms. Besides favouring the adhesion of the bacteria to the host cells, S-layers can protect them from the lytic activity of the immune system [77].

A quite unique function was observed for the S-layer of the cyanobacterium *Synechococcus sp GL24*. This bacterium lives in sea waters of a high mineral content. Its S-layer is able to bind calcium carbonate or gypsum protecting therefore the bacterium from encrustment by continuously shedding S-layer fragments with attached mineral into the environment [78].

### 1.3.5 GENETIC ENGINEERING OF S-LAYERS

In the recent years an important line of development has been directed towards the genetic manipulation of S-layers. Genetic modifications of S-layers have allowed elucidation of the structure-function relationship of distinct S-layer domains and led to the enhancement of the S-layer properties with several novel functionalities [79, 80, 81].

In this sense, by generating various truncated versions of the S-layer protein SbsC of *Bacillus stearothermophilus* ATCC 12980, it could be demonstrated that the N-terminal part is responsible for anchoring the S-layer subunits to the rigid cell wall layer but is not required for self-assembly, nor for oblique lattice structure formation. Studies with the C-terminal truncation variants of this S-layer have revealed that more than 200 amino acids of this part can be deleted without interfering with the self-assembly process.

Similar truncation experiments were performed with the S-layer SbpA of *Bacillus sphaericus* CCM 2177. Results indicated that the SLH domain of the S-layer consisting of the three SLH motifs is responsible for SCWP binding while deletion of more than 300 amino acids from the C-terminal part caused a change of the lattice structure type from square to oblique.

Besides truncation analyses, several S-layer fusion proteins with enhanced application potential were constructed. The S-layer fusion protein consisting of the S-layer protein SbpA and a synthetic analogue of the B-domain of protein A capable of binding the Fc part of IgG [82] was used for coating biocompatible microbeads in order to generate specific adsorbent which should find clinical application in the treatment of various autoimmune diseases. For the treatment of IgE-mediated allergies by



construction of vaccines, Bet v1 allergen was fused to the S-layer protein SbsC of *Bacillus stearothermophilus* ATCC 12980 [83]. The fusion protein proved to be fully functional. To address not only medical needs, a fusion protein with enhanced Ni<sup>2+</sup> binding capacity was constructed by fusing His tags to the N- and C-terminal part of the S-layer protein SlfB of the uranium mining waste pile isolate *Bacillus sphaericus* JG-A12 [84]. This protein is particularly attractive for catalytic purposes or as a template for fabrication of Ni binding filter materials. Other high affinity tags such as Strep tag II were similarly built into the S-layer lattices serving as promising building blocks for nanobiotechnology.

All these fusion proteins were cloned and expressed in *E. coli*. This organism is most often the choice for heterologous expression of prokaryotic proteins not only because of the ease of growth and manipulations of this organism using simple laboratory equipment and the availability of dozens of vectors and host strains that have been developed for maximizing expression but also because a wealth of knowledge about the genetics and physiology of this bacterium. However studies about expressing S-layers in other host such as *S. cerevisiae* and HeLa cells exist as well [85].

### 1.3.6 APPLICATIONS OF S-LAYERS

The specific structural and self-assembly properties of S-layers have led to a broad spectrum of applications in biotechnology, biomimetics and nanotechnology.

#### ***S-layers as ultrafiltration membranes***

Owing to their porous structure with pores identical in size and morphology, S-layers from various *Bacillaceae* strains have been exploited for production of ultrafiltration membranes (SUMs). To this end, S-layers or cell-wall fragments carrying S-layers were deposited on microfiltration membranes and cross linked with glutaraldehyde. Permeability studies using proteins with defined molecular size were performed with the S-layers of *Bacillus stearothermophilus* strains [86]. The S-layers showed sharp exclusion limits between molecular weights of 30,000 and 45,000 Da.

### ***S-layers as matrix for immobilization of functional molecules***

S-layers can serve as a functional surface for coupling of inorganic molecules or biomolecules such as proteins and enzymes. The coupling is achieved by chemical methods and results in a uniform and dense arrangement of macromolecules on the S-layer matrix.

By functionalizing the S-layer with phosphorescence Pt(II) metalloporphyrins, an efficient luminescence based oxygen sensor system could be obtained [87]. These molecules quench upon contact with molecular oxygen and the decrease in the luminescence signal can be used for oxygen monitoring. The S-layer was recrystallized on an optical fiber tip, crosslinked and activated by the EDC method in order to covalently bind the Pt(II) porphyrin molecules. The phase shifts between the excitation and luminescence emission and the change in amplitude have been measured at given oxygen concentrations. Based on the same principle, several other analytes can be sensed and measured.

Similarly a glucose sensor was developed by immobilizing an oxygen sensitive fluorescent dye on the S-layer in close vicinity to the glucose oxidase sensing layer. A decrease in oxygen concentration resulted in a measurable signal via the fluorescent dye [88]. Functionalization of free carboxyl groups of acidic amino acids with carbodiimide was used to immobilize Protein A onto the S-layer of *Clostridium thermohydrosulfuricum* L111-69 [89]. The obtained affinity particles were shown to efficiently bind immunoglobulins and could be used to diagnose type I allergies by detection of serum IgEs.

With the aim of developing new biosensors, the enzymes naringinase and  $\beta$ -glucosidase were immobilized onto S-layer lattices *via* spacers. The enzymatic activity retained was between 60 and 80% and up to 160%, respectively [90].

### ***S-layers as supporting structure for functional lipid membranes***

Recently the reconstitution of biological membranes has been the focus of intensive research. However investigations were primarily impeded by the low stability of artificial planar lipid bilayer systems and liposomes. By recrystallizing isolated S-layer

molecules onto the lipid membranes, the stability of these structures can be increased significantly. Furthermore, the S-layers recrystallized for instance on liposomes [91, 92] can be further exploited as a matrix for coupling of other functional molecules. In this way, the whole system could act as a drug-targeting compound.

### ***S-layers for vaccine development***

*Aeromonas salmonicida* and *Aeromonas hydrophila* can cause disease in salmonids in fresh water and marine environments. Since the S-layer of those organisms are essential for virulence, whole cell preparations, cell sonicates or partially purified cell products have been applied as attenuated vaccines [93, 94]. On the other hand, native and cross-linked S-layers were used as combined carrier/adjuvant systems either against infection with pathogenic bacteria or in the immunotherapy of cancers and in the antiallergic immunotherapy [95, 96].

### ***Patterning of recrystallized S-layers***

Technological applications of surfaces functionalized with S-layers require patterning of the protein lattice. Patterning of the S-layers recrystallized on Si wafers could be achieved by irradiation with deep UV laser through a microlithographic mask having features in the size of 1  $\mu\text{m}$  and 200 nm [97]. Local ablation with ArF radiation has totally removed the S-layer in the exposed areas while the integrity of the protein matrix was retained in the unexposed areas making possible the subsequent binding of biologically functional molecules or attachment of enhancing ligands.

S-layers might also be applied as natural nanoresists. Since S-layers are thinner (only 5-10 nm) than conventional resists, a considerable improvement in edge resolution is expected during the fabrication of submicron structures. In this application the S-layers are reinforced by a thin refractory layer *e.g.* Zr, silylation or electroless metallization in order to yield different etching rates between exposed and unexposed areas for the subsequent reactive ion etching [98].

### ***S-layers as template for formation of regularly ordered nanoparticle arrays***

S-layers as scaffolds have been found to be well suited for the predefined fabrication of ordered metallic and semiconductor particle arrays. Regular cluster array formation was reported on the S-layer of *Bacillus sphaericus* NCTC 9602 by the wet chemical deposition of Pd and Pt, Au and Ag [99]. Fabrication consisted of two steps: incubation of the S-layer with the metal salt for activating the metal deposition and chemical reduction of the salt complexes in order to obtain metallic particles. The last step could be initiated by electron exposure as well [100]. In both cases, the geometrical properties of the particle arrays are completely determined by the underlying protein template. Highly ordered FePt arrays were obtained by deposition of FePt from the gas phase onto the S-layer template [101]. These could meet important nanotechnological applications such as data storage devices.

Gold functionalized S-layer nanotemplates were used for growing silicon nanopillars [102]. In contrast to electron and ion beam lithography which are both costly and slow methods, biotemplated fabrication of nanopillars constitutes a more promising approach. In a first step the S-layer sheets were adsorbed onto silicon substrates and covered with gold nanoparticles. Then the S-layer was removed by O<sub>2</sub> based plasma reactive ion etch treatment which did not disrupt the ordering of the gold colloids acting as a nanomask. Inductively coupled plasma etching process was used to generate silicon pillars-like structures. The resulting pillars had a conical shape, but were arranged in a very disordered manner; probably due to mobility effects that arise during the silicon etch process.

### **1.3.7 THE S-LAYER OF *SPOROSARCINA UREA* ATCC 13881 (Ssla)**

*Sporosarcina urea* ATCC 13881 is a gram positive, motile bacterium living in soil. Taxonomically, it belongs to the family of *Bacillaceae* under the genus *Sporosarcina*. It requires alkaline conditions for growth (pH 8.8 is optimal) and is able to form endospores [103, 104].

For the first time, an outermost protein layer *i.e.* an S-layer, covering its cell surface was described by T.J. Beveridge in 1979 [105]. Isolation from the cell surface and

purification enabled several studies that led to the accumulation of the present knowledge about this S-layer. The three-dimensional structure has been determined to a resolution of 1.7 nm by electron microscopy and image reconstruction. The S-layer shows a tetragonal unit cell with 4 monomers building up 1 unit cell (p4 symmetry) with a lattice constant of 12.9 nm [106]. The monomers have a clear multidomain structure consisting of a massive core, arms connecting adjacent unit cells and spur domains that make contact to the subsidiary fourfold symmetry axes. A general view of the S-layer and its structural details are presented in Figure 1-7.

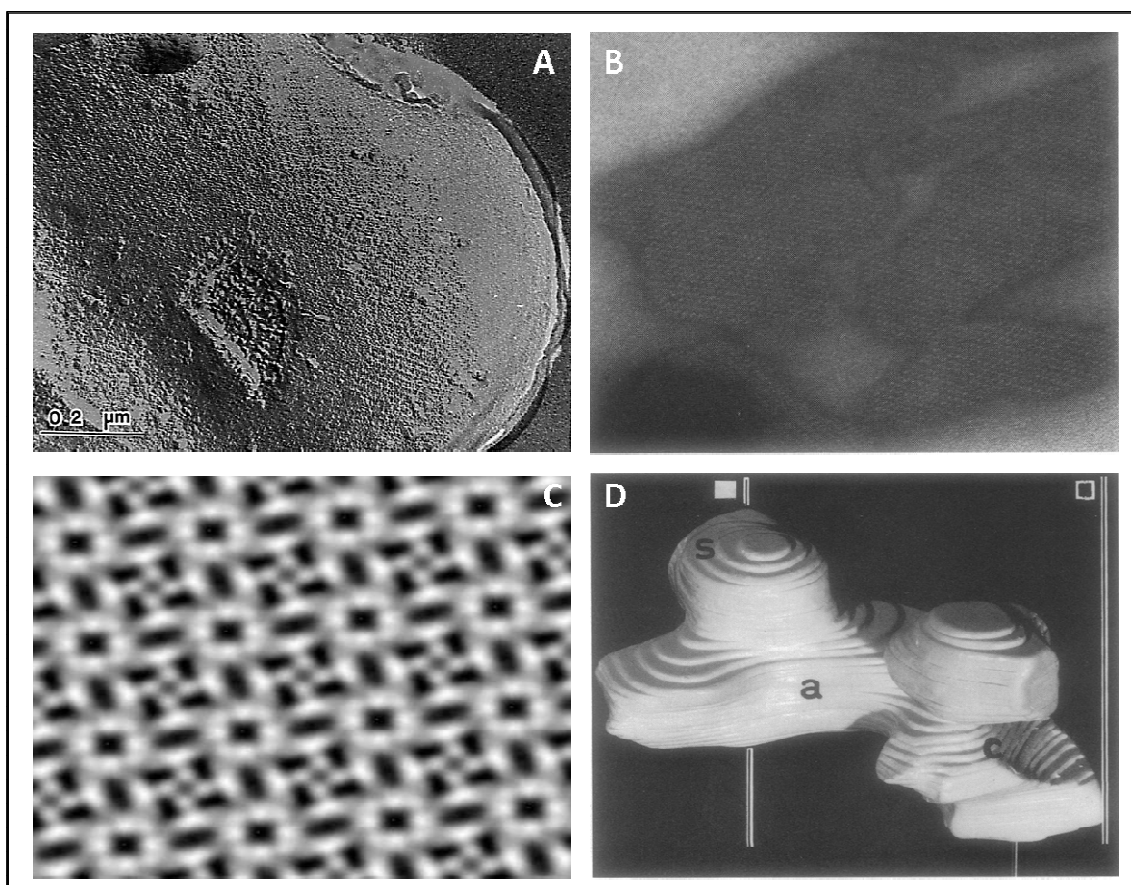


**Figure 1-7 The S-layer of *S. ureae* ATCC 13881**

A) Electron micrograph of freeze etched preparations of intact cells [adapted from [107] B) Negatively stained S-layer sheets that were isolated and adsorbed onto carbon-coated copper grid [adapted from [106] C) Projection map of the negatively stained native S-layer of *S. ureae* obtained after correlation averaging with resolution of 1.7 nm. Protein appears white; the heavily stain-filled pores appear dark D) Wooden model of the putative monomer of the S-layer illustrating the multidomain structure consisting of a core (c), arm (a) and spur (s) domain.

The S-layer has a complex pattern of pores and gaps that are approximately 2 nm wide. Whether the pores are open or closed could not be precisely estimated from electron microscopy investigations since the S-layer is immobilized on a grid, however it was observed that isolated subunits of the S-layer spontaneously associate such that the unit cells are precisely in register and the aligned pores form continuous channels across the two sheets. The thickness of the S-layer was found to be 6.6 nm.

Low stain levels and heavy metal shadowed preparations revealed the inner and the outer surfaces of the S-layer are characteristically different. The outer surface facing the environment is smoother than the inner surface which is connected to the underlying cell envelope (Figure 1-8) having a functional significance [108].

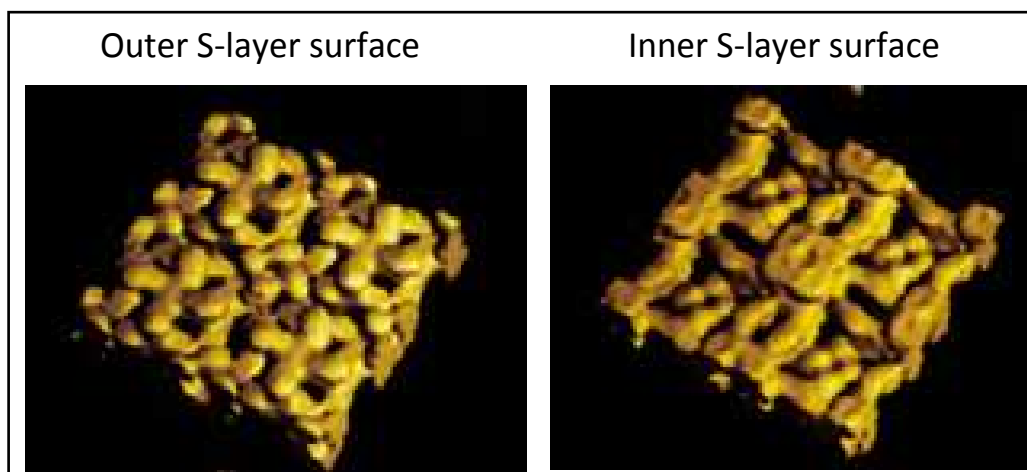


**Figure 1-8** The outer and inner surface of the S-layer of *S. ureae* ATCC 13881

The 3D reconstruction was obtained by surface shading [adapted from [106]].

The S-layer was found to be remarkably sensitive to low pH as judged by the use of acidic negative stains and titration with increasing amounts of acid as well as to proteolytic enzymes, SDS and H-bond perturbants.

The molecular weight of the S-layer protein from the wild type strain is 130 kDa. Infrared spectroscopy investigations revealed that about 35% of the polypeptide has  $\beta$ -structure conformation and that the  $\alpha$ -helix content is low.

Recently the complete gene encoding the S-layer protein (*ss/A*) has been identified [109]. The protein sequence shows a high degree of similarity to other S-layer sequences and consists of 1097 amino acids (AA). It possesses a cleavable N-terminal

secretion signal of 31 amino acids (Figure 1-9). Adjacent to the secretion signal two SLH domain of 43 and 45 amino acids were identified.

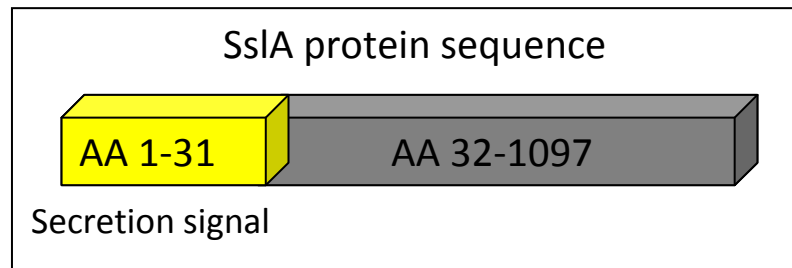


**Figure 1-9 Schematic representation of the SslA protein sequence**

Attempts to heterologously express this S-layer in *E. coli* BL21 (DE3) have shown that the level of synthesis is low, significantly lower than that of other S-layer proteins [110]. In order to improve expression, the use of expression strains bearing rare codons was suggested as a strong bias in the SslA codon usage exists. The protein is not glycosylated as evidenced by staining experiments.

The S-layer of *Sporosarcina ureae* ATCC 13881 has been reported to be an excellent biotemplate for fabrication of highly ordered metal cluster arrays. Pt was deposited onto the isolated protein sheets by first incubating the metal salt with the S-layer followed by a reducing step to obtain metallic Pt particles [111]. As a result, highly ordered nanocluster arrays were formed on the protein template reproducing its square symmetry (Figure 1-10).

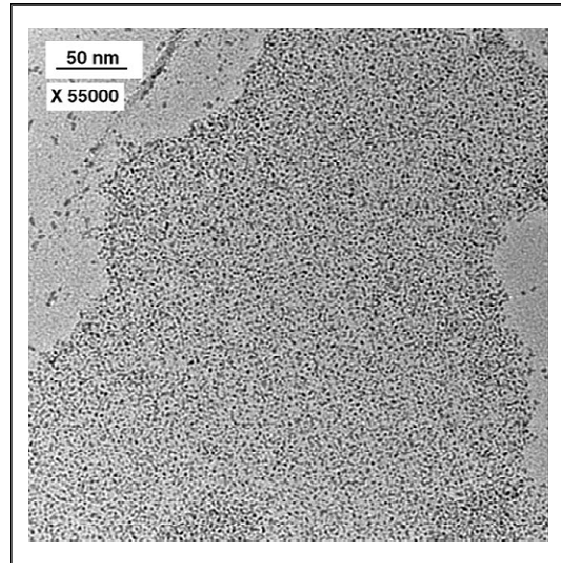


**Figure 1-10 Pt cluster deposition onto the S-layer of *S. ureae* ATCC 13881 [adapted from [111]**

Transmission electron micrographs showed that the Pt clusters were situated in the central pores and gaps of the protein structure. The calculated diameter distribution of the clusters (1.9 nm) was found to be in good agreement with the pore size (~2 nm wide) [106]. Not only the position of Pt but also cluster growth was seen to be controlled by the protein template suggesting that biotemplating (in this case with SslA) can be considered as a new and competitive route for nanostructure fabrication and manipulation.



## 1.4 MOLECULAR BIOTEMPLATING

Nanomolecular patterning with definable size and organization is of integral importance in the drive for further miniaturization in materials science and electronics. Biological systems are an important source of potential templates for the production of such nanoscale structures.

Biomolecular templating uses biomolecules to position nanoscale materials onto substrates. However, single molecules are by far too small to direct the formation of the (supramolecular) complicated shapes and patterns. Instead, ordered structures of biological molecules and assemblies at the nano-scale serve as excellent templates for fabricating inorganic nanostructures.

In nature, biominerals are formed under the structure-directing influence of protein templates. Silaffins in the case of diatoms and silicateins in sponges are capable of self-assembling into larger, structure-directing template aggregates and to induce silica precipitation from precursor compounds. However various other biological entities exist that combine both self-organization and spatial patterning at the nanometer length scale. Template mineralization on lipids, [112, 113] bacterial fibres as well as methods for DNA driven nanocrystal organization [114] and two-dimensional array fabrication using ferritin [115] have been reported.

Ordered structures of biological molecules and assemblies at the nano-scale serve as excellent templates for fabricating inorganic nanostructures. To this end, various biomolecules emerged as an attractive scaffold to which metal nanoparticles can be electrostatically bound. Actin filaments were used as templates for nanowire formation [116] by covalent attachment of gold nanoparticles to the first self-assembled the filaments. Similarly, Au nanoparticles were bound to the phosphate backbone of DNA pieces building up highly ordered molecular assemblies. Metal nanoparticles are very attractive because of their size and shape dependent properties. The optical properties of small metal nanoparticles are dominated by the collective oscillations of conduction electrons from the interaction with electromagnetic radiation. These properties are mainly observed in Au, Ag and Cu

because of the presence of free conduction electrons. The electric field of the incoming radiation induces an electric dipole in the particle and as a response, the particle will compensate for it resulting in a unique resonance wavelength the so-called surface plasmon resonance [117]. The optical properties of gold nanoparticles are of great interest for applications as ultrafast optical switches.

Nucleic acid monomers were used as a template in the synthesis of PbS and CdS [118]. Nanoscale semiconductor crystals exhibit size- and shape-dependent physicochemical properties that are distinct from those of the corresponding bulk solids [119]. These unique properties, arising from size-dependent bandgaps, discrete band structures and confinement of charge carriers enable the diverse applications proposed for semiconductor nanocrystals in the area of physics [120], biology [121, 122] and medicine [123, 124].

Not only covalent or electrostatic interactions but also molecular recognition events can play a role in positioning of distinct molecules within designated nanoregions on a biotemplate. In this sense, the streptavidin-biotin system is the most renowned.

Streptavidin takes its name from the bacterial source of the protein, *Streptomyces avidinii* and from the hen egg-white avidin with which it shares an extraordinary ligand binding affinity ( $K_d=10^{-15}$  M) for biotin [125]. It is a tetrameric protein that consists of 254 amino acids and has a molecular weight of about 60 kDa [126]. Each protomer is an 8-stranded  $\beta$ -barrel with simple up-down topology. Biotin molecules are bound at one of each barrel. The tight and specific interaction between streptavidin and biotin has caused the system to be most widely used not only for patterning and immobilization but also for biomolecule labeling and purification.

Biomolecular templating is fundamental in the development of advanced biosensors, bioreactors, affinity chromatographic separation materials and many diagnostics such as those used in cancer therapeutics [127, 128, 129]. In the future, genetic control over the template properties and coupling will bring to the forefront new platforms and material functionalities that will extend and advance both medicine and nanoscale engineering [130].

## 1.5 AIMS OF THE THESIS

Bottom-up nanotechnology often refers to the emerging use of self-assembly to construct multimolecular assemblies on the nanometer scale and biological systems are prime candidates to this end.

In this respect, surface layer proteins (S-layers) represent a unique self-assembling system. Their remarkable property of self-assembling and their repetitive physicochemical properties down to the nanometre scale led to various applications in the field of bio- and nanotechnology. However, genetic engineering may broaden and advance the S-layer technology.

The S-layer protein of *Sporosarcina ureae* ATCC 13881 observed for the first time in 1979 has not yet been fully characterized with respect to its self-assembling ability. Genetic and structural information as well as studies documenting its excellent property of mediating the formation of highly regular metal clusters exists, however in comparison to other S-layers, there is a lack of knowledge concerning the self-assembling structures it forms under different *in vitro* recrystallization conditions. Moreover, up to now, there is no data available on which part of the protein is responsible for its remarkable self-assembling property.

The present work focuses on the basic principles and self-assembly properties of the S-layer protein of *S. ureae* ATCC 13881. The aim is to provide more information upon the self-assembly structures it forms under different *in vitro* recrystallization conditions, to elucidate protein domains responsible for self-assembly and to modify this domain in order to obtain a functional S-layer with enhanced properties that can be used as a new building block for nanotechnology.

At first, the **native S-layer protein of *S. ureae* ATCC 13881** is investigated. *In vitro* recrystallization studies in solution and on a silicon wafer are performed under different experimental conditions. The influence of several factors such as initial monomer concentration, Ca<sup>2+</sup> ions and pH of recrystallization buffer on the self-assembly process is discussed. Dynamic light scattering experiments provide more insight into the kinetics of the reaction. Further on, the possibility of using this S-layer

as a biotemplate for formation of Au nanoparticle arrays is presented.

In a next step, the self-assembling properties of the **recombinant of S-layer of *S. ureae* ATCC 13881** are analysed by *in vitro* recrystallization experiments in solution and on a silicon substrate. To identify the self-assembly domain of this S-layer, three truncation derivatives are created, heterologously expressed in *E. coli*, purified and their self-assembly investigated. The study is rounded up by the dynamic light scattering measurement.

Finally, for combining the self-assembly properties of this S-layer with a ligand binding function, a chimeric protein is constructed by **fusing streptavidin to the S-layer of *S. ureae* ATCC 13881**. To probe whether the fusion protein retains its ability of self-assembling and the integrated domain remains functional, *in vitro* recrystallization experiments followed by binding of functionalized quantum dots onto the protein template are presented.

## CHAPTER 2

### 2     *THE NATIVE S-LAYER PROTEIN OF SPOROSARCINA UREA* *ATCC 13881*

S-layers are now recognized as one of the most common outermost cell envelope components of prokaryotic organisms. They represent a very versatile self-assembly system with unique features. Their construction principle based on a single constituent protein (or glycoprotein) subunit allows self-assembly into isoporous lattices possessing repetitive physicochemical properties down to the nanometer scale.

In this chapter the native S-layer of *Sporosarcina ureae* ATCC 13881 is studied in detail. The protein is described and characterized with respect to its morphology, *in vitro* recrystallization and functionalization. Factors that influence its self-assembling properties are discussed in detail followed by kinetic studies on the recrystallization process. Furthermore, the possibility of using this S-layer as a biotemplate for fabrication of nanoparticle arrays which could meet important applications in (bio)nanoelectronics is presented.

## 2.1 TOPOGRAPHICAL CHARACTERIZATION

The outer surface of *S. ureae* ATCC 13881 cell envelope comprises a two-dimensional porous crystalline membrane, called an S-layer (or shortly SslA), which is composed of protein monomers that are non-covalently linked to each other. In this way it can be easily isolated from the bacterial cell surface by applying a chemical treatment.

SslA isolation or extraction from the bacterial cell surface is done in several steps in order to separate it from other cell fragments and to obtain a highly pure protein solution. When samples from this protein solution are adsorbed onto a Si substrate, major morphological details of the S-layer sheets can be resolved with AFM (Figure 2-1).

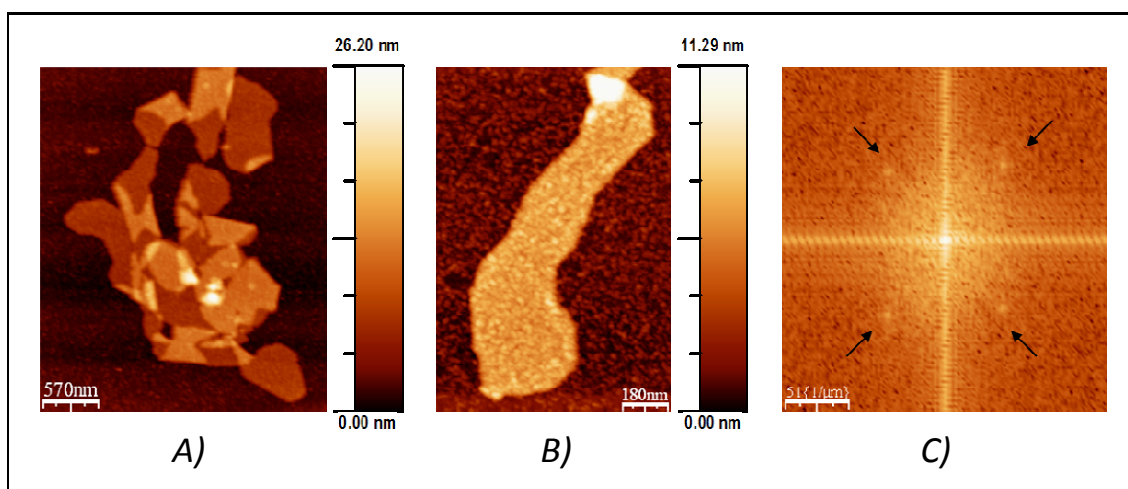


**Figure 2-1 The S-layer protein of *S. ureae* ATCC 13881**

(A) The protein layers were stripped off from the bacterial cell surface and adsorbed onto a Si substrate, (B) Zoomed S-layer sheet for lattice symmetry determination, (C) Fourier analysis based on image B showing the four-fold symmetry (p4). The protein lattice constant is 12.9 nm.

Figure 2-1 A reveals mono and multilayered SslA patches; the latter ones most probably are just folded over the monolayer structures. These patches come off from the bacterial cell surface having different shapes and sizes. Length varies between 300 nm and 1  $\mu$ m. Their thickness of about 6 nm (data not shown) is close to the value

determined by 3D reconstruction (obtained by surface shading [106]), thus air-drying during AFM sample preparation and imaging did not deteriorate dramatically the structure of the protein layer.

In Figure 2-1 C a periodic crystalline structure of SslA can be identified that usually characterizes these S-layer proteins. In order to quantify the lateral periodic structure of the SslA sheets, the digitised AFM image is analysed applying Fourier method. The calculated power spectra shows clear reflexes which contain information about lattice symmetry and periodicity. The SslA lattice of *S. ureae* ATCC 13881 exhibits square-like symmetry (black arrows in Figure 2-1 C) with a center to center spacing of the morphological units of 12.9 nm. This value is in good agreement with the lattice constant reported in literature [106].

The structure of a protein is always related to its function. On the surface of the bacterium, this S-layer protein functions as a protective coat and acts as a molecular sieve between the cell and environment [131].

In order to broaden the application potential of the S-layer protein of *S. ureae* ATCC 13881 and do not limit its use only to the protein layer forms obtained after stripping off from the bacterial cell surface, in the following the self-assembly properties of this S-layer are studied.

## 2.2 SELF-ASSEMBLY OF THE S-LAYER OF *S. UREA* ATCC 13881

S-layer proteins are endowed with the ability to self-assemble into two dimensional arrays. The S-layer monomers interact with each other through non-covalent forces (*e.g.* H-bonds, salt-bridges, ionic bonds or hydrophobic interactions) giving rise to extended protein sheets. A complete disintegration of S-layer lattices into their constituent subunits is generally achieved by treatment of cell wall fragments with hydrogen bond breaking agents or by lowering or raising the pH value. On removal of the disrupting agent, the S-layer monomers reassemble into lattices identical to those observed on intact cells. Such lattices consist of mono- or multilayers

and may have the shape of flat sheets or open ended cylinders [44]. The size and shape of the self-assembly products also depend on several environmental parameters such as protein concentration, temperature, pH, ion composition and ionic strength [132]. Recrystallization parameters must be carefully chosen in order to assure optimal reassembly conditions.

The objective of this section is to understand how the S-layer monomers of *S. ureae* ATCC 13881 (SslA) alone drive the self-assembly reaction and how the different environmental conditions (*e.g.* pH, Ca<sup>2+</sup> ions) influence this reaction. In particular such fundamental knowledge will ultimately enable rational design of long-range ordered single-crystal protein arrays, which will be essential for fully exploiting the functionality of this S-layer protein in nanobiotechnology-based applications.

### 2.2.1 GROWTH STAGES IN THE SELF-ASSEMBLY PROCESS

The S-layer lattices can be disrupted by chemical agents such as guanidinium hydrochloride (GuHCl). Upon removal of the chemical, the monomers reassemble *in vitro* in solution or on a solid support, *e.g.* silicon wafers [133].

For example, in the case of the S-layer of *S. ureae* ATCC 13881 *in vitro* self-assembly was performed first by monomerizing the protein with 5M GuHCl. Reassembly of the protein subunits was initiated by dialysing it against 10 mM CaCl<sub>2</sub> solution. Recrystallization was allowed to proceed in solution for several days or even longer *e.g.* 1 month. After recrystallization, the S-layer was shortly adsorbed to 3-aminopropyltriethoxysilane (APTES) functionalized silicon surface and imaged by Atomic Force Microscopy (AFM). Figure 2-2 shows the S-layer structures obtained:



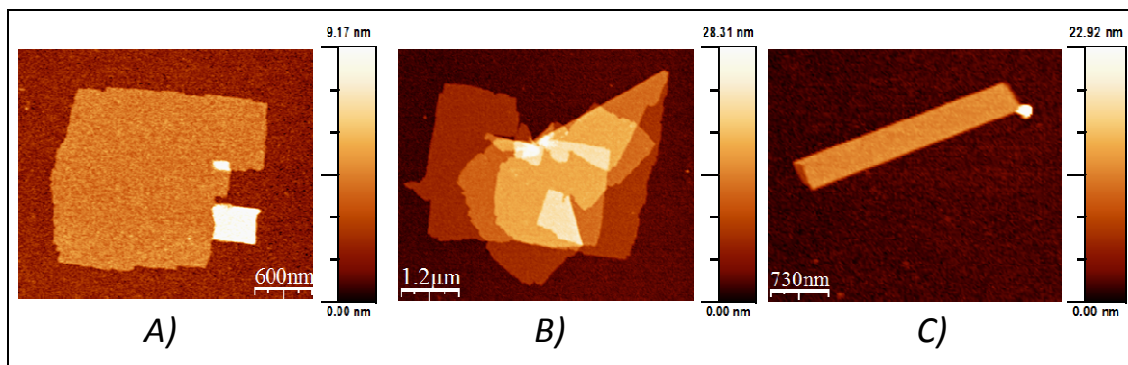


**Figure 2-2 Growth stages in the S-layer self-assembly process.**

The native S-layer of *Sporosarcina ureae* ATCC 13881 was recrystallized at A) low protein concentration (0.29  $\mu\text{g}/\mu\text{l}$ ) over a time period of 1 month, B), C) higher protein concentration (0.79  $\mu\text{g}/\mu\text{l}$ ) over a time period of 12 days.

Monolayered and multilayered sheets as well as tube like structures can be observed in Figure 2-2. The layers exhibit the same p4 lattice symmetry (data not shown) meaning that the self-assembly property is an intrinsic ability of this S-layer given that the appropriate experimental conditions are ensured.

All the different structures have been formed in solution over a certain (longer or shorter) time period. The reason for growing all these different morphologies may lie in the mechanism of the self-assembly process.

S-layer self-assembly involves a nucleation and a growth step determined to a large extent by kinetics. Kinetics refers to the way protein molecules move in solution, the rate at which they are transported and the way they are incorporated into the protein lattices. During nucleation, the monomers in solution collide and join together to form dimer, trimer and higher order clusters. These clusters are defined as nucleation points or nuclei. Upon appropriate conditions, given that these nuclei are big enough; they can grow up into protein patches. The critical size of the nuclei depends first of all on the supersaturation of the solution with protein monomers. By further incorporation of protein monomers into these patches, large, crystalline protein layers are formed. When the layers are large enough, due to an intrinsic curvature, they can fold into a tube. However, there is also the case, when patches agglomerate. These structures are not crystalline but can contain defects such as grain boundaries or amorphous regions.

Obviously, the S-layer of *S. ureae* ATCC 13881 under the mentioned experimental conditions shows the same growth stages: small patches, layers, even multilayered structures and tubes (Figure 2-2). However, experimental parameters chosen for recrystallization have an influence on the final S-layer shape. The initial monomer concentration and the time allowed for recrystallization differs by almost 3 orders of magnitude in this case. At lower initial protein concentration (0.29  $\mu\text{g}/\mu\text{l}$ ) and over a time period of 1 month, flat, planar monolayer has developed while at higher protein concentration (0.79  $\mu\text{g}/\mu\text{l}$ ) and after 12 days of recrystallization multilayered and tube like structure can be observed.

From the above observation it follows that by varying the experimental parameters it is possible to manipulate the self-assembly process and obtain the desired S-layer morphologies. This is advantageous, because for certain applications only a protein monolayer or tubes might be required. But to be able to vary the crystallization parameters depending on the specific aim of application, a deeper understanding of all factors that influence the self-assembly process is necessary. In the following this issue was addressed.

### 2.2.2 FACTORS THAT INFLUENCE THE SELF-ASSEMBLY PROCESS

Besides the complex molecular structure of the SsIA protein monomers determining the p4 symmetry of the protein lattice, the various experimental parameters acting together during the self-assembly process determine the shape and morphology of the final S-layer structures. Recrystallization parameters must be carefully chosen in order to assure optimal reassembly conditions. Therefore the influence of the initial monomer concentration, growth time,  $\text{Ca}^{2+}$  ions, pH of the monomer solution as well the presence of a silicon substrate during the self-assembly reaction is investigated in this section. This is a first time study concerning this particular S-layer protein.

### 2.2.2.1 INITIAL MONOMER CONCENTRATION

To investigate the influence of initial monomer concentration on the self-assembly properties of the S-layer of *S. ureae* ATCC 13881, *in vitro* recrystallization experiments in solution at 2 different protein concentrations were conducted. In particular, 4.5 mg/ml and 0.38 mg/ml initial monomer concentrations (concentration in dialysis) were chosen.

The experiments were performed as follows: the protein was first monomerized with 5M GuHCl for 2 hours. The chemical was subsequently removed by dialysis against 10 mM CaCl<sub>2</sub> at 4 °C for 18 hours and aliquots of the protein solution were adsorbed on cleaned Si wafers at different time intervals: immediately after dialysis, 4 days and 1 week after dialysis. After an adsorption period of 1 hour, the samples were washed gently with ddH<sub>2</sub>O, stained with uranyl acetate and analyzed by scanning electron microscopy (SEM). Examples of self-assembly structures of this S-layer protein grown are shown in Figure 2-3:

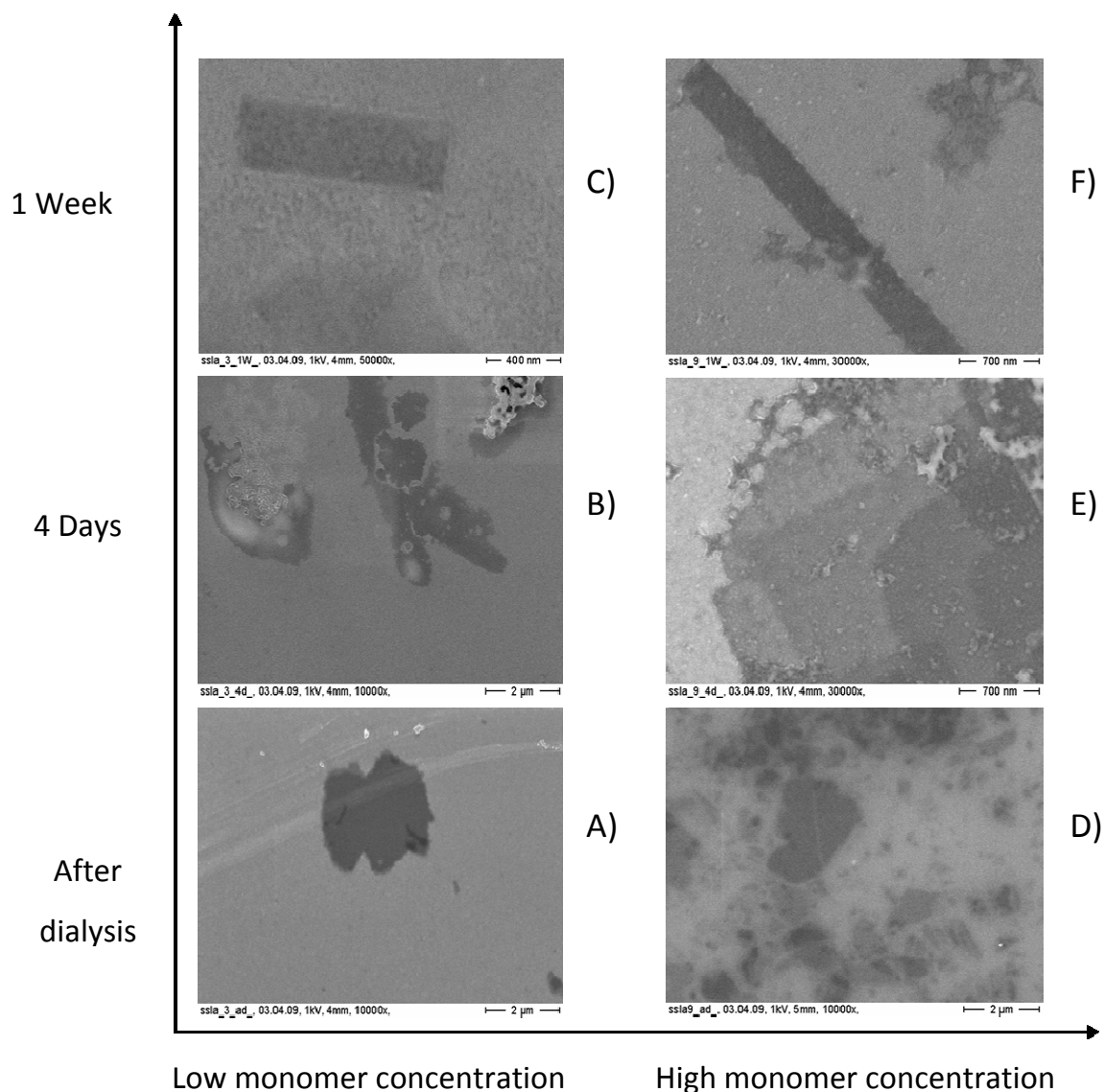


**Figure 2-3 Influence of initial monomer concentration on the self-assembly.**

The native S-layer of *S. ureae* ATCC 13881 was *in vitro* recrystallized at A) low and D) high initial monomer concentration. The patches were adsorbed onto a Si wafer right after dialysis. Note that, many small patches develop at high initial monomer concentration; while one larger patch is observed in case of low initial monomer concentration. E) In time, *i.e.* after 4 days, when the number of protein monomers in the solution is high, patches are growing into multilayers. B) However at low protein concentration, only a few sheets are observed. C) After 1 week allowed for recrystallization, tubes can be observed in the protein solution. F) Tubes are longer in case of high initial monomer concentration, diameter however is of the same size in both cases.

Figure 2-3 shows S-layer patches that have formed during dialysis at different initial monomer concentrations. These patches are different in number and size depending on the protein concentration brought into the self-assembly reaction. At high initial monomer concentration (4.5 mg/ml) a large number of patches can be seen on the silicon substrate having a size between 2  $\mu\text{m}$  and a few hundred nm and various shapes ranging from quadratic until elliptic ones (Figure 2.3 D). These patches are densely distributed over the wafer surface and by a closer inspection even small double patches can be observed, meaning one patch on top of another. They are crystalline, but the crystal symmetry could not be resolved by SEM.

However, in case of low initial monomer concentration (0.38 mg/ml), only one large patch with a size overwhelming 2  $\mu\text{m}$  is displayed (Figure 2-3 A). Other patches can be hardly seen.

All these different structural aspects are related to the mechanism by which the S-layers form in solution, *i.e.* the self-assembly process.

The process of self-assembly and formation of protein crystals starts with nucleation in which small molecular clusters appear in the supersaturated protein solution. The size and number of the critical nuclei formed in a solution is strongly concentration dependent. At high monomer concentration (high supersaturation) the critical size of the nuclei is small; therefore many small clusters will be supercritical and can grow. These plenty supercritical clusters give rise to a large number of patches which soon stop growing due to a fast consumption or depletion of the monomers present in the protein solution. At low monomer concentration (low supersaturation) the critical size of the nuclei is high and only few nuclei can attain this size and stably grow into larger patches. These few large patches may fold into tubes.

If one wants to find the optimal conditions where nice large sheets are grown, it is necessary to choose a working monomer concentration at which enough critical nuclei are formed. If the concentration is too high, many clusters will form, but all will tend to grow and the process will soon run into depletion. In case of a small monomer concentration depletion occurs at a later time point, but there will be not enough critical nuclei in order to grow many large protein sheets.

Patch growth is also affected by attachment of oligomers not only monomers. Large patches can be easier formed by self-assembly or aggregation of oligomeric structures.

In order to see how the patch size of this S-layer evolves in time, the crystallization reaction was let to proceed for several days. After 4 days, protein samples were taken from the recrystallization solution, adsorbed onto a Si wafer, stained with uranyl acetate and imaged by SEM. Results are depicted in Figure 2-3 B and E. These images show different growing pattern of this S-layer protein depending on the initial monomer concentration. A few layers have grown at low protein concentration (Figure 2-3 B) while at high concentration a multilayered structure can be observed (Figure 2-3 E). The layers are formed by further monomer incorporation into the existing patches, however there is always a competitive adsorption and desorption of the monomers happening in the solution. Hence, patches evolve into layers in time. At low initial monomer concentration the amount of monomers is less, meaning that the chance for a layer to grow is limited to the number of protein molecules available in solution. Are there more monomers present in the protein solution, the S-layer patches will grow easier into large layers or even into multilayers.

Nucleation and growth can occur either in solution or on the silicon substrate and it is difficult to distinguish between these two cases. Patches or layers can be formed in solution (homogeneous nucleation) and then these will adsorb onto the substrate or nucleation can start on the silicon substrate (heterogeneous nucleation) and layers are build up. In this latter case, the very first layer will not be well ordered and may present some defects. The formation of the second layer is driven by the interaction of the monomers with the first layer. As it is known that S-layer of *S. ureae* ATCC 13881 has a different charge distribution on its inner and outer surface [106], the growth mechanism resembles the layer-by-layer deposition of polyelectrolytes where the sequential adsorptions of anionic and cationic polyelectrolytes allow the construction of multilayer films [134].

In order to further monitor the self-assembly process, samples from the recrystallization solution were taken after 1 week as well, adsorbed onto a Si

substrate, stained with uranyl acetate and imaged by SEM. Images in Figure 2-3 C and F show that in this time tubes were formed no matter if the initial monomer concentration was low or high.

These SslA tubes are hollow, open ended cylinders having between 450 and 600 nm in diameter (radius) and between 1.1 and 4.5  $\mu\text{m}$  in length. The density of the tubes is not very high.

However, the tubes differ in length, being longer in case where the protein concentration was higher (Figure 2-3 F) which is normal since at high monomer concentration it is possible to grow large layers which can fold up into tubes. Interestingly, the tubes formed at two different monomer concentrations differ only in length and not in diameter.

Tube formation occurs after a patch has grown to a certain size that it can fold. With increasing patch size, patch edges meet each other and form a tube. On the molecular level this morphology is favoured because the unsaturated chemical bonds at the edges of the layer or patch will be reduced.

As tubes are observed in the later stage of the crystallization process, *e.g.* after 1 week in case of the S-layer of *Sporosarcina ureae* ATCC 13881, one might suppose that there is a critical size under which tube formation does not take place.

Patches can exhibit an intrinsic curvature. Besides the molecular structure of the SslA monomers, the patch curvature can be influenced by the solvent or recrystallization buffer which affects surface charges on the S-layer surface. These surface charges are different on the inner and outer surface of the S-layer (SslA) due to different chemical moieties (groups) that are present. Hence, changes in pH value, ionic strength or salts will have an influence on these surface charges and indirectly on the patch folding.

The folding mechanism is related to the crystal symmetry of the SslA lattice. Folding happens not on the diagonal but on the axis parallel to the patch edges. This fact is exemplified in Figure 2-4:

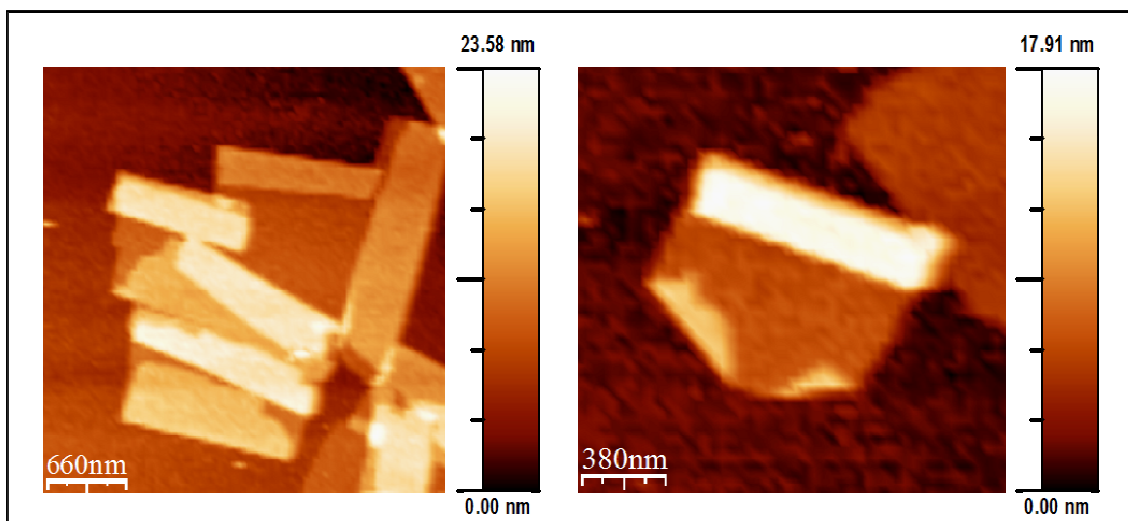


**Figure 2-4 Tube formation in case of the S-layer of *S. ureae* ATCC 13881**

The tubular form is particularly attractive because it provides access to three different contact regions: inner and outer surfaces as well as both ends. Nature does create and use successfully such tubular structures at the molecular or nanoscale and in this sense, most probably, microtubules are a more than fabulous example. The living cell is able to build the large tube like structures by the repetitive assembly of the small subunits. The cytoskeletal polymer combines strength and adaptability because they are built out of multiple protofilaments - long linear strings of subunits joined end to end - that associate laterally. Contrarily to this example, the S-layer tubes form by rolling up sheets that were assembled by the adhesion of individual protein monomers to each other.

Cylinders are observed not only under synthetic experimental conditions *i.e. in vitro* recrystallization of native SslA but also when expressed in different host organisms. The S-layer of *Bacillus stearothermophilus* ATCC 12980 (SbsC) is a good example for this latter case. This S-layer was expressed in *E. coli* [135] and the self-assembly products found in the cytoplasm of the host organism were organized as closely packed spirally wound sheets. Modification of the same S-layer protein structure by genetic engineering *e.g.* fusion to green fluorescent protein (eGFP) led to similar filamentous, cylindrical structures in *S. cerevisiae* cells [136].

The potential utility of the mentioned S-layer tubular architectures in a variety of



chemical, biological and material science applications will depend largely on the understanding of the underlying formation mechanism as well as on the ability to precisely manipulate such nanoscale objects.

### *Ca<sup>2+</sup> ions*

As a next potential factor, the influence of Ca<sup>2+</sup> ions on the self-assembly of the authentic S-layer protein of *Sporosarcina ureae* ATCC 13881 was monitored.

Previous studies conducted by Pum and Sleytr have suggested that calcium ions are essential for the self-assembly of the SbpA and that concentration of this ion is a critical parameter that determines the shape and size of the recrystallized S-layer lattices [137]. Hence, there was a strong interest to know whether this is true in case of this S-layer protein as well.

In order to analyze the effect of Ca<sup>2+</sup> on the recrystallization of SslA, the self-assembly reaction was followed in the presence versus absence of CaCl<sub>2</sub> at a protein concentration of 1.3 mg/ml. Experimentally, the purified native S-layer solution was monomerized with 5M GuHCl followed by a dialysis step. The dialysis was performed separately against 10 mM CaCl<sub>2</sub> and 10 mM Tris/HCl pH 8 overnight at 4 °C. Protein samples were adsorbed after 3 days and 1 week following dialysis onto a cleaned Si wafer for 10 minutes, than washed with distilled water, dried with N<sub>2</sub> and imaged with SEM. Figure 2-5 shows the self-assembly products obtained:

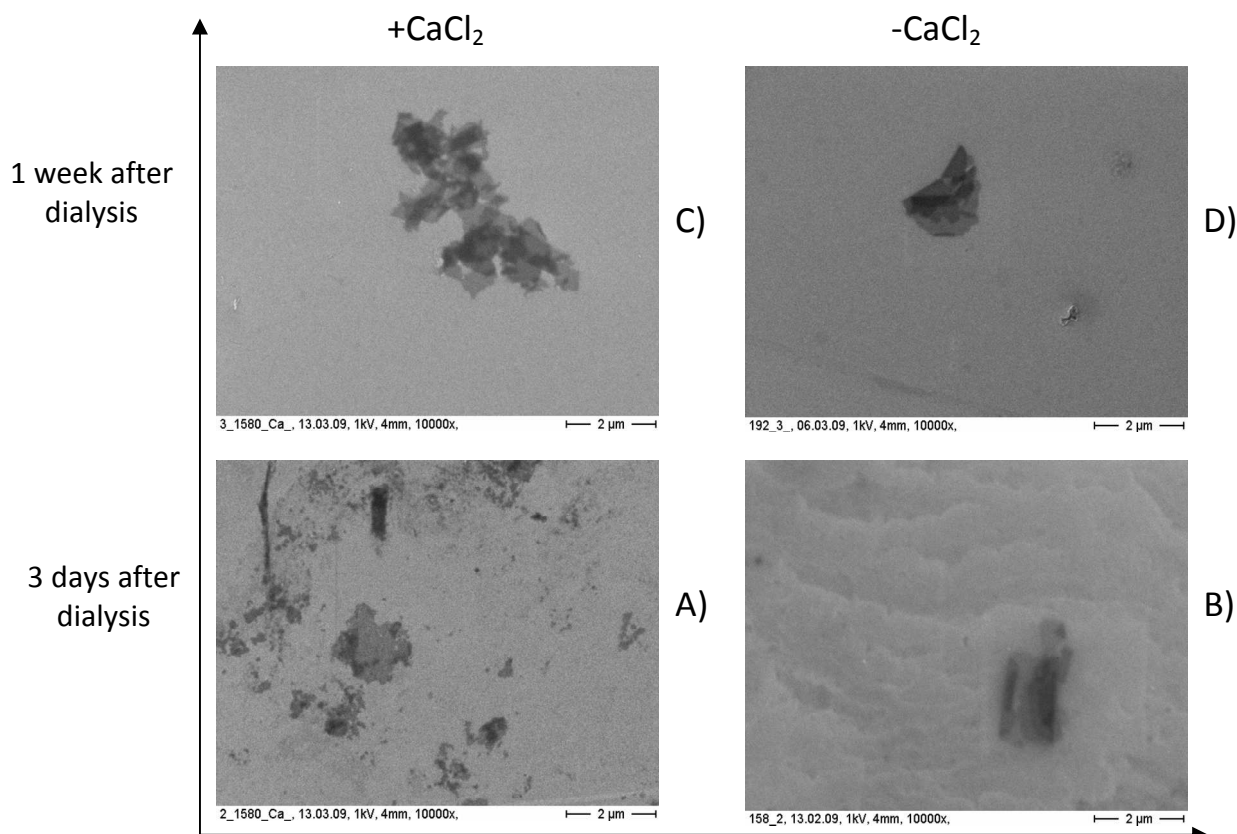


**Figure 2-5 Influence of  $\text{Ca}^{2+}$  ions on the self-assembly of the S-layer of *S. urea* ATCC 13881**

The *in vitro* recrystallization reaction was carried out by first monomerizing the protein with 5 M GuHCl, than dialysed against A) 10 mM  $\text{CaCl}_2$  and B) 10 mM Tris/HCl pH 8, respectively. Self-assembly products were adsorbed onto a Si substrate after 3 days following dialysis. C) After 1 week following dialysis many S-layer patches/ layers have formed in the presence of  $\text{Ca}^{2+}$  ions while D) only a larger layer can be observed in the absence of  $\text{Ca}^{2+}$  ions (dialysed against Tris/HCl pH 8) after 1 week following dialysis.

More S-layer patches can be observed when self-assembly occurs in the presence of  $\text{Ca}^{2+}$  ions (Figure 2-5 A) having a well defined, square like shape. Some are seen folded. In case where the self-assembly happened in the absence of  $\text{Ca}^{2+}$  ions *i.e.* in Tris/HCl buffer, there are only a few sheets formed (Figure 2-5 B). These protein layers are larger in size and similarly, folded. In time, this difference is even more obvious. While in the presence of  $\text{Ca}^{2+}$  ions numerous other SsIA patches can be observed (Figure 2-5 C), in the absence of  $\text{Ca}^{2+}$  ions just an extended sheet like structure formed (Figure 2-5 D). It follows that for the same recrystallization time and protein concentration, there is a faster patch formation observed in the presence of  $\text{Ca}^{2+}$  ions. Monomer binding to the patches is enhanced and the growth of stable patches accelerated. It appears that  $\text{Ca}^{2+}$  influences the rate constant of the self-assembly reaction (nucleation and growth

rate), fact which can be explained by the electrical double layer theory. The isoelectric point of SslA is 5.21. At pH 8 it is therefore negatively charged. In the absence of salt, the electric double layer of the SslA molecule is thick and its influence is strong. The mobility of the protein molecule is low because as it moves it drags the double layer surrounding it. In the presence of salt, the surface charges of the protein molecule are screened by counterions in the solution, which decreases the thickness of the double layer around the protein [138, 139]. Therefore the effective size of the protein molecule also decreases which results in the increase of molecular mobility. The presence of salt increases the volume transport rate of protein molecules in the bulk to the incorporation surface. However, the surface integration, penetration and rearrangement is influenced by the intrinsic properties of the protein molecules, such as their conformations. The presence of the salt however does not change the conformation and rigidity of the protein molecules.

In conclusion,  $\text{Ca}^{2+}$  ions have an electrostatic steering effect and are increasing the association constant of the SslA monomers, therefore the number of S-layer patches assembled in solution is significantly higher, phenomena that could be of interest for applications where a large number of protein layers are required. However other experimental parameters should be also taken into consideration. For instance, Satiropoulou *et. al.* [140] have monitored the ionic interaction of the S-layer of *D. radiodurans* with cations and anions using electrochemical impedance spectroscopy. They found that a strong interaction between calcium ions and the S-layer occurs due to the penetration of this ions into the Helmholtz plane of the double layer (adsorption site for ions on the S-layer) and that  $\text{Ca}^{2+}$  ions are transported through the vertex regions of the S-layer lattice, molecular process guided mainly by electrical gradients presumed to originate from negative charges on the surface of the protein.

The role of calcium ions in case of SslA can be presumed to be either: mediate the interaction between the protein monomers or bind to a specific site on the protein monomer thereby modifying its structure and exposing sites relevant for the self-assembly process or the ions just simply screen the negative charges on the surface of protein monomers facilitating the self-assembly reaction.

## *pH of recrystallization buffer*

Next, the self-assembly properties of SslA with respect to the recrystallization buffer pH were explored. *In vitro* recrystallization experiments were carried out at a protein concentration of 0.38 mg/ml by treatments with buffer solutions having different pH values.

To this end, the purified S-layer solution was first monomerized with 5M GuHCl than dialysed overnight at 4 °C against 10 mM Tris/HCl buffer having pH 3, 5 and 9 respectively. Samples from the dialysate were adsorbed onto cleaned Si substrates for 10 minutes and subsequently rinsed by repeated immersion in distilled water and dried under N<sub>2</sub> stream. AFM was used to investigate the S-layer structures obtained. These are shown in Figure 2-6:

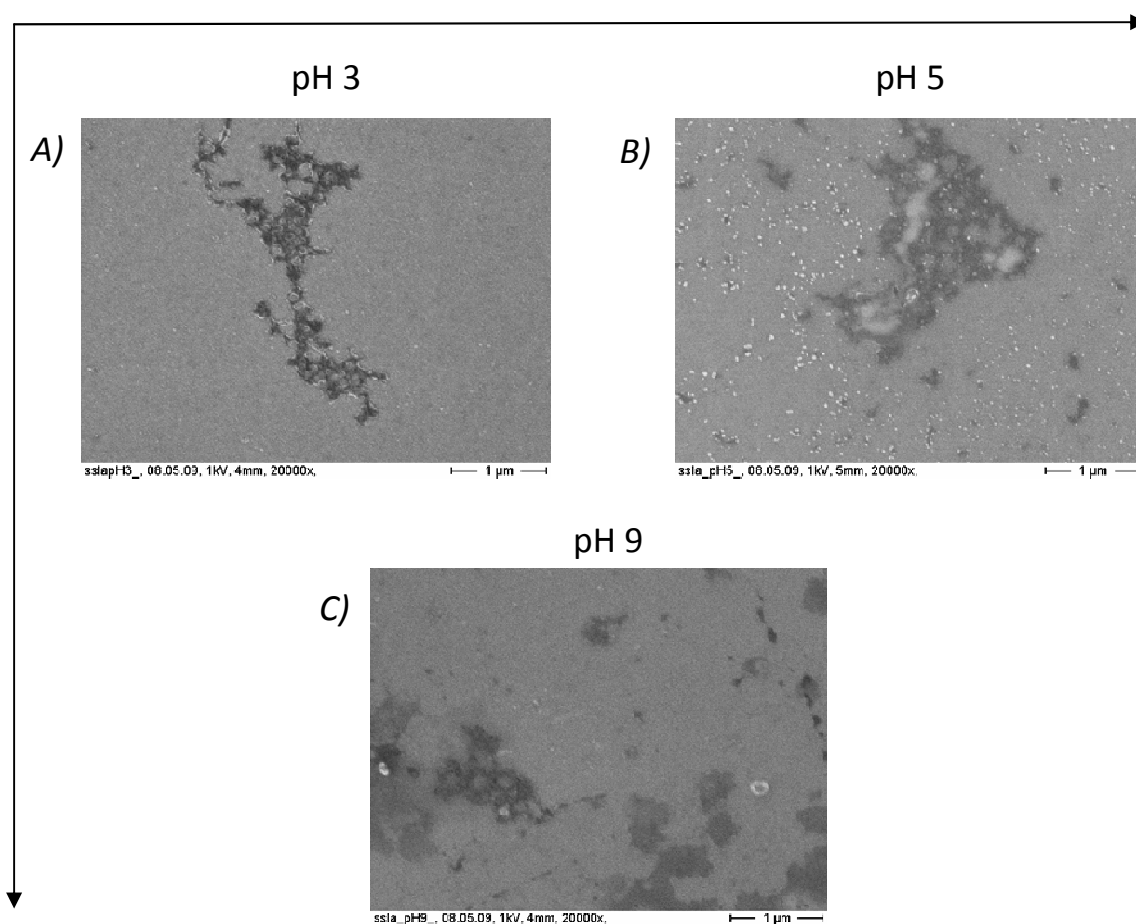


**Figure 2-6 Influence of buffer pH on the self-assembly of the S-layer of *S. ureae* ATCC 13881**

For *in vitro* recrystallization, the protein was at first monomerized with GuHCl, than dialysed against buffer having A) pH 3, B) pH 5 and C) pH 9.

The self-assembly reaction was performed here in solution and the images in Figure 2-6 show S-layer structures that do not have the typical layer or patch conformation when recrystallized at pH 3 (Figure 2-6 A) and pH 5 (Figure 2-6 B). The low pH caused the denaturation of the protein.

Low pH induces the protonation of carboxylic and amine groups in the hydrophilic shell and causes therefore a new distribution of charges that induces conformational changes.

However, at pH 9 small patches can be observed (Figure 2-6 C) meaning that in this case monomers could bind to each other, form critical sized nuclei which after a certain size, could stably grow into patches or small layers.

When performed, intact layers of this S-layer protein are kept overnight in a low pH buffer *e.g.* pH 3, the normal S-layer lattice structure and shape is preserved (Anja Blüher personal communication). Similarly, the S-layer sheets did not suffer structural modifications when treated with higher pH buffers as well (pH 5, 9 and 11). It seems that under the applied acidic conditions the H bonds that connect the protein monomers in the S-layer lattice were not disrupted and that it does not influence the stability of the protein structure.

However, a buffer of pH 3 has denatured the S-layer protein of *Bacillus sphaericus* CCM2177 (SbpA) too [141]. In this case, at first a silicon substrate was immersed into the monomer solution. Recrystallization was let to proceed overnight and as a result, protein layers have formed on the silicon substrate. Next, the substrates containing the protein layers were introduced into a buffer of pH 3 and the effects were imaged with AFM. An irreversible denaturation and loss of conformation was detected. Interestingly, recrystallization on the secondary cell wall polymer (SCWP), a natural environment for the protein layer and chemical crosslinking with glutaraldehyde made the same S-layer more resistant towards pH exposure and structural deformations.

Motivated by these observations, recrystallization experiments of the S-layer of *S. ureae* ATCC 13881 were performed at low pH in the presence of a Si substrate as well. A solution of monomers was obtained by monomerization with 5M GuHCl which was then dialysed overnight at 4 °C against 10 mM Tris/HCl pH 3 in the presence of an

APTES functionalized silicon substrate. After dialysis, the silicon substrate was rinsed with distilled water, dried in a stream of N<sub>2</sub> and analysed with AFM. Figure 2-7 depicts the resulted self-assembly structures:

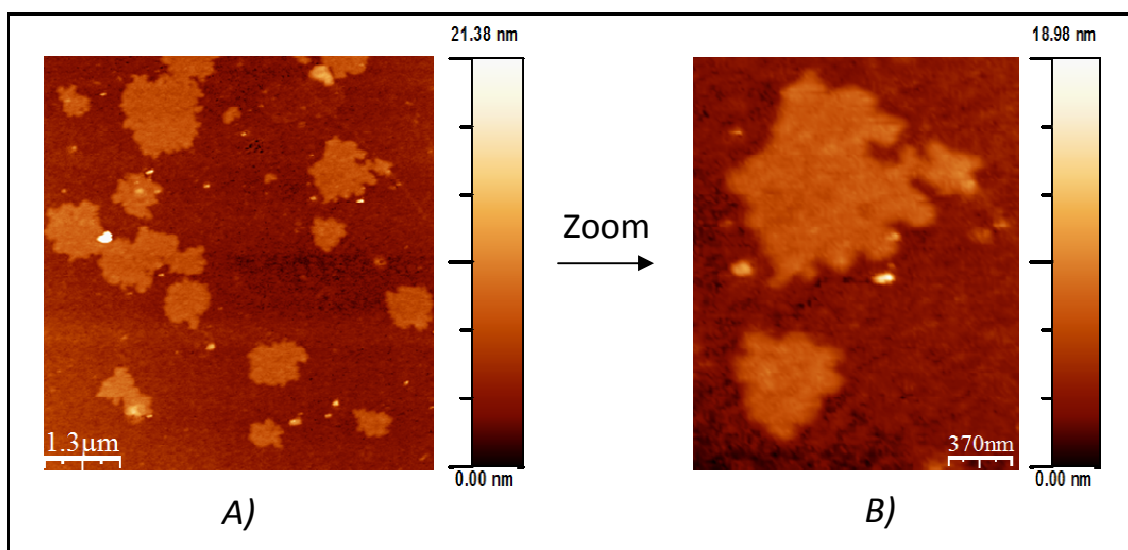


**Figure 2-7 Influence of the Si substrate on the self-assembly performed at low pH**

The native S-layer of *S. ureae* ATCC 13881 was monomerized with GuHCl and dialysed against 10 mM Tris/HCl buffer pH 3 in the presence of an APTES functionalized Si surface.

Many S-layer patches have formed when recrystallization was done in the presence of a substrate even though at pH 3. These patches displayed in Figure 2-7 have planar, circle like shapes with rough edges and sizes between 700 nm and 1.3 μm.

It seems that the substrate facilitates the self-assembly of the monomers. In this regard, functionalization with APTES may play a role. APTES reacts with silicon surfaces in a way that the silane part anchors to the silicon surface and the NH<sub>2</sub> group remains exposed. In aqueous solution and under acidic conditions (in this case pH 3) the NH<sub>2</sub> group gets protonated and the surface becomes positive charged. The acidic condition will further cause the protein molecules to carry a net positive charge (pI of the protein is 5.2) while buffer molecules are similarly positively charged. Thus a strong repulsion from the substrate and buffer molecules will facilitate formation of small patches in solution (homogeneous nucleation) that will fall onto the substrate when the *in vitro* recrystallization is stopped, *i.e.* when the silicon substrates is taken out for analysis and imaging.

In conclusion, when *in vitro* recrystallization is performed in solution at pH 3 in the absence of a silicon substrate, self-assembly does not occur and the protein molecules aggregate. In the presence of the APTES silicon surface, monomers are able to self-assemble into small patches with distinct shapes.

### *Si substrate*

Many applications like using S-layers as protein templates or as patterning elements require a stable and large coverage of wafer surfaces. Direct recrystallization on such wafers over adsorption of preformed S-layer sheets should constitute a better approach, however it is important to know and establish experimental conditions under which this can be achieved. Therefore further on, the *in vitro* recrystallization behaviour of the authentic S-layer of *S. ureae* ATCC 13881 on a functionalized Si wafer is studied, aiming at exploring the effect of this hydrophilic and positively charged silicon surface as a last factor influencing the self-assembly process.

In this case the *in vitro* self-assembly of the S-layer of *Sporosarcina ureae* ATCC 13881 (SslA) was done according to a protocol by Sleytr *et. al.* 2008 [142]. The experimental steps included monomerization of the purified protein with 2M GuHCl and dialysis against double distilled water for 3 hours followed by the centrifugation of the dialysate at 14 000 g for 5 minutes. The supernatant was diluted with 0.1 mM CaCl<sub>2</sub> and 0.5 mM Tris/HCl pH 9 to a protein concentration of 0.1 mg/ml. Cleaned and APTES functionalized Si pieces were incubated with the diluted protein solution and recrystallization was allowed to proceed for 4 hours at room temperature. AFM has been involved in analysing the shape and structure of the obtained S-layers and the result is displayed in Figure 2-8:

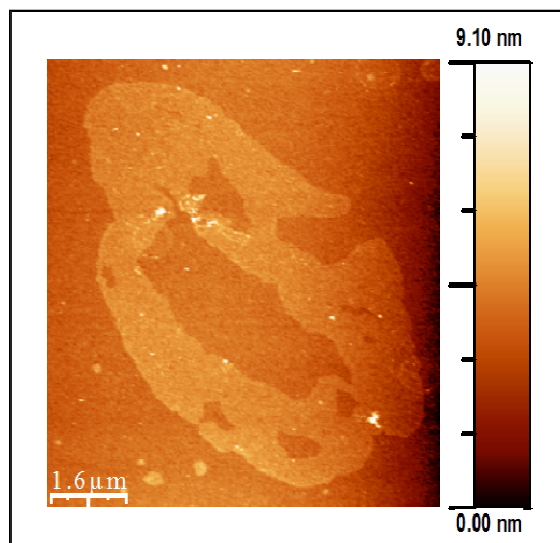


**Figure 2-8 Influence of Si substrate on the self-assembly of SslA**

The S-layer was *in vitro* recrystallized in the presence of an APTES functionalized Si surface.

As Figure 2-8 shows, the S-layer recrystallized onto the Si substrate into a large monolayer having a size of more than 5 μm in length though the layer is not continuous, regular or coherent. Height is about 2.5-3 nm (data not shown) and most probably a flattening and a loss of the hydration shell happens after drying with N<sub>2</sub> and before imaging.

The protein concentration in this case was 1 mg/ml and the self-assembly is initiated in the presence of Ca<sup>2+</sup> ions and Tris/HCl buffer having pH 9. At this pH, the protein carries an overall net negative charge and repulsion from the substrate and buffer molecules in this case is diminished, therefore monomers can nucleate on the silicon substrate (heterogeneous nucleation) and grow into large crystalline layers. With further optimization of the recrystallization reaction, a total coverage of the Si surface can be foreseen.

Tube formation in this case is greatly impeded mainly due to the good binding of the S-layer to the silicon substrate. Surface tension is not enough for allowing adoption of a certain curvature and tube formation would only be possible after the delamination of the S-layer from the silicon substrate. Tubes will therefore only form in solution, by homogeneous nucleation which is advantageous for some of the applications involving S-layer proteins.



The fact that a large monolayer is formed is of great importance since it offers the possibility of being used as a molecular template or biotemplate for various bio- or nanotechnological applications.

And finally, this also proves that SslA monomers are able to self-assemble not only on the natural support *i.e.* cell wall polymer, but also on inorganic, synthetic surfaces such as Si wafer.

In summary, it was demonstrated and explained how environmental parameters such as initial monomer concentration, Ca<sup>2+</sup> ions, pH of recrystallization buffer or the Si substrate affect the self-assembly of the S-layer of *S. ureae* ATCC 13881. The information obtained contributes and eases the way for obtaining the desired S-layer structures for a certain application.

### 2.2.3 KINETIC STUDIES ON THE SELF-ASSEMBLY PROCESS

In order to better understand how SslA monomers alone drive the self-assembly reaction, the *in vitro* self-assembly kinetics of SslA in real time was followed by dynamic light scattering (DLS). This method is able to monitor the development of microstructures in colloidal suspensions. It was shown that light scattering can quickly detect abrupt and polydisperse amorphous aggregation of a protein under certain conditions [143].

In particular, the influence of protein concentration on self-assembly was investigated in the presence of 30 mM CaCl<sub>2</sub>. Samples for the SslA self-assembly reactions were prepared by first monomerizing a desired amount of protein stock solution with 1 ml 5M GuHCl (395 µg and 1 mg respectively) than dialysing it against pure water for two hours. After dialysis, the protein solution was centrifuged and the supernatant (containing the SslA monomers) was mixed with CaCl<sub>2</sub> for the assembly reaction initiation. The mixture had a final volume of 1 ml and was subjected to DLS measurements immediately after mixing.

DLS measurements were performed at two different protein concentrations: 0.38 and 1 mg/ml (number of measurements: 60, number of runs: 10, run duration: 18

sec). The results are shown in Figure 2-9 where each data point corresponds to the Z-average diameter obtained from the DLS measurement and is plotted as a function of time. The Z-average diameter is defined as the intensity weighted mean average for the ensemble collection of particles in the sample derived from the slope of the linearized form of the correlation function. As the light scattering signal intensity is proportional to the square of the molecular weight, it is very sensitive to subtle changes in the oligomeric state of the protein.

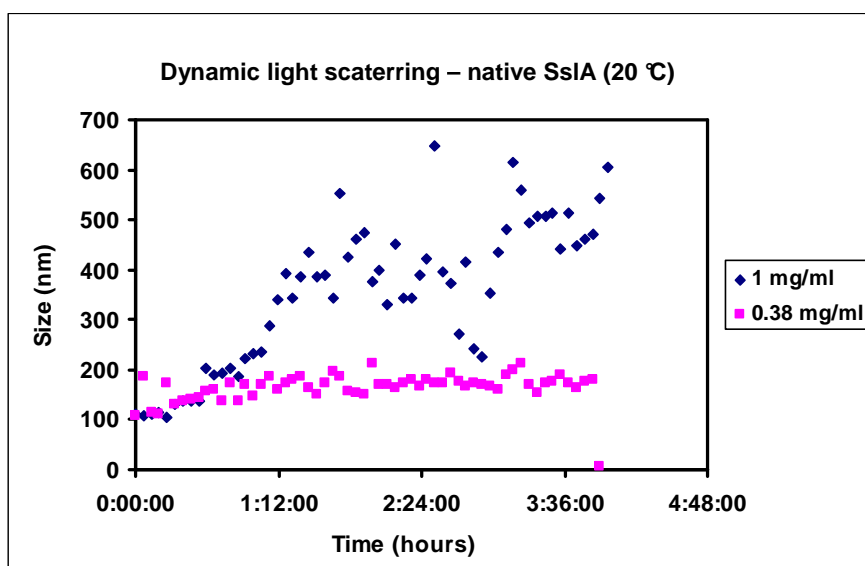


**Figure 2-9 Influence of protein concentration on the kinetics of SsIA self-assembly**

Kinetics was monitored by DLS under low and high protein concentration (0.38 mg/ml and 1 mg/ml respectively) at a constant calcium concentration of 30 mM and a temperature of 20 °C.

Although monomers should constitute the majority of the molecules in solution after dialysis, the initial Z average diameter of ~100 nm observed from the plot reflects the presence of oligomeric or even higher order structures of SsIA in solution.

The first part of the plots - low and high protein concentration - shows a similar pattern, a slight growth until a certain time point. The growth corresponds to the self-assembly process resulting in structures which are larger in size *e.g.* patches and protein layers. However for low protein concentration this size is only approximately 150-200 nm and afterwards growth ceases, phenomenon that can be attributed to the depletion of the monomers. A few S-layer structures that have already assembled and

cannot grow anymore due to the low concentration of monomers present in the solution, which are rapidly consumed stopping the assembly reaction. These are stable structures.

In case of a higher protein concentration, the assembly and accumulation of larger structures *e.g.* 350-400 nm in size was observed. These constitute a population of larger patches or layers that have coagulated and are now present in the solution. Due to a higher density of protein structures it is possible to form larger assemblies. During coagulation, the protein lattices upon collision or agglomeration might also often break resulting in smaller structures as shown by the fluctuations at larger times along the curve proving the existence of additional mechanisms at this stage.

Interestingly, the size difference between the structures assembled at low and high protein concentration is approximately the double value. In fact, this can be related to the concentration. The amount of protein molecules brought into the self-assembly reaction differs by the order of two and one can even say that the layers or larger patches formed at high protein concentration correspond actually to the agglomeration of 2 patches resulting in patch dimers.

In order to obtain information about the thermodynamics of S-layer crystallization, the effect of temperature was also analyzed. Figure 2-10 shows the dependence of SslA self-assembly reaction on temperature. The protein samples were similarly prepared like in the previous case and dynamic light scattering measurements performed at 20 °C and 25 °C, respectively.

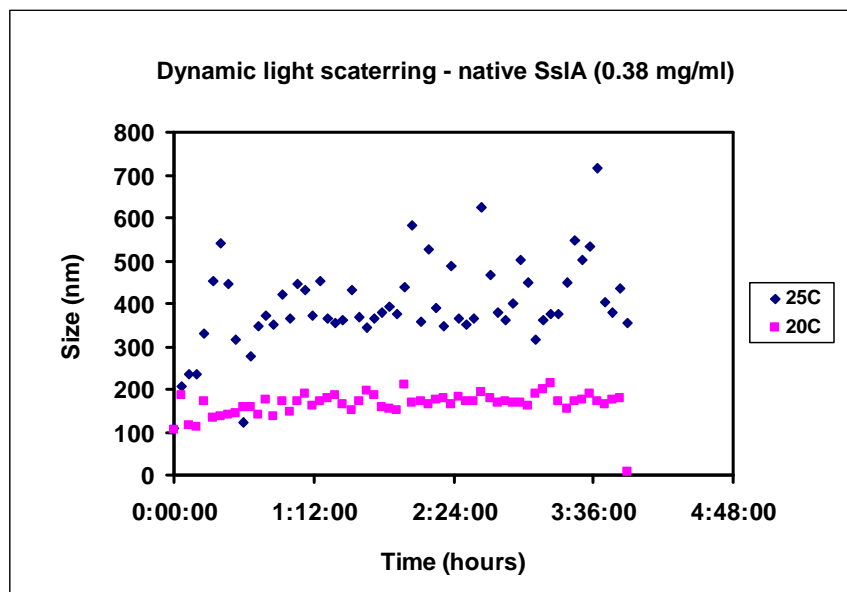


**Figure 2-10 Influence of temperature on the kinetics of SslA self-assembly**

Kinetics was monitored by DLS under two different temperatures 20 °C and 25 °C at a constant protein concentration of 0.38 mg/ml and a calcium concentration of 30 mM.

Figure 2-10 shows that by increasing the temperature, there is a fast assembly of protein lattices resulting in larger patches or layers with a size distribution from 350 to 400 nm. While at 20 °C there are protein structures that have assembled to a size of 150-200 nm and remain stable over the time, at 25 °C for the same protein concentration growth units agglomerate into higher order structures. The difference can be attributed to the increased molecular mobility of the protein structures that are able to coagulate in solution into larger entities and the behaviour looks similar to the case of high protein concentration. Fluctuations along the curve show that these large layers are highly dynamic; they fuse and broke apart. The coagulation is also supported by the fact that sizes differ by an order of 2 when measured at 20 °C and 25 °C. While at 20 °C the structures are in the size range of 150-200 nm an increase in temperature to 25 °C cause the appearance of patch assemblies that have size of 400 or even 600 nm. These sizes can be attributed to the patch dimers, trimers that organize in various shapes.

In conclusion the dynamic light scattering measurements have shown that the assembly of the S-layer protein structures is concentration and temperature dependent. At higher protein concentrations and temperature coagulation of the

## THE NATIVE S-LAYER OF *S. UREA* ATCC 13881

---

protein lattices occurs with a size of about 400 nm. In this case, the information obtained relates to the assembly of already formed protein entities which have a size of about 100 nm. Most probably the assembly reaction started earlier than the DLS measurement *e.g.* during the dialysis process and was not induced by the addition of CaCl<sub>2</sub>. Therefore the effect of CaCl<sub>2</sub> cannot be estimated.

Finally, DLS does not provide information on growing patch number during the self-assembly reaction, only about the time dependence of the patch size.

### 2.3 FUNCTIONALIZATION OF THE SSLA PROTEIN TEMPLATE WITH GOLD NANOPARTICLES

Previous studies on S-layers have shown that the periodic structure can be exploited as a template for the in situ nucleation of inorganic particles formed from vapour deposition [144, 145] electron-beam irradiation of metal salts [146] or wet chemical deposition [147]. Although these methods result in semiregular, crystalline arrays of nanoparticles with spacings in register with the underlying S-layer lattice, they are not readily adapted to controlling the particle size and hence the contact distances between the particle surfaces, both of which are important in quantum phenomena.

Furthermore, A. Blüher 2008 [189] has shown that depositing presynthesized colloidal Au nanoparticles of 5 nm in diameter have patterned the S-layer protein sheets, however some parts of the S-layer *i.e.* a folded part, was found to be more densely decorated than the neighbouring, *i.e.* unfolded region. This ununiform distribution of particles may depend on the different S-layer surface exposed which on the same time may be determined by the underlying substrate *i.e.* silicon wafer properties. Up to now, patterning experiments with preformed Au nanoparticles were not performed for the S-layer of *S. ureae* ATCC 13881. Therefore, the aim of this section is to investigate up to which extent this S-layer facilitates the ordered spatial arrangement of Au nanoparticles under different adsorption conditions onto treated silicon substrates.

To this end, the S-layer protein was adsorbed onto pure as well as onto functionalized silicon substrates, then the gold nanoparticles were deposited onto the protein lattice. Prefabricated, negatively charged gold nanoparticles (purchased from Invitrogen) with a diameter of 5 nm were chosen for the experiments.

At first a reference sample was prepared by adsorbing 10  $\mu$ l from the Au colloid solution onto a cleaned Si for 10 minutes, than fluid was dragged with filter paper. Figure 2-11 A shows randomly distributed Au cluster agglomerates on the silicon

surface.

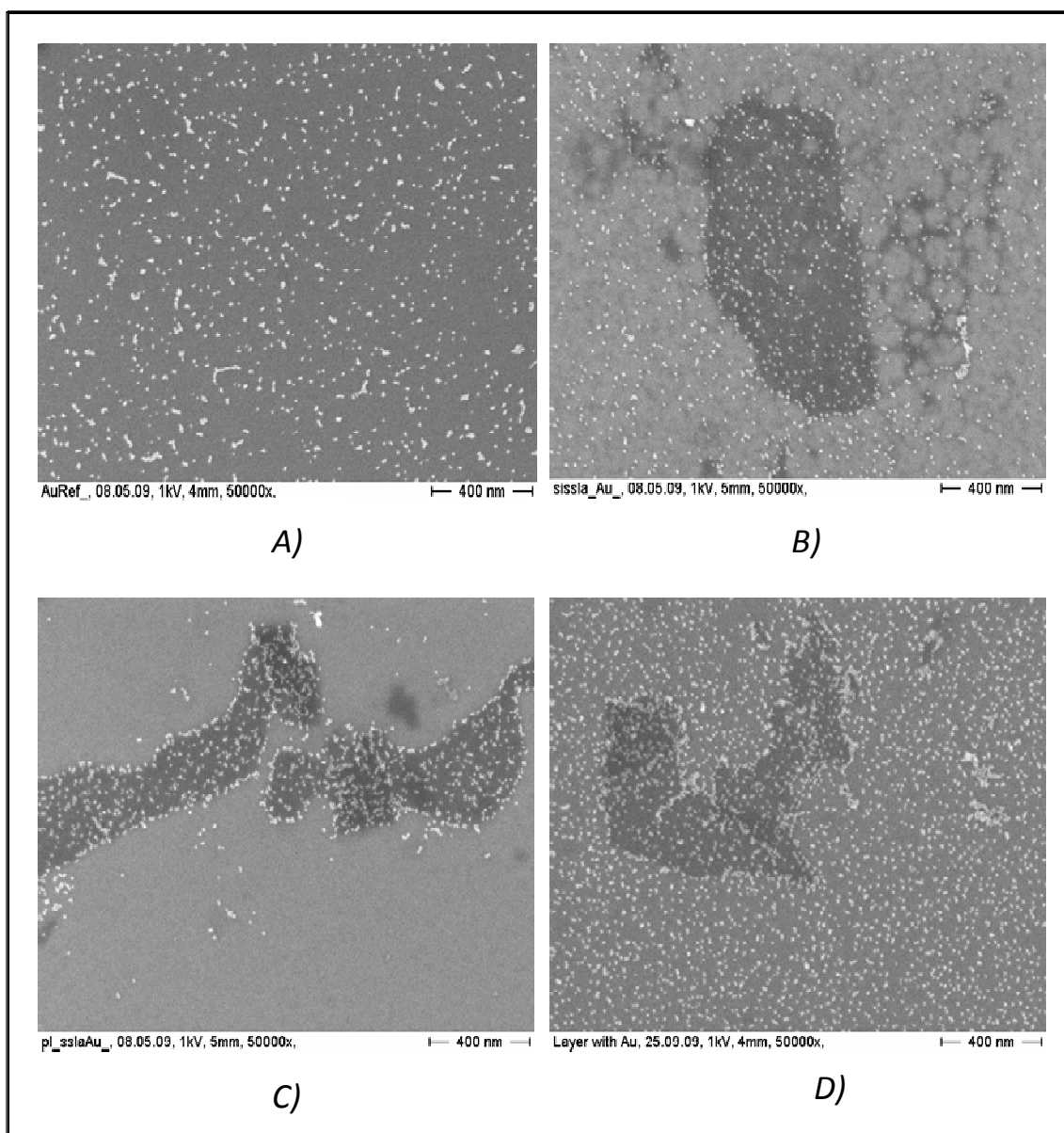


**Figure 2-11 Functionalization of the S-layer of *S. ureae* ATCC 13881 with Au nanoparticles**

White dots represent gold colloids which were A) adsorbed onto the native oxide Si substrate (reference sample) or bound onto the S-layer protein template which was first adsorbed onto B) native oxide Si surface C) plasma treated Si surface and D) APTES treated Si surface.

Next, the Au nanoparticles were deposited onto the two-dimensional crystalline surface layer protein of the bacterium *Sporosarcina ureae* ATCC 13881.

Before the deposition of gold particles, the S-layer was immobilized onto the Si surface. Due to the different physicochemical properties of the S-layer surface, one

side being hydrophilic while the other hydrophobic [106], it was adsorbed onto different Si substrates: native oxide Si surface, plasma treated Si and APTES functionalized Si for one hour. After adsorption, the S-layer was exposed to 10  $\mu$ l of aqueous Au colloid solution for 10 minutes. Finally, samples were blot-dried using filter paper and imaged by scanning electron microscopy. Figure 2-11 B, C and D shows the coverage of the protein templates with the Au nanoparticles.

The distinct adsorption patterns of the S-layer protein onto the silicon surface will strongly influence the deposition of the gold clusters.

In order to understand the deposition pattern of Au nanoparticles onto the S-layer lattice, at first the adsorption behaviour of the S-layer protein fragments on various types of substrates has to be considered.

Electrostatic interaction is important when surfaces are charged in aqueous solutions, because proteins molecules are also charged depending on the particular solution pH conditions. Under neutral pH conditions, the Si surface has a net negative surface charge arising from the dissociation of silanol groups [148]. As the citrate-stabilized gold nanoparticles used in this work are negatively charged in aqueous solution (at pH 7), electrostatic interactions are expected to dominate the behaviour of the colloidal system. In this way the S-layer screens the negative charges of the Si surface and offers local positive charges for gold cluster adsorption, fact that can be observed in Figure 2-11 B. It has to be kept in mind that each side of the S-layer surface has a heterogeneous distribution of positive and negative charges, and a net charge which could be positive or negative depending on the pH.

When the Si surface is plasma treated, the density of the negative charges on the Si surface is expected to be higher. Visual inspection of the Figure 2-11 C reveals that similarly, the S-layer sheet has adsorbed onto the Si surface and is densely decorated with gold nanoparticles. The nanoparticles clearly display a dramatically decreased level of nonspecific binding. Due to their net negative charge they are strongly repelled from the Si surface.

Under neutral pH conditions, silicon substrates modified with an APTES layer are positively charged, typically displaying a high density of protonated amino groups



to the adjoining aqueous phase [149]. The interaction between a protein and an oppositely charged surface is intuitively expected to be attractive. In this case, it is likely that the S-layer adsorption results from long-range electrostatic interactions occurring between the positively charged amino groups of the silane and acidic, negatively charged sites on the protein. In this case too, the S-layer template offers binding sites for the gold nanoparticles and Figure 2-11 D shows that these are abundantly present on the protein layer.

The observation that a significant amount of nonspecific binding is associated with the APTES Si surface is consistent with the general supposition that the gold nanoparticles experience long range electrostatic attractions with positively ionized APTES molecules ( $-\text{NH}_3^+$ ) covering the surface of the silicon substrate.

Based on the above mentioned observations, the best Si surface onto which the best S-layer adsorption and gold nanoparticles coverage can be achieved, is the plasma treated Si.

As reported in literature [106], the unit cell of the *S. urea* S-layer consists of 4 monomers with a complex molecular structure. Therefore the question of where exactly the gold clusters bind arises. Engelhardt *et. al.* [150] defined three sites on this p4 S-layer lattice, namely the minor fourfold symmetry axis (*A*), the twofold symmetry axis (*B*), and the major fourfold symmetry axis (*C*). Wahl *et. al.* [151] have shown that Pd metal particles synthesized by chemical reduction of metal salt complexes in the presence of the protein template were bound mainly to the (*A*) site and fewer particles to (*B*) and (*C*) sites respectively. Interestingly, qualitatively the same result was reported by Queitsch *et. al.* [152] who have analyzed the occupation of specific affinity sites of the S layer of *B. sphaericus* NCTC 9602 with FePt clusters deposited from the gas phase.

From the images displayed in Figure 2-11 the exact position of the particles cannot be precisely estimated. However, on a zoomed image shown in Figure 2-12, a regular distribution of the gold nanoparticles can be observed.

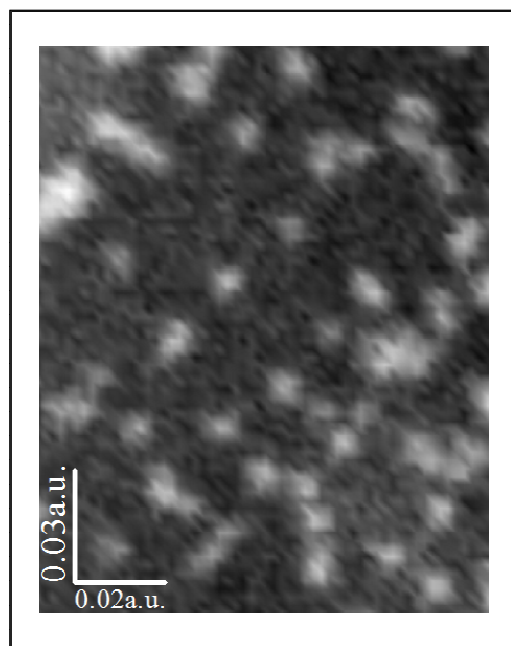


**Figure 2-12 Arrangement of Au nanoparticles on the SslA template**

The control over the interparticle spacing can be achieved through judicious choice of the type and dimensions of the metallic nanoparticles.

Other metal particles such as Pt, Pd, Ag or even Au have been deposited onto this S-layer but they were produced by chemical synthesis by reducing a specific metal salt solution [99]. The method of depositing already synthesized nanoparticles is however more advantageous since it is faster and more straightforward.

In conclusion, it was shown that the S-layer of *S. ureae* ATCC 13881 has the potential to act as a biotemplate and initiate a regular arrangement of gold nanoparticles.

It is very effective as a seamless template and the nanoparticle array on the S-layer surface offers significant advantages for several nanotechnological applications *e. g.* as a bottom-up biological-based route to nanostructure fabrication in the field of molecular electronics and optics or catalysis and sensing applications. In how far this patterning principle may be employed for all these applications, is yet to be explored.

### 2.4 CONCLUSIONS AND OUTLOOK

The aim of this chapter was to characterize the authentic S-layer of *Sporosarcina ureae* ATCC 13881 (SslA) with respect to its morphology, self-assembling properties and functionalization. To this end, SslA was stripped off from the bacterial cell surface and purified. AFM analysis revealed entangled S-layer patches of different sizes and shapes, exhibiting square lattice type (p4 symmetry) with a lattice constant of 12.9 nm. Upon disintegration of these patches by a chemical treatment, the SslA subunits were able to self-assemble and reform the lattices; however this process yields protein monolayers, multilayers or tubes. It turned out that the emergence of all these various structural shapes is greatly influenced by several experimental factors involved in the *in vitro* recrystallization reaction. Factors such as initial monomer concentration, Ca<sup>2+</sup> ions, pH of recrystallization buffer or the Si substrate onto which the *in vitro* recrystallization of the S-layer is initiated were studied in detail. It became clear that at high initial monomer concentration many small patches form, while a low initial monomer concentration favours the growth of fewer and therefore larger patches. In time, these patches further expanded according to the governing laws of the self-assembly process. When compared to the structures obtained by the same protein when stripped off from the bacterial cell surface, the multilayered SslA structures formed at this stage prove to be a unique ensemble of the *in vitro* self-assembly process; fact showing that upon appropriate experimental conditions, the self-assembly property of this S-layer protein can be exploited to create protein surfaces that can be employed as functional templates for building in 3D at the nanoscale.

When SslA mono- or multilayers have grown to a certain size, they folded into tubes. The advantage of a tubular S-layer structure may lie in its potential to serve as a hollow object that may possibly encapsulate and release certain molecules or inorganic crystals on purpose.

Experiments have further shown that Ca<sup>2+</sup> ions are accelerating the self-assembly reaction of the SslA monomers. However, at low pH and in the absence of a solid substrate (*e. g.* APTES functionalized silicon), the monomers are not able to build the S-

layer lattices, but alkali pH of the recrystallization buffer exerts exactly the opposite effect. Going from *in vitro* recrystallization in solution to self-assembly onto surfaces like for example silicon wafer, crystalline and coherent protein monolayer with repetitive morphological and physicochemical features was obtained. The surface charges of the substrate play a major role here. With further optimization of the process, whole wafer coatings can be envisioned which will ultimately have a great application potential in bionanotechnology or other related fields.

Fusion of SslA patches having sizes between 100 and 200 nm has been captured by dynamic light scattering measurements. The process proved to be concentration and temperature dependent. Layer growth with preformed stable patches dominates the self-assembly. It remains to be investigated in how far this method can be used to obtain more information about the kinetics of the self-assembly reaction, *e.g.* starting with the spontaneous association of the S-layer monomers.

Finally, it was possible to show that SslA can be used as a biotemplate for ordered assembly of gold nanoparticle arrays. Density of the particles on the S-layer template varied according to the surface of the protein exposed, which instead was affected by the choice of the underlying Si substrate (in case of functionalization, surface charges proved to be relevant). Further optimizations of the introduced biotemplate assisted self-assembly process may lead to various other nanoparticle superstructures depending on the particle size and surface interactions between the S-layer and gold. Ultimately, the resulted ordered array structure could display enhanced properties suitable for bottom-up fabrication of novel types of nanoelectric devices.

## CHAPTER 3

### 3 THE RECOMBINANT S-LAYER OF *S. UREA* ATCC 13881

Recombinant proteins are more adequate for technological reasons as they represent the homologous population of molecules with controlled sequence which can be simply modified by site directed mutagenesis. Furthermore, they can undergo cheap mass production and have a high level purity.

Modifications of S-layers by recombinant DNA technology can significantly influence the development of applied S-layer research and broaden the application potential for S-layers.

The *sslA* gene of *Sporosarcina ureae* ATCC 13881, which was already identified by Ryzkov *et. al.* 2007, encodes a surface layer protein of 1097 amino acids [109]. This is the prerequisite for recombinant expression of SslA and its modification for different nanotechnological applications.

The following part of the work is contributed to the characterization of the recombinant S-layer of *Sporosarcina ureae* ATCC 13881. After cloning and expression of the protein, the ability of this recombinant S-layer to self-assemble in solution and on silicon wafer is investigated. Further on, the focus is to reveal distinct segments of this protein that are self-sufficient and responsible for self-assembly of the S-layer subunits into protein lattices. To this end, truncation derivatives were created and their self-assembling behaviour as well as factors influencing this process are investigated in detail.

## 3.1 CHARACTERIZATION OF THE RECOMBINANT SSLA

The nucleotide sequence of the S-layer gene of *S. ureae* ATCC 13881 (*sslA*) encodes a protein of 1097 amino acids [109]. The first 31 amino acids of this protein were assigned to a secretion signal and the remaining sequence of 1066 amino acids constitutes the mature SslA protein. Further on, this will be quoted as SslA<sub>32-1097</sub>.

So far, the self-assembly structures formed under different *in vitro* recrystallization conditions have not been studied in detail. For this purpose, at first, the PCR product encoding SslA<sub>32-1097</sub> is cloned and expressed in *E. coli* Rosetta Blue cells. After isolation and purification, its ability to self-assemble in solution and on a silicon wafer is analysed. The information obtained can be used for further modifications of this recombinant protein for various bio- and nanotechnological applications.

### 3.1.1 CLONING

Difficulties in cloning the S-layer genes have been encountered by many researchers [153, 154, 155]. In a number of cases, conventional cloning techniques have failed to result positive clones bearing the full version of the S-layer genes or simply the S-layer genes could not be cloned at all.

Cloning SslA<sub>32-1097</sub> with commonly used DNA cloning procedures has also failed. It was impossible to obtain positive clones after restriction enzyme (RE) digestion and ligation of the insert DNA into the pET23b+ vector and transformation of the recombinant molecule into the cloning host, despite several trials. SslA<sub>32-1097</sub> could only be cloned by using the Ek/Lic cloning strategy and the pET46 Ek/Lic vector. With this method, positive clones were found right after the first trial.

The pET-46 Ek/LIC vector used in the cloning experiment is prepared for rapid, directional cloning of PCR-amplified DNA for high level expression of polypeptides. Furthermore it encodes for an N-terminal His<sub>6</sub> fusion tag sequence which is cleavable due to the presence of Lic site (enterokinase cleavage site).

## THE RECOMBINANT S-LAYER OF *S. UREA* ATCC 13881

---

The successful application of this cloning strategy has been shown for the S-layer gene of *slfB* of the uranium mining waste pile isolate *Bacillus sphaericus* JGA12 [84].

In order to obtain the SslA<sub>32-1097</sub> construct, at first genomic DNA from *Sporosarcina ureae* ATCC 13881 was isolated (see Appendix). A polymerase chain reaction (PCR) product derived from PCR amplification using primers Pforp46\_p4 and Prevp46\_p4 encoding the gene SslA<sub>32-1097</sub> was annealed with the pET46 Ek/lic (Novagen) vector. The recombinant vector pET46Ek/lic-SslA<sub>32-1097</sub> was transformed into *E. coli* Nova Blue Giga Singles competent cells. Positive clones were found via colony PCR and the correct insertion of the SslA<sub>32-1097</sub> gene was proved by sequencing.

The *ssla* gene consists of 3198 bps which translates to 1066 amino acids. After cloning, the protein sequence will additionally contain an N-terminally encoded His<sub>6</sub> tag (six tandem histidine residues) and the Lic arm introduced by the PCR primers.

Using specifically designed primers which include the Lic arms, SslA<sub>32-1097</sub> could be efficiently amplified and cloned without the need for restriction digestion or ligation.

### 3.1.2 HETEROLOGOUS EXPRESSION IN *E. COLI*, ISOLATION AND PURIFICATION

*E. coli* is the bacterial system that is most widely and routinely used for the expression of heterologous gene products of prokaryotic origin. Since this S-layer originates from a prokaryotic organism and because it does not require any glycosilation or other posttranslational modifications [110], *E. coli* was chosen as a suitable host for expression. Subsequently, this S-layer protein was purified from *E. coli* cells by metal chelating affinity chromatography. The results are outlined below.

For the heterologous expression of SslA<sub>32-1097</sub> the recombinant plasmid pET46Ek/lic-SslA<sub>32-1097</sub> was established in the expression strain *E. coli* Rosetta Blue (DE3). Expression was monitored by taking culture samples for SDS-PAGE analysis before and after 1, 3 and 5 hours following induction with 1 mM IPTG (final concentration). These samples have been further treated as described by Laemli (1970) and separated on a 12% SDS-PAA gel followed by staining with Coomassie Brilliant Blue protein stain. Results of expression are shown in Figure 3-1:

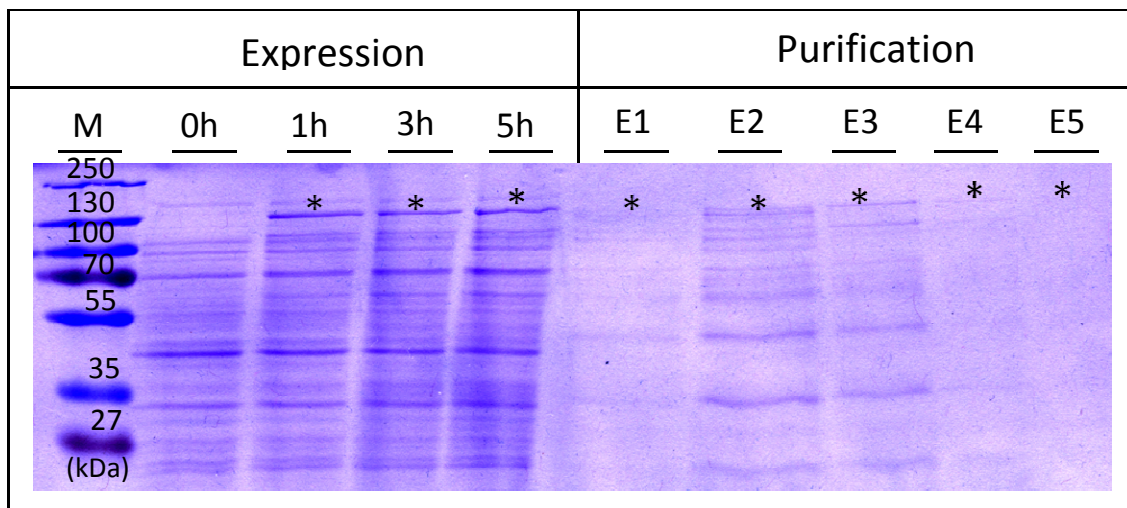


**Figure 3-1 Heterologous expression of SsIA<sub>32-1097</sub> in *E. coli* and purification**

The Coomassie stained protein gel shows expression in Rosetta Blue (DE3) whole cell lysates after 0, 1, 3, and 5 hours of induction with 1 mM IPTG (20 µg protein loaded per lane). E1-E5 mark the elution fractions of the Ni<sup>2+</sup> affinity chromatography. M-protein ladder (Page Ruler™ Plus Prestained). Recombinant protein position is marked with star.

In comparison to *E. coli* cells harvested before induction with IPTG (Figure 3-1 0h), an additional protein band with an apparent molecular mass of 130 kDa can be observed on the SDS-PAGE gel that corresponds to the SsIA<sub>32-1097</sub> protein (Figure 3-1 1h, 3h and 5h). Already 1 hour after induction the protein is present in the cells. However the level of expression is low and does not increase with the induction time. Similar observation was reported by Ryzkov [110] for this S-layer protein when expressed in *E. coli* B21 (DE3) strain. The reasons might imply: toxicity of the S-layer with regard to *E. coli* cells (hindrance of cell proliferation) or rare codon usage. Furthermore, a delay in growth measured by OD<sub>600</sub> was observed when compared to uninduced *E. coli* Rosetta Blue (DE3) cells (data not shown). Despite the fact that this strain supplies tRNAs for codons rarely used in *E. coli* cells, the expression level remains rather low hinting to other mechanisms impeding production of SsIA<sub>32-1097</sub> in *E. coli*.

SsIA<sub>32-1097</sub> could be isolated from the soluble fraction of *E. coli* cell lysate (data not shown). Very frequently, proteins are produced in *E. coli* cells in insoluble form, as a consequence of protein misfolding, aggregation and sequestration into “inclusion bodies”. It can require a considerable amount of effort to resolubilize and refold the protein in a proper way. This phenomenon was also reported for S-layers. In the case



## THE RECOMBINANT S-LAYER OF *S. UREAE* ATCC 13881

---

of *Caulobacter crescentus*, inclusion body formation was observed after the expression of a recombinant S layer, which did not form any regular structure [156]. However in case of SslA<sub>32-1097</sub> 50 % of the proteins could be extracted in soluble form without the need of solubilising and refolding it.

After isolation, the soluble fraction containing the S-layer was subjected to Ni affinity chromatography. Due to the His<sub>6</sub> tag, SslA<sub>32-1097</sub> could be purified via this method under native conditions. Fractions containing the purified protein were pooled, dialysed against distilled water for 12 hours at 4 °C. The successful purification was assessed by SDS-PAGE and the S-layer protein was found to be present in all elution fractions (Figure 3-1 E1-E5). These results indicate that the His<sub>6</sub> tag fused to the N-terminus of the recombinant S-layer protein was able to bind to the Ni-NTA resin. The purification procedure yielded more than 1 mg/ml protein. More precisely, 25 mg of purified recombinant SslA<sub>32-1097</sub> protein could be obtained from ~ 3 L culture.

The purification of large amounts of recombinant S-layer proteins from the cytosolic fraction of *E. coli* is usually time and material consuming in comparison to S-layer purification from wild type strains. However, by expressing this protein together with a His<sub>6</sub> tag, as demonstrated here, constitutes a relatively easy purification method of this recombinant protein by Ni-chelating chromatography.

Purification is extremely important for the subsequent recrystallization process. Pure protein solutions allow an easier identification of the self-assembly structures and do not disturb or inhibit self-assembly.

Addition of protease inhibitors during the isolation and purification step was helpful in preventing protein degradation.

### 3.1.3 SELF-ASSEMBLY

The ability of the recombinant S-layer monomers to self-assemble in suspension and to recrystallize on solid supports into monolayers or tubes has attracted much attention for a wide range of applications in the fields of nanotechnology and biomedicine [157]. After having the pure recombinant SslA protein produced and extracted from *E. coli* cells, it was therefore of great importance to investigate its self-assembling abilities.

The following issues were the focus of investigations and discussion:

- Is the recombinant protein able to self-assemble *in vitro*? If yes, under which conditions?
- What are the self-assembling structures it forms?
- Can the p4 symmetry as in case of the native SslA be observed?
- What factors will influence the self-assembly process?

To answer all these questions, *in vitro* recrystallization experiments were conducted in solution and on a Si wafer.

#### ***In vitro* recrystallization in solution**

At first *in vitro* recrystallization experiments in solution were carried out. To this end, the purified S-layer protein was disintegrated with 5M guanidinium hydrochloride (GuHCl) which was subsequently removed by dialysis (the protein concentration being 0.38 mg/ml) against 10 mM CaCl<sub>2</sub> solution at 4 °C for 24 hours. 1 week following dialysis, samples from the dialysed solution were adsorbed for 1 hour on cleaned Si substrates. After adsorption, the substrates were gently washed with distilled water and the S-layer structures stained with uranyl acetate and analysed by SEM. Results are shown in Figure 3-2:

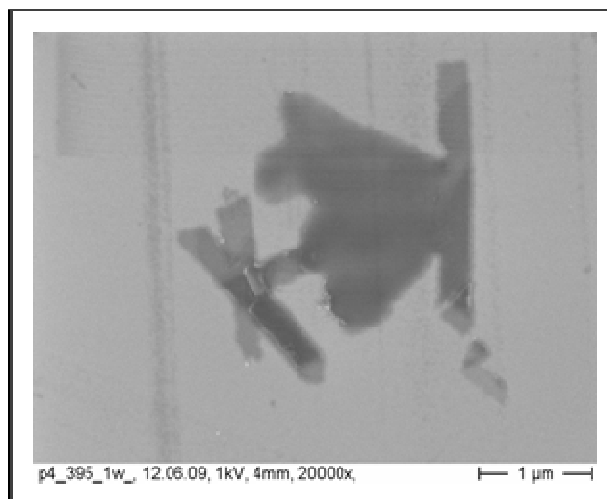


**Figure 3-2 *In vitro* recrystallization of SslA<sub>32-1097</sub> in solution**

SEM image showing SslA<sub>32-1097</sub> recrystallized in solution at a protein concentration of 0.38 mg/ml and adsorbed onto a Si wafer 1 week after dialysis.

As shown in Figure 3-2, under the above mentioned experimental conditions SslA<sub>32-1097</sub> was able to *in vitro* self-assemble in solution. After monomerization and dialysis, in the time course of 1 week, SslA<sub>32-1097</sub> monomers reassembled into multilayered sheets and into open ended monolayer and double layer cylinders (Figure 3-2). The diameter of the monolayer cylinders is in the range of 300 nm. Length varies from 1 μm to 2.5 μm. However the lattice symmetry could not be determined from this image.

Interestingly, when compared to the tube like structures formed by the native SslA protein, which had a measured diameter of 450-600 nm and a length between 1.1 and 4.5 μm, these recombinant S-layer tubes appear thinner and shorter.

Tube like structures were found in the case of the S-layer *Bacillus stearothermophilus* ATCC 12980 (SbsC) as well. These tubes had a diameter of 100 nm and a length of 1-3 μm [136].

Tube formation represents a later stage of the self-assembly process, as seen already in the case of the authentic SslA. It occurs after S-layer patches have grown to a certain size and their ends, due to the acquired curvature, tend to fold into a cylindrical, hollow, open ended structure; a process that requires a considerable amount of time. At a protein concentration of 0.38 mg/ml only after 1 week tube like structures could be observed. Right after the dialysis, at this protein concentration, which is considered to be low, only a very small patch was formed (Figure 3-3 A). This phenomenon can be

explained as follows: at low supersaturation the small nucleation rate leads to the growth of a few patches which finally may evolve into tube like structures.

However, when recrystallization reaction was performed at a higher initial monomer concentration, *e.g.* 2 mg/ml, already after dialysis, tubes could be observed (Figure 3-3 B).

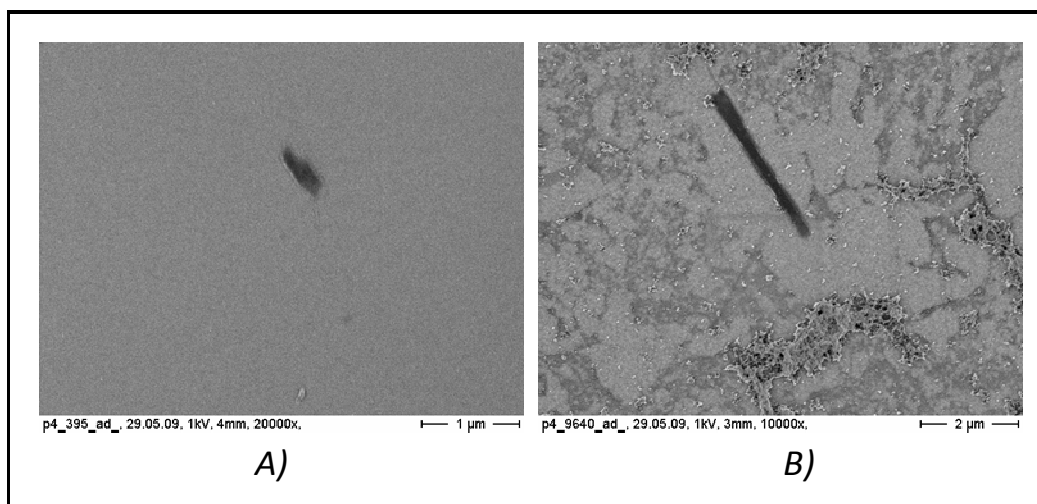


**Figure 3-3 SslA<sub>32-1097</sub> self-assembly at low versus high initial monomer concentration**

*In vitro* recrystallization was performed at A) 0.38 mg/ml and B) 2 mg/ml initial monomer concentration. The resulted self-assembly structures were adsorbed onto a Si wafer right after dialysis.

In this case, the nucleation rate is increased and self-assembly reaction proceeds faster. The higher supersaturation favored therefore the self-assembly and growth of the S-layer lattices. At an even higher supersaturation *e.g.* 4.5 mg/ml (the protein concentration at which the native SslA was recrystallized) many small patches and no tubes could be observed hinting that the kinetics of the process is so fast that layer formation is impossible due to the fast depletion of the monomers in the protein solution.

Of course, 4.5 mg/ml represents a higher concentration as in case of recombinant SslA, *e.g.* just 2 mg/ml, but in the latter case a higher initial monomer concentration could not be achieved because the recombinant protein is extracted at a much lower concentration from *E. coli* cells than the S-layer stripped from the bacterial cell surface. The recombinant protein after extraction is purified, than mixed with storage buffer and the concentration must be set after this step accordingly, in solution.

### ***In vitro* recrystallization on Si substrate**

The functionalization of inorganic surfaces with monomolecular layers of biopolymers has already attracted much attention in the field of supramolecular engineering.

S-layers possess the capability to reassemble *in vitro* in suspension into protein lattices with varying size and morphology. More importantly, there are several studies reporting on the capability of numerous S-layer proteins, mainly derived from *Bacillaceae* species to reassemble on solid substrates. Solid supports such as silicon wafers, silicon nitride, gallium arsenide wafers, mica, glass and graphite were successfully applied whereby the size of the coherent protein lattices was only limited by the size of the substrate [158]. Not only authentic bacterial S-layers stripped from the cell surface have been shown to recrystallize on such surfaces but also recombinant S-layers [142].

As shown in the previous section, SslA<sub>32-1097</sub> recrystallizes in solution *in vitro* into protein sheets and open ended tubes and the recrystallization conditions have a strong influence on the self-assembly process (*e.g.* initial monomer concentration). Reassembly of this S-layer on solid substrates would open up new approaches towards applications in the fields of nanotechnology and biomedicine (biosensors) especially with the possibility of enhancing its properties by genetic engineering. Therefore in this section the recrystallization behaviour of this S-layer on a functionalized Si wafer was explored.

To this end, recrystallization experiments were carried out by first monomerizing 0.5 mg of the purified S-layer with 5M GuHCl. After monomerization, 1/5 of the protein solution was dialysed against 10 mM Tris/HCl buffer pH 3 at 4 °C in the presence of APTES functionalized Si substrate. After 2 hours, the substrates were taken out, washed in distilled water and dried on air. Atomic force microscopy was used for imaging the topography of the recrystallized S-layer lattices on the silicon wafer. Figure 3-4 shows the structures obtained.

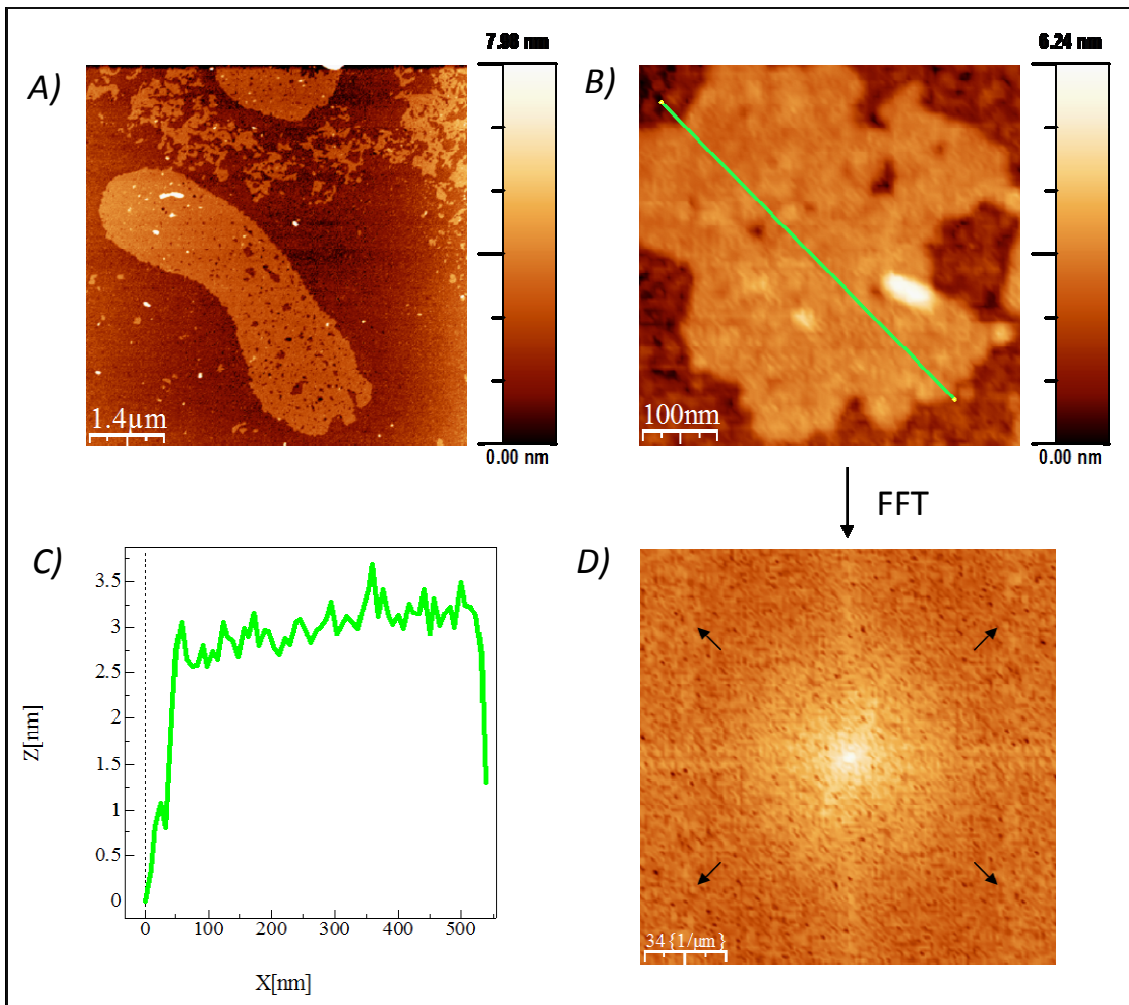


**Figure 3-4 Morphology and lattice structure of SslA<sub>32-1097</sub> *in vitro* recrystallized on Si wafer**

(A) The S-layer structures formed during recrystallization in the presence of an APTES functionalized Si surface, (B) Zoomed image of an individual S-layer patch, (C) Height profile and (D) Fast Fourier Transformation and lattice symmetry estimation based on image B.

The image in Figure 3-4 A shows, that only monolayers were formed on the silicon substrate. The extensive monolayer displayed in the image has several micrometers in length ( $\sim 6 \mu\text{m}$ ) and its height between 2.5 and 3 nm (data not shown). Many smaller patches can be observed as well. These are similarly crystalline and monolayered, and their height corresponds to 2.5 - 3 nm as shown in Figure 3-4 C.

It can be assumed that the substrate provides active centres for nucleation, hence the name of heterogeneous nucleation. However, currently there is no reliable model that describes in detail the heterogeneous nucleation and kinetics of protein crystallization on solid substrates.

## THE RECOMBINANT S-LAYER OF *S. UREAE* ATCC 13881

---

The growth of the various small patches could be initiated due to the existence of several randomly oriented nucleation points. The formation of such nucleation centres would require a reorientation of the adsorbed S-layer subunits until an orientation with a minimum of strain within the small crystallites is reached. Subsequently, protein crystal growth might be advanced in plane by incorporation of new subunits and terminated by neighbouring, also growing, crystalline areas. The size of the individual crystalline domains formed in this way is in the range of 200 nm and 500 nm in length (see length of a patch in Figure 3-4 C). Alternatively, it could be assumed that small patches have been nucleated and grown not only on the silicon surface but also in solution. These patches are then deposited onto the substrate. By both mechanisms a closed mosaic of crystalline domains would be generated (Figure 3-4 B) in one point. However, the entire silicon surface was not covered by a coherent monolayer after this recrystallization time of approximately 2 hours.

The size and structure of the crystalline domains and the crystallization speed depend not only on the particular S-layer species but also on the surface properties of the substrates. Under neutral pH conditions, APTES-modified silicon substrates typically present a positively charged surface. At low pH, like used in this recrystallization experiment, the monomers and buffer molecules carry a positive charge as well (pI of SslA<sub>32-1097</sub> is 5.5). Thus a strong repulsion from substrate, buffer and neighbouring molecules might facilitate orientation and attachment of the protein monomers giving rise to nuclei that can grow into patches and further on into an extensive layer.

Interestingly, no tubes were observed. It is supposed that tube formation in the presence of a substrate it is greatly impeded due to the strong binding of the protein to the substrate.

The protein concentration in the recrystallization experiment is rather low. This might also influence the self-assembly pattern observed on the Si wafer.

Fast Fourier Transformation (FFT) analysis of AFM images were performed in order to derive the lattice structure of the self-assembly structures formed by SslA<sub>32-1097</sub>. As observed on the image in Figure 3-4 D, the symmetry of the morphological unit of the S-layer lattice is p4 (4 dots can be pointed out) with a period of 12.2 nm which is in good agreement with data obtained for native S layer produced and exposed on the

surface of *Sporosarcina ureae* (p4 and 12.9 nm lattice constant). The morphological unit consists of four monomers arranged in p4 symmetry.

In conclusion, the recombinant SslA is able to self-assemble *in vitro* onto Si surfaces into large monolayers. Consequently, it may be used for a biological functionalization of silicon surfaces as a geometrically and physicochemically precisely defined immobilization matrix.

### 3.2 TAILORING THE RECOMBINANT SSLA - TOWARDS ELUCIDATION OF SSLA PROTEIN DOMAIN RESPONSIBLE FOR SELF-ASSEMBLY

S-layers possess the intrinsic ability of self-assembling into porous protein lattices and form periodic structures of oblique (p1, p2), trimeric (p3), square (p4) or hexagonal (p6) lattices.

This remarkable property of self-assembling *in vivo* and *in vitro* has been extensively explored and studied. For instance, in a previous study it was demonstrated that the N-terminal part of the S-layer of *Bacillus stearothermophilus* ATCC 12980 is responsible for anchoring the S-layer subunits to the cell wall and is required neither for the self-assembly nor for generating the lattice structure. Self-assembly is mediated by the central part of the S-layer while a fragment consisting of 219 AA can be deleted from the C-terminal part without interfering with the self assembly process or formation of the lattice structure [159].

The native as well as the recombinant S-layer of *Sporosarcina ureae* ATCC 13881 (SslA) is able to self-assemble *in vitro* in solution and on solid supports. However, up to now there exists no data as to which part of this S-layer protein is responsible for the self-assembly into lattices bearing p4 symmetry. In order to elucidate the structure-function relationship of distinct segments of SslA with respect to the self-assembly ability, three truncation derivatives of this protein were generated based on multiple sequence alignment data performed with sequences of S-layer proteins of *Bacillus stearothermophilus* ATCC 12980 (SbsC) and *Bacillus sphaericus*



CCM 2177 (SbpA). The PCR products encoding the SslA derivatives were cloned and expressed in *E. coli*. After isolation and purification, their ability to self-assemble was investigated. The information obtained would allow modifications of the protein that preserves its self-assembling ability but supplements it with novel properties.

It is generally agreed on the fact that cloning of S-layers is difficult as it is the cloning of large genes. Truncated S-layer forms with preserved self-assembly potential would facilitate further genetic modifications and broaden the application potential of this S-layer protein. Besides the metabolic cost for producing the S-layer even *in vivo* circumstances is very high; the S-layer can constitute up to 10 % of the total protein of cells in the exponential growth phase [160]. Therefore it would be advantageous to have proteins that are smaller in size and less costly for the cells to produce allowing even their large scale synthesis.

### 3.2.1 MUTAGENESIS AND MOLECULAR CHARACTERIZATION OF SSLA

#### TRUNCATION DERIVATIVES

In order to define which parts of the SslA protein are subject to truncation, an alignment of the SslA protein sequence was carried out with sequences of other S-layers for which an extensive truncation analysis was already done. As described in literature, truncation analysis was performed for 2 S-layers, namely SbsC of *Bacillus stearothermophilus* ATCC 12980 [135] and SbpA of *Bacillus sphaericus* CCM 2177 [161]. ClustalW alignment results have shown that both S-layers show a high sequence similarity to the SslA sequence [110]. The sequences have the highest sequence similarity in their N-terminal parts, followed by the central protein part while their C-terminal parts exhibited the lowest sequence similarity. This is well in line with the alignment data for most of the S-layer proteins, indicating the highest sequence similarity for the N-terminal protein part that is primarily involved in the cell wall attachment and a moderate sequence similarity for the central part responsible for self-assembly. The C-terminal S-layer sequence was described in literature as the part involved in cell wall anchoring and that it most probably leads to quite diverse cell surface properties [69].

From the results of SbpA truncation assays it is known that cutting the N-terminal 202 amino acids and the C-terminal 237 amino acids does not affect its self-assembling properties; the S-layer was still able to form self-assembly products with p4 lattice symmetry [161]. Indeed truncation derivatives consisting of only the N-terminal 318, 468, 618 or 768 amino acids of the protein sequence had lost the ability to self-assemble and formed unstructured aggregates. Moreover, the deletion of the 350 C-terminal amino acids was linked to a change in lattice type from square to oblique (p1). In case of SbsC, with the various truncated forms it was demonstrated that the protein part between amino acids 258 and 880 is necessary for self-assembly and the C-terminal 179 amino acids can be deleted without affecting the oblique lattice structure [159].

Based on the comparison of these sequence data, truncations lacking the N-terminal 341 amino acids and the C-terminal 172 amino acids were created plus a derivative lacking both of these SslA protein parts. The design of these derivatives is depicted in Figure 3-5:

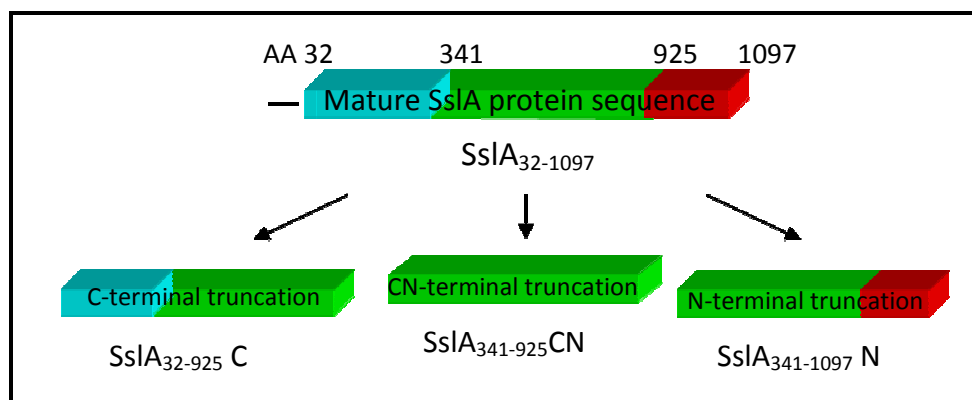


**Figure 3-5 Creation of SslA truncation derivatives**

By deletion of the N-terminal part of the SslA protein sequence (amino acids 1-341),  $SslA_{341-1097} N$  is created. Similarly, by deletion of the C-terminal part (amino acids 925-1097),  $SslA_{32-925} C$  was constructed. Finally a construct having both N- and C-terminals truncated (amino acids 1-341 and 925-1097) named  $SslA_{341-925} CN$  was designed.

**The N-terminal truncation** of the S-layer of *S. ureae* ATCC 13881 is the protein version lacking the N-terminal 341 amino acids shortly termed  **$SslA_{341-1097} N$** . This SslA derivative has a calculated molecular weight of 84 kDa and a theoretical pI value of

5.31.

Like in the case of SsIA<sub>32-1097</sub>, this truncation derivative could only be cloned with the Ek/Lic strategy. The gene encoding SsIA<sub>341-1097N</sub> was first amplified by PCR from genomic DNA with primers Pfor341Licp2 and Prevmatp4Licp2 (see Appendix). The PCR product was ligated into the pET 51b+ Ek/Lic (Novagen) using the EK/Lic Strategy.

*E. coli* Nova Blue Giga Single cell were transformed with the recombinant plasmid pET51Ek/Lic-SsIA<sub>341-1097N</sub> carrying the desired gene sequence. Positive clones were at first screened by colony PCR and confirmed by sequencing (the successful cloning was confirmed by the restriction analysis of the inserts and partial sequencing).

SsIA<sub>341-1097</sub> is encoded by 2387 bps but the final protein structure contains additionally a His<sub>10</sub> tag fused to its C-terminal part and the Lic arm and consists therefore of 794 amino acids.

**The C-terminal truncation derivative** of the recombinant S-layer of *Sporosarcina ureae* ATCC 13881 was obtained by cleavage of the last 172 amino acids of the recombinant SsIA protein sequence and named **SsIA<sub>32-925C</sub>**. The gene encoding this SsIA derivative consists of 2724 bps which translates into an S-layer protein of 907 amino acids with a molecular weight of 97 kDa and pI of 5.46. The final protein structure contains additionally a His<sub>6</sub> tag. Plasmids carrying the desired gene sequence were a kind leftover of Pavel Ryzkov [110].

**The CN-terminally truncated SsIA derivative** was created by deletion of both, the N-terminal 341 amino acids and the C-terminal 172 amino acids resulting in a construct containing just the central part of this recombinant S-layer termed **SsIA<sub>341-925CN</sub>**.

This SsIA derivative is encoded by a gene of 1828 bps only. The protein itself consists of 599 amino acids including a His<sub>6</sub> tag with a calculated molecular weight of 64 kDa and a pI of 5.42. Plasmids carrying the desired gene sequence were a kind leftover of Pavel Ryzkov [110].

### 3.2.2 HETEROLOGOUS EXPRESSION IN *E. COLI*, ISOLATION AND PURIFICATION

For the expression of all three SsIA truncation derivatives, *E. coli* was chosen as host organism. The choice was motivated by the facts that *E. coli* is a desirable organism for

## THE RECOMBINANT S-LAYER OF *S. UREAE* ATCC 13881

heterologous expression of proteins owing to its easy of manipulation, the availability of a variety of cloning vectors, well understood genetics and low cost of the culture [162]. Furthermore, it was successfully used in expressing the mature form of SslA.

For heterologous expression of the N-terminal truncation, the recombinant plasmid pET 51Ek/Lic-SslA<sub>341-1097</sub>N was established in the expression strain *E. coli* BL21 (DE3) according to the advices of the manufacturer providing the Ek/Lic plasmid. The C-terminal truncated SslA derivative and the CN-terminal derivative were established in the expression strain *E. coli* Rosetta Blue (DE3) because this strain supplies tRNAs for codons rarely used in *E. coli* cells that would be necessary to translate the foreign S-layer DNA sequence. Protein expression was induced with 1 mM IPTG (final concentration) and monitored by taking samples from cultures before and 1 and 3 hours following induction. The optimal temperature during expression was found to be 30 °C. Samples taken were then prepared for SDS-PAGE analysis as described by Laemli (1970) and separated on a 10% SDS-PAA gel followed by staining with Coomassie Brilliant Blue which is a protein stain. The results of the expression are shown in Figure 3-6:

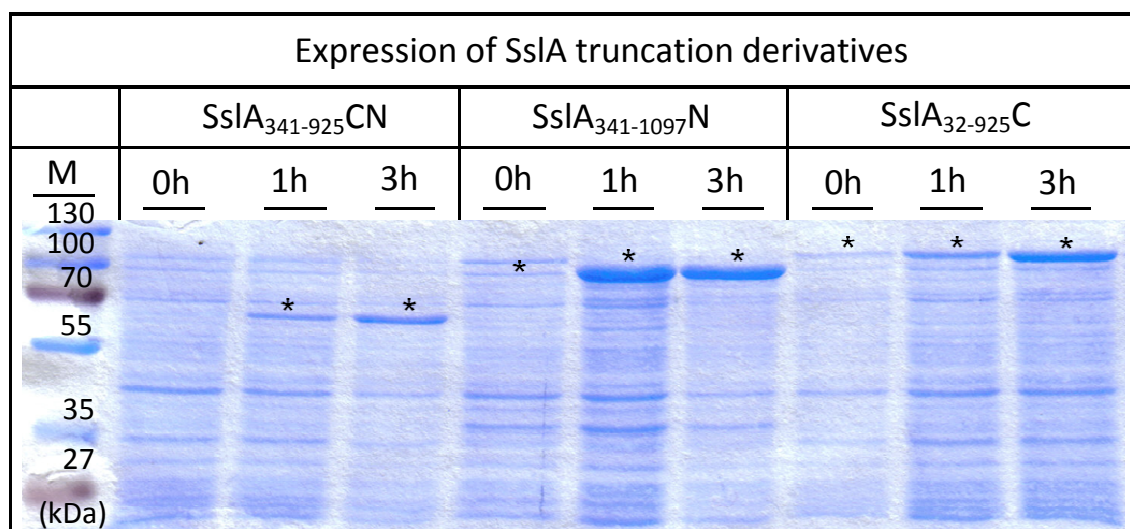


**Figure 3-6 Heterologous expression of SslA truncation derivatives in *E. coli***

The Coomassie stained protein gel shows expression of SslA<sub>341-925</sub>CN and SslA<sub>32-925</sub>C in *E. coli* Rosetta Blue (DE3) and of SslA<sub>341-1097</sub>N in BL21 (DE3) whole cell lysates after 0, 1, and 3 hours of induction with 1 mM IPTG (20 µg protein loaded per lane). M-protein ladder (Page Ruler™ Plus Prestained). Recombinant protein position is marked with star.

## THE RECOMBINANT S-LAYER OF *S. UREAE* ATCC 13881

---

The N-terminal derivative has a calculated size of 84 kDa. A protein of this size can be observed on the SDS-PAGE gel indicating that the entire SslA<sub>341-1097N</sub> had been produced in *E. coli* cells (Figure 3-6 0-3h SslA<sub>341-1097N</sub>). Already after 1 hour following induction, a thick protein band corresponding to the size of this SslA protein derivative can be observed on the gel (Figure 3-6 1h SslA<sub>341-1097N</sub>). Moreover, at this time point expression is the most efficient, since after 3 hours following induction the amount of the protein produced is lower as indicated by the reduced thickness of the protein band on the gel (Figure 3-6 3h SslA<sub>341-1097N</sub>). Interestingly, even without induction, a slight protein band can be observed (Figure 3-6 0h SslA<sub>341-1097N</sub>), however such a basal protein expression was not present in the case of the mature recombinant SslA form.

A protein band corresponding to the size of the C-terminal derivative (97 kDa) can be further identified on the gel image (Figure 3-6 0h-3h SslA<sub>32-925C</sub>) confirming the successful expression of this derivative in the *E. coli* cells. Contrary to the N-terminal derivative, the level of expression seems to increase with the induction time, *i.e.* the highest after 3 hours following induction, as evidenced by the thickness of the protein bands seen on the gel (Figure 3-6 1h and 3h SslA<sub>32-925C</sub>). However, even without induction, the protein is expressed in the cells and this fact could be connected to the leakiness of the vector molecule.

The SDS-PAGE pattern shows apparently no basal expression for the CN-terminal truncation derivative. A protein band corresponding to the calculated molecular weight of this protein *i.e.* 64 kDa can be observed only after 1 hour following induction with IPTG (Figure 3-6 1h SslA<sub>341-925CN</sub>). The expression level further increases as indicated by the protein band thickness on the gel (Figure 3-6 3h SslA<sub>341-925CN</sub>).

SslA derivatives accumulated mainly in the soluble fraction of the lysed *E. coli* BL21 (DE3) and Rosetta Blue (DE3) cells (data not shown). After isolation, the supernatant containing the S-layers was subjected to Ni affinity chromatography. Elution fractions containing the purified proteins were pooled and dialysed against distilled water for 12 hours at 4 °C.

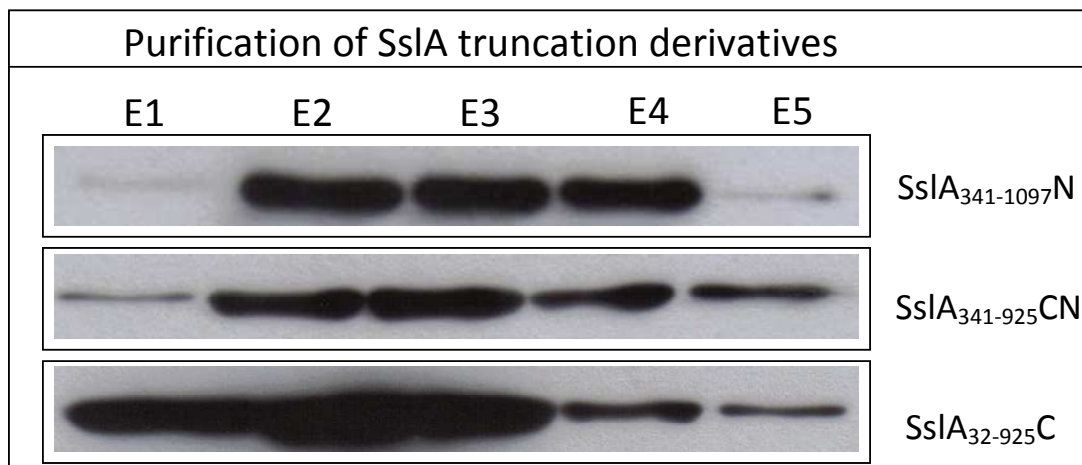


**Figure 3-7 Purification of SslA truncation derivatives**

E1-E5 mark the elution fractions of the Ni<sup>2+</sup> affinity chromatography. Samples from elution fractions of SslA<sub>341-1097</sub>N, SslA<sub>341-925</sub>CN and SslA<sub>32-925</sub>C were subjected to Western Blot analysis using the anti-His antibody.

SslA<sub>341-1097</sub>N is expressed with a His tag consisting of 10 Histidine amino acids, which allowed a relatively easy purification via Ni affinity chromatography. The S-layer protein was present in all elution fractions (Figure 3-7 E2-E4 SslA<sub>341-1097</sub>N). Since this SslA construct contains an N-terminal Strep-tag II as well, an alternative purification method would have been via the Strep tag.

SslA<sub>32-925</sub>C bears similarly a C-terminal His<sub>6</sub> tag which facilitated its purification from the whole cell lysate of *E. coli* cells. This derivative eluted at the expected molecular mass and on immunoblots a strong cross reaction was observed between this protein and the anti-His antibody (Figure 3-7 E1-E5 SslA<sub>32-925</sub>C). The elution fractions containing SslA<sub>32-925</sub>C had a high purity. The available His<sub>6</sub> tag on the C-terminal part of SslA<sub>341-925</sub>CN allowed for a relatively simple purification of this protein as well. The protein could be detected in the elution fractions (Figure 3-7 E1-E5 SslA<sub>341-925</sub>CN). The purification resulted approximately 30 mg of pure protein which was further on used for self-assembly experiments. A lower amount of protein could be extracted in case of the C-terminal protein *i.e.* 26 mg and 22 mg pure protein in case of the N-terminal derivative, respectively.

In conclusion, all three SslA truncation derivatives were successfully expressed in *E. coli* and purified via Ni affinity chromatography. The addition of protease inhibitors was helpful in reducing protein degradation in case of all the expressed derivatives.

### 3.2.3 SELF-ASSEMBLY

Previous attempts to produce recombinant S-layers often resulted in proteins unable to form crystalline arrays [156]. However, in some cases such as SbsA and SbsD, recombinant S-layer proteins were produced and purified, which re-assembled into flat sheets or cylinders that exhibited the wild-type structures [154]. Truncated recombinant forms of SbsC of *G. stearothermophilus* ATCC 12980 re-assembled exclusively into monolayer cylinders (N-terminal truncation form) or into flat sheets, showing no regular lattice structure (C-terminal truncation forms) [159]. These forms differed from the self-assembly products formed by the wild-type SbsC that showed double-layer sheets and double-layer or monolayer cylinders exhibiting an oblique structure.

After the successful expression and purification of the SslA truncation derivatives, their self-assembling properties and lattice symmetry formation are investigated in this section. Are these derivatives able of self-assembling *in vitro* or is this ability lost with certain amino acid deletions? If self-assembly is preserved, how do the self-assembling structures look like? Can the p4 symmetry as in case of the native SslA be observed? Which factors will influence the self-assembly process? To answer all these questions, *in vitro* recrystallization experiments were conducted in solution and on a silicon wafer.

#### ***In vitro* recrystallization in solution**

To investigate the self-assembly properties of isolated recombinant SslA truncation derivatives in solution, the purified proteins were monomerized with 5M GuHCl which was subsequently removed by dialysis (the protein concentration was 2 mg/ml) against 10 mM CaCl<sub>2</sub> solution at 4 °C for 24 hours. After dialysis, samples of the dialysed solutions were adsorbed for 1 hour onto cleaned Si substrate. After adsorption, the substrates were gently washed with distilled water and analysed by AFM. Results are shown in Figure 3-8:

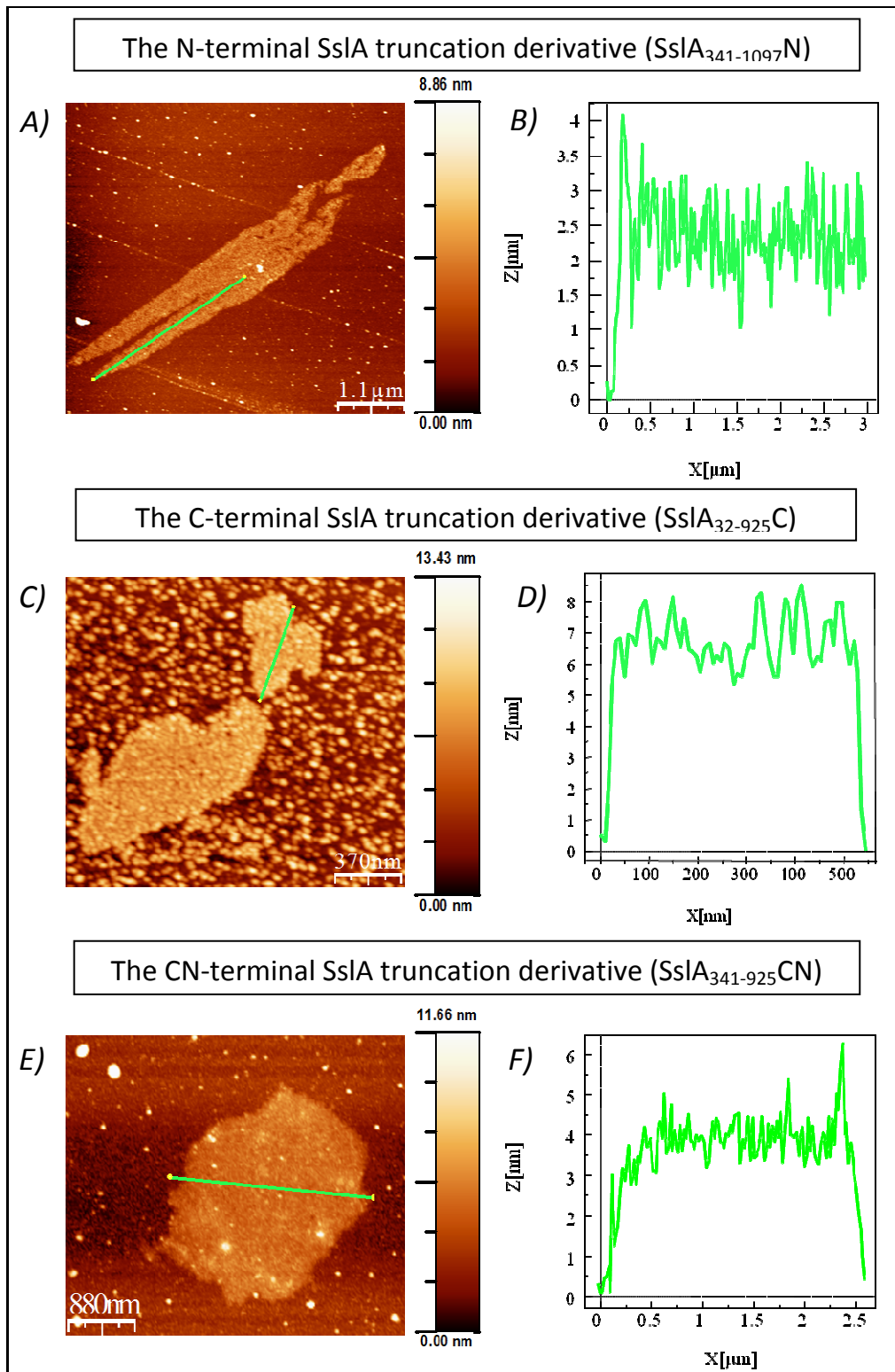


**Figure 3-8** Self-assembly of the recombinant SsIA truncation derivatives in solution

AFM micrographs show A) SsIA<sub>341-1097</sub>N, C) SsIA<sub>32-925</sub>C E) SsIA<sub>341-925</sub>CN recrystallized *in vitro* in solution and adsorbed onto Si substrate after dialysis. The corresponding height profiles of the protein layers are presented in B), D) and F).



## THE RECOMBINANT S-LAYER OF *S. UREAE* ATCC 13881

---

As Figure 3-8 shows, all truncation derivatives were able to self-assemble under the above mentioned experimental conditions into layer like structures. In case of the N-terminal truncation (**SsIA<sub>341-1097</sub> N**), *in vitro* recrystallization in solution generated long protein layers extending to a length of more than 4  $\mu\text{m}$  and a diameter of more than 1  $\mu\text{m}$  (Figure 3-8 A). These layers are observed in the form of a monolayer with a height between 2.5 and 3 nm (Figure 3-8 B). The C-terminal SsIA truncation (**SsIA<sub>32-925</sub> C**) has self-assembled similarly into monolayers during the *in vitro* recrystallization reaction. These layers or patches are smaller in size, having only 400 nm or up to 1  $\mu\text{m}$  (Figure 3-8 C), however their height corresponds to 6 nm as seen from the AFM measurement (Figure 3-8 D). This structural difference can be perhaps related to hydration processes. The C-terminal part is localized outside the cell, therefore it is less charged. By cutting it, the N-terminal part would favour the formation of a thin water film, which due to the capillary forces occurring between the AFM tip and the hydrated S-layer domain results in a larger thickness *i.e.* 6 nm. This structural difference is observed not only in the case of *in vitro* recrystallization in solution but also when recrystallization was done on a solid substrate (see next section).

Shape of protein layers formed by the C-terminal truncation is also different; they are not elongated but rather more rounded up, elliptic, a fact that is most probably related to the mechanism of the assembly process that drives the joining of the S-layer monomers and growth of the layers. Figure 3-8 C contains a dense background of individual S-layer monomers (caused by the high monomer concentration *i.e.* 2 mg/ml and the high resolution of AFM) which compete for being incorporated into the protein lattice. More about these aspects of the self-assembly of the truncation derivatives is discussed in section 3.2.4. The CN-terminal truncation derivative (**SsIA<sub>341-925</sub> CN**) was also able to self-assemble and forms similarly, layer like structure under these experimental conditions. More precisely, Figure 3-8 E shows a protein monolayer having a size between 1.5 and 2.5  $\mu\text{m}$ . Its height is approximately 3 nm (Figure 3-8 F). (However, drying and surface tension might cause a decrease in height for all S-layer truncation structures; in AFM this height is measured). Interestingly, the S-layer sheet has square shaped edges that resemble the structural form of native S-layers and hints to the square (p4) lattice symmetry. However, at this stage symmetry

## THE RECOMBINANT S-LAYER OF *S. UREAE* ATCC 13881

---

could not be determined (it will be reviewed in the following section again). Indeed for the C-terminal truncation, the four fold symmetry (p4) with a lattice constant of 13.1 nm (data not shown) could be detected, which is in good agreement with the lattice constant reported for the native SslA variant [106]. For the N-terminal truncation, determination of the lattice symmetry was not possible with the available data.

All in all, the truncated SslA forms created have preserved their ability to self-assemble into protein sheets. Compared to the truncation analysis of SbsC, this result could be somehow suspected owing to the high sequence similarity and function of the two S-layers.

It was already shown for SbsC that the N-terminal part is responsible for anchoring the S-layer to the rigid cell wall and is not required for the self-assembly. From the results of SbpA truncation assays it is known that cutting the N-terminal 202 amino acids does not affect its self-assembling properties. Since the N-terminal SslA truncation (**SslA<sub>341-1097</sub> N**) did also self-assemble it can be speculated that its N-terminal part is similarly involved in cell wall attachment and its deletion therefore does not impede its intrinsic property of self-assembling into protein lattices.

However, cutting the C-terminal part of SslA might affect its self-assembling ability, since in case of SbsC, three C-terminal truncations have lost this property (SbsC<sub>31-713</sub>, SbsC<sub>31-844</sub> and SbsC<sub>31-860</sub>). But in this case the SslA C-terminal derivative is composed of amino acids 31-925 and its self-assembling ability is preserved. (A similar result was obtained for SbsC<sub>31-880</sub>, SbsC<sub>31-900</sub> and SbsC<sub>31-920</sub>). It can be concluded that this part of SslA is not directly responsible for self-assembly and the last 172 amino acids of this S-layer protein can be deleted without interfering with the self-assembly process and without having an impact on the lattice structure (p4). But one might think that cutting even more than the first 341 amino acids or the last 172 amino acids will indeed affect the self-assembly of SslA. The image in Figure 3-8 E proves that the deletion of these both domains still does not have a negative impact on the self-assembly property of SslA. This derivative (**SslA<sub>341-925</sub> CN**) was still able to form S-layer sheets. This SslA domain might be however the minimal part that is sufficient for the assembly. In case of SbsC, with the various truncated forms it was demonstrated that the protein part between amino acids 258 and 880 are necessary for self-assembly. Truncation results

from this work show that for SslA this minimal part can be set between amino acids 341 and 925. For SbsC, the C-terminal 179 amino acids can be deleted without affecting the oblique lattice structure [159]. For SslA this is true for the C-terminal 172 amino acids, except that this S-layer forms square lattice type. In case of SbpA, deletion of C-terminal 237 amino acids does not affect its self-assembling properties; the S-layer was still able to form self-assembly products with p4 lattice symmetry [161].

In conclusion, neither the N-terminal, nor the C-terminal is the SslA protein domain is responsible for self-assembly. Both of these parts can be deleted and the resulting protein will still self-assemble into protein lattices. Therefore, the central SslA-domain is self sufficient for the self-assembly.

### ***In vitro* recrystallization on substrate**

S-layers are endowed with the ability to self-assemble into two dimensional arrays *in vitro* not only in solution but also on a solid support. For example the S-layer SbsB of *Bacillus stearothermophilus* PV72/p2 forms monocrystalline lattices with individual areas larger than 10  $\mu\text{m}$  in diameter on silicon wafers within 4 hours [132].

The truncation derivatives of the S-layer of *S. ureae* ATCC 13881 were able to form sheet like structures in solution. Therefore in this section results are outlined concerning its assembly on a Si wafer.

For investigating the self-assembly properties of the SslA truncation derivatives on a solid substrate, the proteins were recrystallized on a functionalized Si surface at a protein concentration of 0.5 mg/ml. In particular, the purified S-layer solutions were at first dissolved in 5M GuHCl and 1/5 of the solution dialysed against Tris/HCl buffer pH 3 for 2 hours at 4 °C in the presence of an APTES functionalizes Si substrate. After dialysis, the Si substrate was washed with distilled water, dried on air and analysed by AFM. For the N-terminal truncation derivative the resulting self-assembly structures are shown in Figure 3-9:

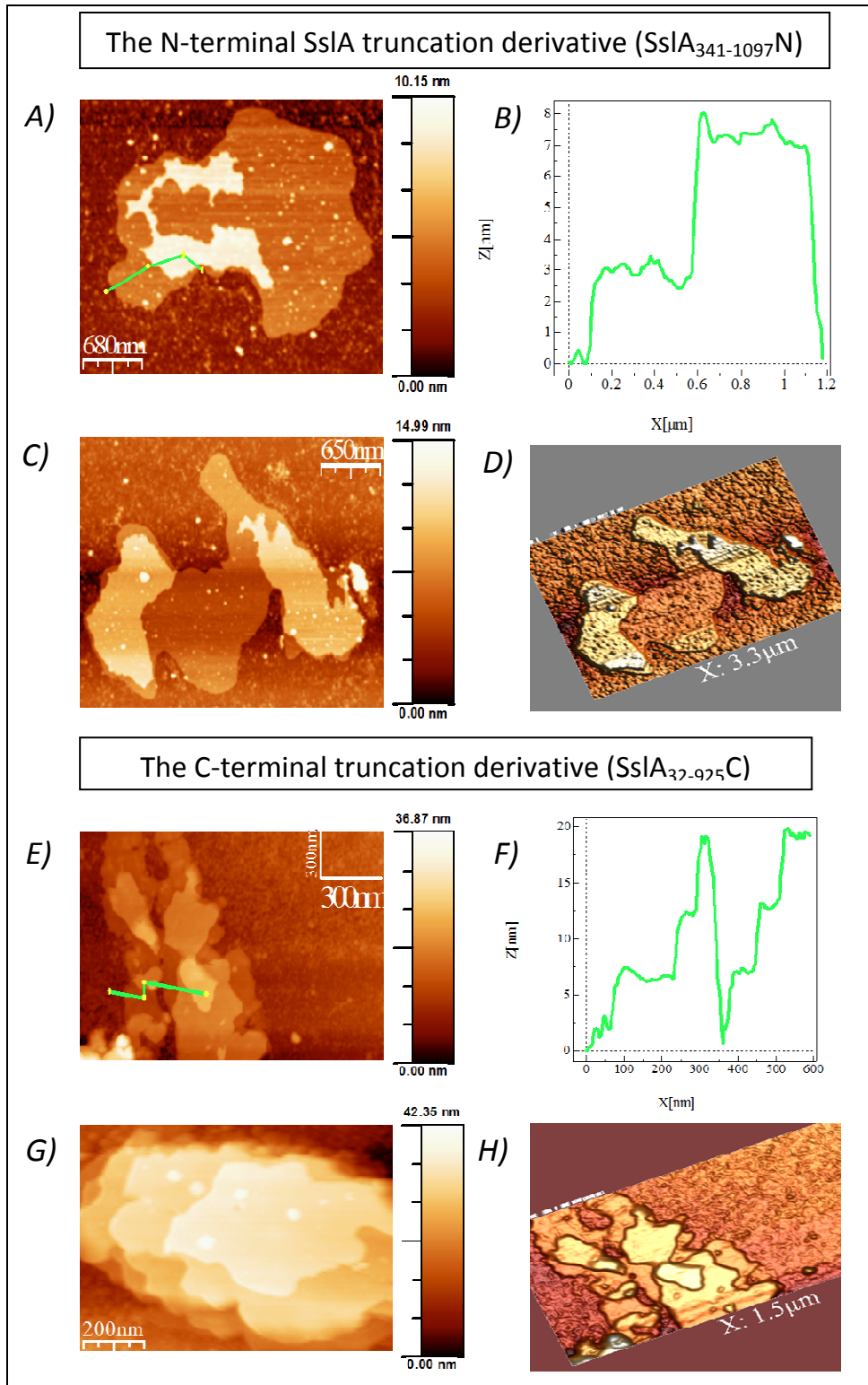


**Figure 3-9** Self-assembly of the recombinant SsIA truncation derivatives on a Si wafer

AFM micrographs show (A), (C) SsIA<sub>341-1097</sub>N, (E),(G) SsIA<sub>32-925</sub>C recrystallized *in vitro* at pH 3 in the presence of an APTES functionalized Si substrate. All truncation derivatives have kept their self-assembly ability and form multilayers. (B) Height profile and (D) 3D line rendering of SsIA<sub>341-1097</sub>N based on image A, (F) Height profile and (H) 3D line rendering of SsIA<sub>32-925</sub>C based on image E.

Figure 3-9 shows that the N-terminal SslA truncation derivative was able to self-assemble under the above mentioned *in vitro* recrystallization conditions. The resulting self-assembly structures take the form of crystalline protein multilayers extending to sizes between 1 and 3  $\mu\text{m}$  (Figure 3-9 A, C). A 3D reproduction of the multilayer structure is shown in Figure 3-9 D. The thickness of one layer is approximately 3 nm as indicated by the cross section profile displayed in Figure 3-9 B. A similar height was measured for this derivative when recrystallized in solution. Yet, recognition of the lattice structure is not possible with the obtained images.

**SslA<sub>341-1097</sub>N** bears an N-terminal Strep-tag II and a C-terminal His<sub>10</sub>-tag. None of them interferes with the self-assembling ability of this derivative. The result is important because it demonstrates that SslA can be functionalized and the protein still gives crystalline nanostructures that expose high affinity tags. Strep-tag II binds strongly streptavidin, while His-tag is able to coordinate Ni<sup>2+</sup> ions; in this way, the S-layer might represent a functional template either for binding biotinylated molecules through streptavidin or for metallization. Accessibility of the tags can be investigated with single molecule force spectroscopy. Strep-tag II fusions were already done for SbpA, the S-layer protein of *Bacillus sphaericus* CCM 2177 [142]. Similarly, the genetic modification did not disrupt its layer formation ability and the Strep-tag moiety was also accessible in the protein lattice. However, an S-layer construct with preserved self-assembling properties having both, Strep-tag II and His-tag has not yet been reported in the literature. But more importantly, the *in vitro* recrystallization experiment on the silicon substrate demonstrates once again that the N-terminal part of SslA can be deleted without interfering with its self-assembling ability.

The C-terminal SslA truncation derivative retained its self-assembling property as well. *In vitro*, on a Si wafer, the monomers have arranged into multilayers as it can be observed from Figure 3-9 E and G. In contrast to the N-terminal SslA truncation derivative, these protein layers have a measured height of approximately 6 nm (Figure 3-9. F). The size of the layers however is smaller, being in the range from 300 nm to 1.5  $\mu\text{m}$ ; indeed they are multiple. A 3D profile of the layers is shown in Figure 3-9 H.

Formation of the square lattice structure could not be determined for the C-terminal SslA truncation derivative.

Under the same *in vitro* recrystallization conditions, large, coherent and crystalline monolayer was observed for the CN-terminal SslA truncation derivative (Figure 3-10 A and C). The size of this monolayer is in order of micrometers. Height corresponds to 2.5 -3 nm (Figure 3-10 B). Fourier analysis clearly shows the p4 square lattice type symmetry (Figure 3-10 D black arrows) with a period of 13.2 nm which is in good agreement with data obtained for native SslA produced and exposed on the surface of *Sporosarcina ureae* (p4 and 12.9 nm) [106]. This demonstrates that truncation of both, the N- and C-terminal part, has no influence on the formation of the square lattice type.

However, a smaller lattice size corresponding to 6.6 nm could be measured as well. This data may hint to substructures present in the protein lattice. So far no such data was reported in the literature for any of the S-layer proteins studied.

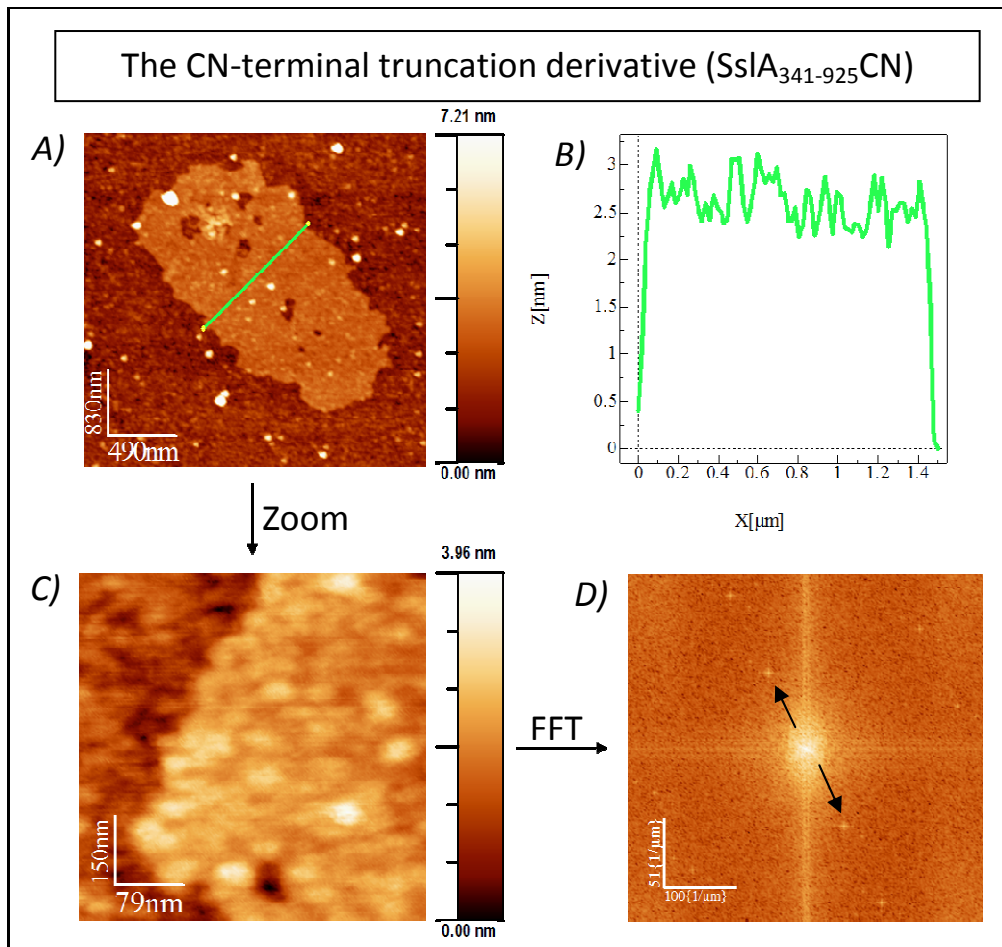


**Figure 3-10 Self-assembly of SsIA<sub>341-925</sub>CN on a Si wafer**

AFM micrographs show (A) the S-layer recrystallized *in vitro* at pH=3 in the presence of an APTES-Si substrate (B) Height profile based on image A, (C) Zoomed image for lattice symmetry estimation, (D) FFT analysis based on high quality image B showing the p4 symmetry (see black arrows).

Truncation analysis of SbsC revealed that the C-terminal 179 amino acids are not required for the formation of the oblique lattice structure. In case of this smallest SsIA derivative, the C-terminal 172 amino acids were deleted and the square lattice type still could be formed; fact that corroborates the view that this SsIA part does not contribute to the lattice formation properties. More importantly, upon assembly, it could be once again demonstrated that deletion of both, N- and C-terminal parts does not hinder self-assembly supporting the view that this central SsIA protein domain might be sufficient and responsible for the self-assembling properties of this S-layer.

It is however remarkable that in just only 2 hours, the SsIA truncation derivatives have generated such extensive layers on the Si wafer. When recrystallized in solution, the

self-assembly structures required more time to form, *i.e.* 24 hours. The difference may lie in the kinetics of the self-assembly reaction, that happens in the two different environments. In the presence of a substrate heterogeneous nucleation occurs. Generally, heterogeneous nucleation takes place more quickly since the substrate acts as a scaffold for the crystal lattice to grow on, thus eliminating the necessity of creating a new surface and the incipient surface energy requirements. Hence, the faster assembly resulted compared to homogeneous nucleation occurring in solution.  $\text{Ca}^{2+}$  ions have accelerated the self-assembly process when the native SslA protein was recrystallized in solution. In case of the *in vitro* recrystallization on the substrate, there are no  $\text{Ca}^{2+}$  ions involved, indeed the reaction proceeds at low pH, *i.e.* pH 3. At this pH, the SslA protein monomers are positively charged. Buffer molecules carry a similar, positive charge while the functionalized silicon surface presents as well positive charges. Hence strong repulsion effects are forcing the monomers to join and adopt the most optimal conformation for cluster formation and organization as well as for growth on the solid substrate.

In conclusion, the SslA truncation derivatives created have kept their ability to self-assemble *in vitro* in solution and on a Si wafer. The proteins formed crystalline nanostructures that depending on the application can be considered promising building blocks for nanobiotechnology. Furthermore, the recrystallization experiments have demonstrated that the central SslA protein part is sufficient for self-assembly and for the square lattice symmetry formation. The result opens up new possibilities for further genetic modifications of this recombinant S-layer towards interesting applications in nanobiotechnology.

### 3.2.4 FACTORS THAT INFLUENCE THE SELF-ASSEMBLY PROCESS

In the preceding sections it was shown that SslA truncation derivatives have kept their self-assembling properties and formed monolayer and multilayer structures. In most cases, the structural form and size of the S-layer self-assembly products depends also on several environmental parameters. In this section, factors and their influence on the *in vitro* recrystallization reaction in solution and on a Si substrate are presented.



### ***Influence of initial monomer concentration on the self-assembly in solution***

Protein crystallization or specifically the self-assembly process involves a nucleation and growth step determined to a large extent by kinetics. Protein nuclei formed by collision can only grow into crystal lattices if they have reached a critical size and overcome the free energy barrier. Nucleation without preferential nucleation sites is called homogeneous nucleation and it occurs spontaneously and randomly in the volume of ideally pure solutions, *i. e.* solutions constituted of solvent and solute molecules only.

Bonding between the protein subunits will mainly determine the assembly route, the final reassembly form and the possibility to form mono- or double layers. However other parameters such as initial protein concentration (and growth time) will also affect the structural form and size of the self-assembly products which have tremendous importance for certain (nano)technological applications. In order to experimentally evidence it, recrystallization was performed at high (2 mg/ml) versus low (0.38 mg/ml) initial monomer concentration and the structures of self-assembly products compared. In more detail, the truncation derivatives were at first monomerized with 5M GuHCl which was subsequently removed by dialysis against 10 mM CaCl<sub>2</sub> (neutral pH) for 24 hours at 4 °C. After dialysis, aliquots of the protein solutions were adsorbed onto cleaned silicon substrates for 1 hour followed by the gentle washing of the substrates in distilled water and staining with uranyl acetate. The protein structures formed were visualized by means of SEM and are presented in Figure 3-11.

The S-layer self-assembly is initiated by removal of denaturant GuHCl from the monomer solution and proceeds by assembly of the monomers into higher order structures *e.g.* protein lattices. In this sense, at high initial monomer concentration, the N-terminal SsIA truncation derivative recrystallized into large layer which furthermore folds up into a tube like structure (Figure 3-11 B).

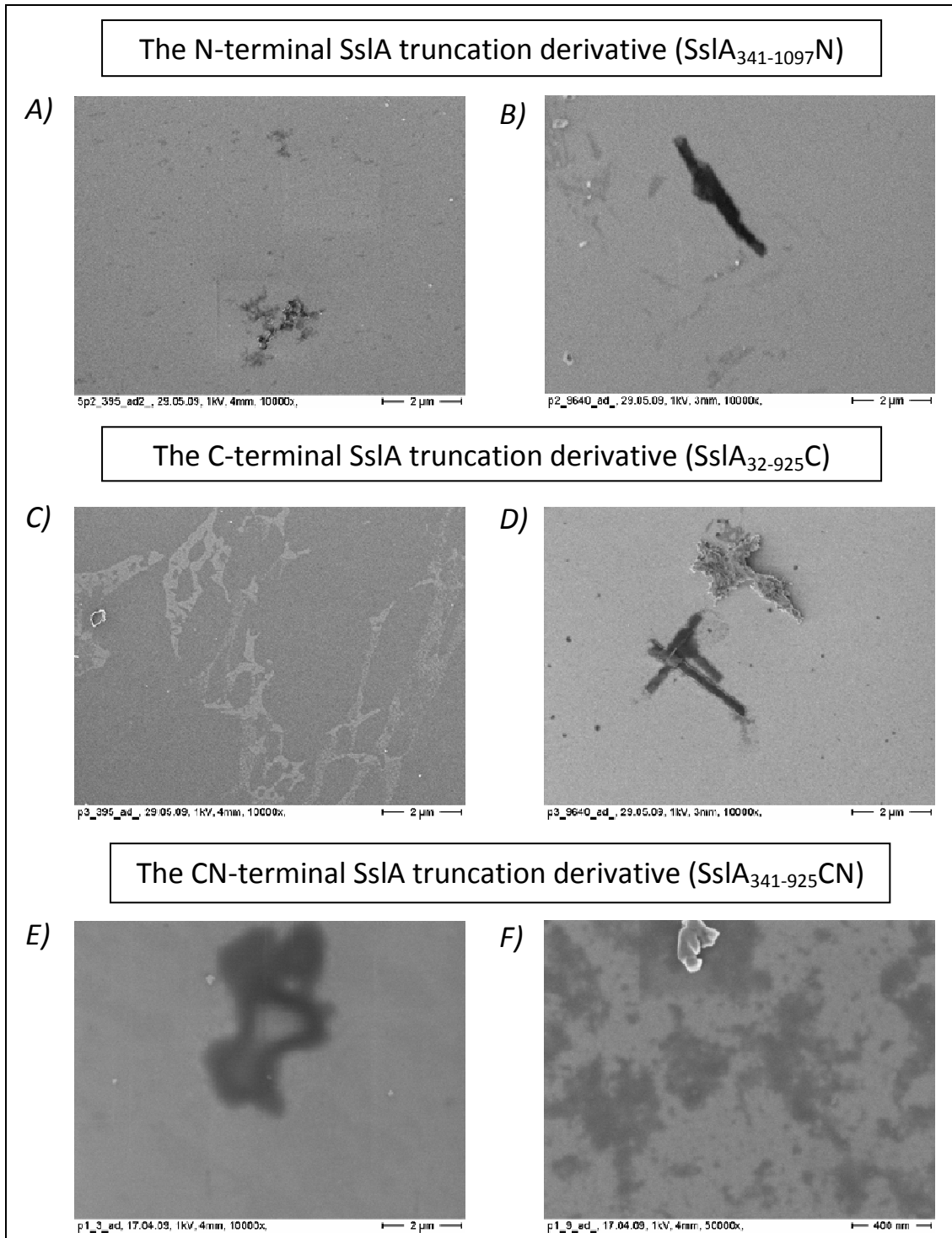


**Figure 3-11 Influence of initial monomer concentration on the self-assembly of the SsIA truncation derivatives in solution**

SEM micrographs show SsIA<sub>341-1097</sub>N recrystallized *in vitro* in solution (A) at low and (B) high initial monomer concentration, similarly SsIA<sub>32-925</sub>C recrystallized at (C) low and (D) high initial monomer concentration and SsIA<sub>341-925</sub>CN recrystallized at (E) low and (F) high initial monomer concentration. All self assembly products were adsorbed onto a Si wafer right after dialysis.

## THE RECOMBINANT S-LAYER OF *S. UREAE* ATCC 13881

---

This tubular structure of SslA<sub>341-1097</sub> N has a length of about 2  $\mu\text{m}$  and a diameter of approximately 300 nm. Similar structure has been observed for the mature recombinant SslA when it was *in vitro* recrystallized at the same initial monomer concentration *i.e.* 2 mg/ml. The diameter of these tubes does not differ from those formed by the N-terminal SslA truncation. Interestingly, truncation of the S-layer, more precisely deletion of its N-terminal 341 amino acids, does not affect tube formation.

At a low initial monomer concentration SslA<sub>341-1097</sub> N formed only small patches (Figure 3-11 A). The phenomenon can be attributed to the low number of monomers present in the protein solution which assemble into few critical nuclei but growth is impeded due to the fast consumption of the molecules. Contrarily, for the same initial monomer concentration brought into the self-assembly reaction, large crystalline layers can be observed in case of the C-terminal SslA truncation derivative (Figure 3-11 C). SslA<sub>32-925</sub>C presents tubular architectures when recrystallized at high initial monomer concentration (Figure 3-11 D). These are monolayered tubes and most probably the adoption of such morphology is caused by accumulation of additional charges on the N-terminal part due to the absence of the C-terminal SslA domain.

In case of the CN-terminal SslA truncation derivative, at low initial monomer concentration large S-layer sheets were formed with sizes greater than 1.5  $\mu\text{m}$  (Figure 3-11 E), while at high initial protein concentration many small patches can be observed (Figure 3-11 F). These latter structures are much smaller in size, being less than 400 nm and most probably formed due the high density of nuclei which all tend to consume the monomers therefore, due to a fast depletion, they cannot be extended into sheets. The patches observed could be nucleated in solution (homogeneous nucleation) and deposited on the silicon substrate or nucleated on the surface of the silicon substrate (heterogeneous nucleation) followed by the growth process. To estimate exactly which is the dominating process in this case, is very difficult. However dynamic light scattering experiments, which will be presented in section 3.2.5 suggest, that heterogeneous nucleation and growth of the patches on the silicon wafer occurs with a higher probability.

Tubes are not formed, fact that can be related to the size of the protein. This derivative is lacking the N-terminal 341 amino acids and the C-terminal 172 amino

acids resulting in a protein of 584 amino acids totally. The diminished monomers form patches but there is not enough driving force for adopting a certain curvature.

Obviously the initial monomer concentration has a great influence on the self-assembly process of SslA derivatives.

### **FACTORS THAT INFLUENCE FORMATION OF SslA SHEETS ON SOLID SUBSTRATE**

The CN-terminal SslA truncation derivative (SslA<sub>341-925</sub>CN) was able to self-assemble *in vitro* on functionalized silica wafer into nanosheets. However, for certain technical applications, morphology and size of the protein template is relevant which in fact is greatly determined by several experimental factors. In this section the experimental parameters and conditions influencing the recrystallization process of this truncated recombinant S-layer protein form are studied in detail.

#### ***Cumulative effect of initial monomer concentration, growth time and pH of the recrystallization buffer***

Protein recrystallization on surfaces is a rather complex process. It begins with nucleation meaning the fluctuational appearance of small molecular clusters. Upon addition of further protein molecules, these clusters grow and protein layers form. The number of protein molecules involved in these reactions, the rate of incorporation and the final shape of the protein crystals depends largely on crystallization conditions and kinetics.

Experiments were performed with regard to the initial monomer concentration, growth time and the charge of buffer molecules. *In vitro* recrystallization was done by first monomerizing the purified protein (initial monomer concentration of 0.43 mg/ml) with 5M GuHCl than dialysing 1/6 of the protein solution against Tris/HCl pH 7.5 for 2 hours at 4 °C without addition of any salt and in the presence of APTES functionalized silicon substrate (the substrate was added into the dialysis bag along with the protein solution). After dialysis, the substrate was washed with distilled water, dried on air and self-assembly structures imaged with AFM.

## THE RECOMBINANT S-LAYER OF *S. UREAE* ATCC 13881

Figure 3-12 A shows that under these crystallization conditions, on the Si substrate many small patches have formed on a bottom protein layer. Large layers cannot be observed. In this case the substrate bears positive charges due to the amino residues of APTES.

Keeping all the experimental parameters constant but performing the recrystallization at lower initial monomer concentration (0.17 mg/ml) and for only 1 hour, the number and shape of patches found on the functionalized Si wafer differs greatly, as seen in Figure 3-12 B. There are no more well defined patches on the Si wafer but layer like structures. The phenomena can be attributed to the lower protein concentration. Fewer monomers have the opportunity to better organize on the substrate while depletion is slower.

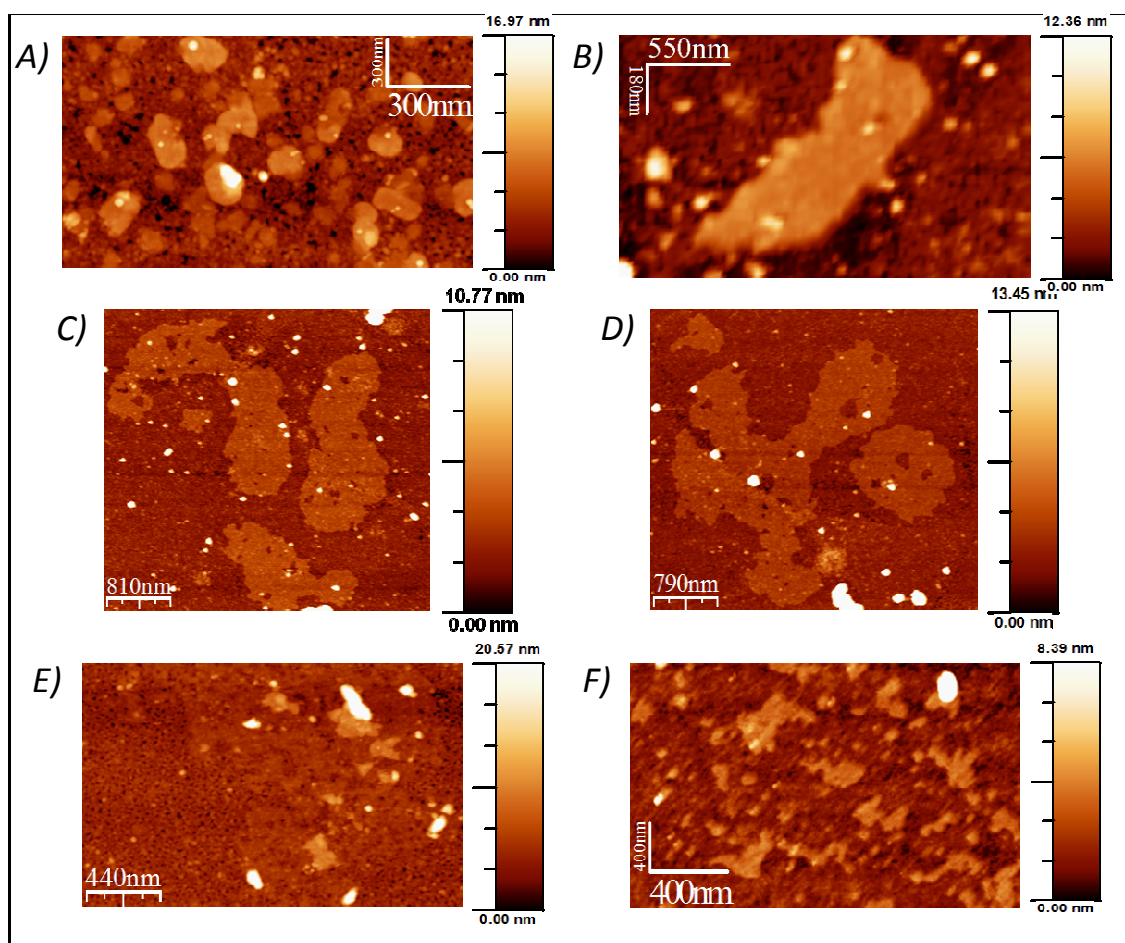


**Figure 3-12 Influence of several factors on self-assembly of SslA<sub>341-925</sub> CN on a Si wafer**

AFM images show self-assembly products recrystallized *in vitro* in the presence of an APTES-Si substrate: A) At the initial monomer concentration of 0.43 mg/ml and 2h dialysis time against Tris/HCl pH 7.5 many small patches have formed, B) Lowering the monomer concentration to 0.17 mg/ml and dialysis time to 1 hour results in layer like structures, C) and D) Large layers are obtained when the monomer concentration is increased to 0.39 mg/ml and dialysis is performed for 2 hours against Tris/HCl having pH 3, E) Increasing pH *i.e.* Tris/HCl pH 5 results only in the formation of small patches and F) There is only random deposition of the monomers when further increasing pH *i.e.* to pH 7.

When the initial monomer concentration was increased to 0.39 mg/ml, growth time to 2 hours and the pH of the recrystallization buffer set to 3, nice large layers were obtained on the Si wafer. They are shown in Figure 3-12 C and D. They are over 1  $\mu\text{m}$  long and with FFT the p4 symmetry was detected (presented in Figure 3-10).

It is mentioned in literature, that the low pH has a disrupting effect on the S-layer proteins by breaking the hydrogen bonds holding the monomers together [53]. But in this case, dialysis against a buffer of low pH, *i.e.* pH 3 facilitated the formation of protein sheets. It is commonly known that pH influences charges of the protein

molecules, their mobility and therefore the nucleation rate constant. This additional parameter in the crystallization experiments can explain the large S-layer structures obtained (Figure 3-12 C and D). Patch growth is the result of the competition between random attachment and detachment of monomers at the edges of a patch. The probability of the monomers to be desorbed depends largely on the buffer pH and surface charges of the silicon substrate. At pH 3 the monomers carry a net positive charge (pI of SslA is 5.4). Therefore, low pH *i.e.* pH 3 as additional parameter in the recrystallization experiment seems to favour proper attachment of monomers giving rise to extended protein monolayers. Monomers can bind lattice sites with maximum binding energy.

When the S-layer is recrystallized in the presence of a higher pH buffer, *e.g.* pH 5, only small patches can be observed on the APTES Si surface (Figure 3-12 E). At this pH, the SslA molecules are in equilibrium bearing no net positive or negative charges, therefore they are attracted to the silica surface. Desorption is not so fast anymore and many small nuclei form; they all tend to grow. Therefore small protein patches can be observed for which the lattice symmetry could not be estimated from the AFM images.

At an even higher pH *i.e.* pH 7, the random adsorption to the substrate is more accentuated due to the net negative charge of the protein molecules. In this case even the patch formation is difficult since due to a lack of proper orientation, the next molecules will not be able to assemble, as illustrated in the Figure 3-12 F.

### ***Influence of substrate properties***

The size and structure of the S-layer self-assembly products depends not only on the particular S-layer but also on the surface properties of the substrate. Based on this idea, a comparative study on the self-assembly of the CN-terminal truncation derivative of the recombinant S-layer of *Sporosarcina ureae* ATCC 13881 (SslA<sub>341-925</sub>CN) on two different substrates was conducted.

In particular, mica and gold substrates were used. The experiments were performed at a protein concentration of 0.64 mg/ml involving the usual steps of monomerization

## THE RECOMBINANT S-LAYER OF *S. UREAE* ATCC 13881

with 5M GuHCl and dialysis against 0.5 mM Tris/HCl pH 7.5 containing in addition 10 mM CaCl<sub>2</sub> for 2 hours at 4 °C. The dialysate was centrifuged and the supernatant containing the S-layer monomers was adsorbed on the substrates for 30 minutes in the presence of 25 mM MgCl<sub>2</sub>. After adsorption, the substrates were washed in distilled water, dried in a N<sub>2</sub> stream and imaged with AFM. Results are displayed in Figure 3-13.

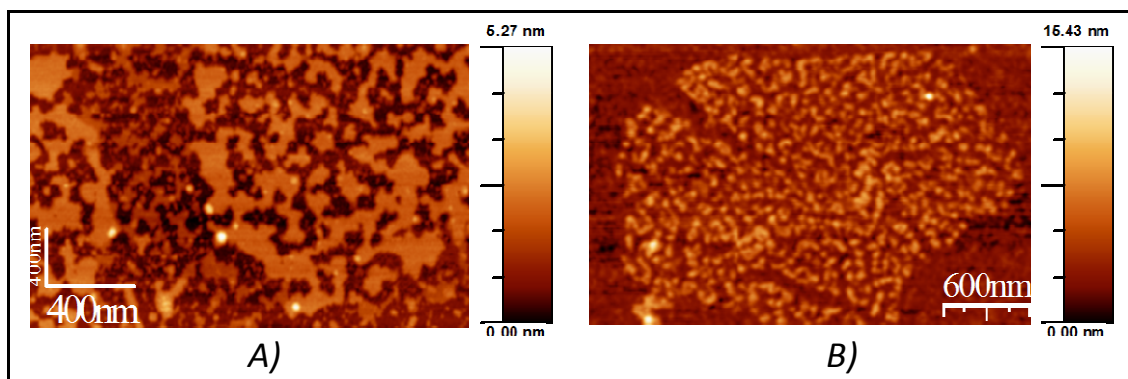


**Figure 3-13 SsIA<sub>341-925</sub>CN *in vitro* recrystallized on different substrates**

AFM micrographs show self-assembly structures formed on (A) mica and (B) gold substrate.

Distinct nucleation centres are observed on gold surface which has hydrophobic properties and an accentuated roughness (Figure 3-13 B). The monomers are only randomly organized and there is no coherent patch or layer formation. However for the same assembly time, on the mica surface already patches can be observed which tend to further grow into protein layers (Figure 3-13 A). The explanation is given with the charge of the substrate. The charge and roughness of the surface exerts a strong impact on the process of protein crystal nucleation. Under the crystallization pH (7.5), the mica is negatively charged and regarded as an atomically flat surface while the gold surface is hydrophobic. The protein monomers under these conditions bear similarly, an overall negative charge. Evidently, the electrostatic repulsion between the negatively charged mica and protein molecules favours organization and attachment of S-layer monomers to each other rather than to the substrate giving rise to the observed patches; on the other hand, the S-layer molecules are strongly attached to the gold surface and further assembly is impeded or taking place more slowly. This slow nucleation and growth on gold surfaces was already reported in the literature for



the S-layer protein SbsB of *Bacillus stearothermophilus* PV72/p2. This S-layer forms monocrystalline lattices with individual areas larger than 10  $\mu\text{m}$  in diameter on silicon wafers within 4 hours, whereas on gold surfaces the recrystallization proceeds slower and the monocrystalline areas are much smaller in comparison to silicon [158].

### 3.2.5 KINETIC STUDIES ON THE SELF-ASSEMBLY PROCESS

As shown in the preceding section, the CN-terminal SslA truncation derivative (SslA<sub>341-925</sub>CN) was still able to self-assemble into protein layers in solution and on silicon surfaces despite mutagenesis.

The objective of this section is to understand how the SslA<sub>341-925</sub>CN monomers alone drive the self-assembly reaction. To this end, the *in vitro* self-assembly kinetics was followed in real time in solution by dynamic light scattering (DLS). As the light scattering signal intensity is proportional to the square of the protein molecular weight, this technique can monitor subtle changes in the oligomeric state of the protein.

In particular, the influence of the protein concentration on the self-assembly reaction was studied. Therefore, the DLS experiments were performed at two different protein concentrations: 0.38 and 1 mg/ml, respectively. Samples were prepared by first monomerizing the desired amount of lyophilized S-layer protein with 5M GuHCl followed by removal of the chemical by dialysis against distilled water for 2 hours at 4 °C. After dialysis, the suspension was centrifuged at 14 000 g for 10 minutes and the supernatant mixed with CaCl<sub>2</sub> (final concentration 30 mM) for the assembly reaction initiation. The DLS measurements were started immediately after mixing at a total volume of 1 ml. The results are shown in Figure 3-14.

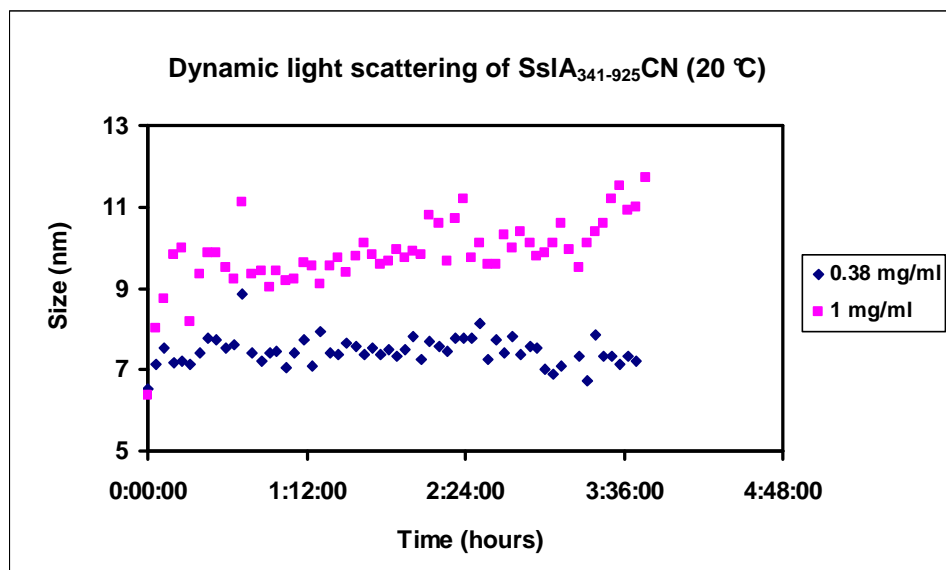


**Figure 3-14 Kinetics of SslA<sub>341-925</sub>CN self-assembly monitored by DLS**

Measurements were performed under low (0.38 mg/ml) and high (1 mg/ml) protein concentration, at 30 mM calcium concentration and a temperature of 20 °C.

Each data point shown in Figure 3-14 corresponds to the Z-average diameter obtained from the DLS measurement and is plotted as a function of time. The Z-average diameter is defined as the intensity weighted mean average for the ensemble collection of particles in the sample derived from the slope of the linearized form of the correlation function.

As observed from Figure 3-14, the self-assembly reaction proceeds differently at low and high initial monomer concentration. Initially the truncated SslA molecules present in solution have a size of approximately 6.5 nm and this size corresponds to the size of an individual monomer. At low monomer concentration, *i.e.* when there are only a few monomers in the protein solution, this size is not substantially increased, meaning that there is no self-assembly. Over the time, the SslA molecules do not associate and form the lattice structure.

However at high protein concentration, there is self-assembly occurring and the size of the self-assembled structures is in the range of 11 or 12 nm. Interestingly, these stable clusters are in the size range of the S-layer unit cell. However, formation of larger layers is not observed over the time period of 4 hours.

Contrarily to this behaviour, the native SslA does self-assemble into larger structures

(200 - 400 nm in size) under the same experimental conditions (see section 2.2.3). The difference is most probably caused by the truncation of the protein. By deletion of both, N- and C-terminal parts, the aggregation probability is diminished and as a consequence, self-assembly or growth of the clusters does not occur.

### 3.3 CONCLUSIONS AND OUTLOOK

The focus of this chapter was to characterize the recombinant S-layer protein of *Sporosarcina ureae* ATCC 13881. After the successful cloning with the help of the Ek/Lic cloning strategy, the mature form of this recombinant S-layer protein could be expressed in *E. coli* cells; however the level of expression was low. The His<sub>6</sub> tag on its N-terminal part facilitated purification from the host cells and as concluded from the *in vitro* recrystallization experiments, it did not interfere with its self-assembling properties. When self-assembly proceeded in solution, the recombinant SslA recrystallized into sheet and tube like structures. The reaction proved to be concentration and time dependent; that is for a higher initial monomer concentration tube formation could be detected at an earlier time point than in case, when less monomers were brought into the self-assembly reaction. *In vitro* recrystallization on a Si wafer resulted micrometer sized, crystalline monolayers exhibiting the p4 symmetry, the lattice structure resembling the one of authentic S-layer of *Sporosarcina ureae* ATCC 13881. The remarkable property of isolated recombinant SslA subunits to *in vitro* self-assemble as well as the repetitive morphological feature of the obtained monolayers combined with a high porosity make them an attractive candidate for biological functionalization of surfaces, *e.g.* in case of Si-based sensors or even as novel organic coatings. The tubular structures may find applications in encapsulation and release of molecular cargoes on purpose.

With the various truncated SslA forms cloned, expressed and purified from *E. coli* cells, it could be demonstrated that the N-terminal part of this S-layer protein is not required for the self-assembly. Similarly, the C-terminal part can be deleted without interfering with the self-assembly process. Moreover, the deletion of both, the N- and

C-terminal SslA domains does not have an influence on the self-assembly properties; the resulting protein is able to form extended monolayers that exhibit the p4 lattice symmetry. The lattice constant of 6.6 nm revealed substructures in the S-layer lattice, data that until now was not at all reported for any of the S-layer proteins studied. But more importantly, it became clear that this central protein part is self-sufficient and most likely responsible for the intrinsic ability of this S-layer to self-assemble in solution and on a solid substrate *i.e.* on Si wafer. At the moment there is no available crystal structure of the SslA protein, although this would allow a precise positioning and determination of the amino acids that contribute to this intrinsic ability. A 3D model indeed would provide substantial information. In case of proteins, this can be accomplished by fold prediction. Preliminary data alignment (not presented in this work) has confirmed the finding of an appropriate fold from a Surface Protein with a high score, making therefore possible in the future a 3D model building of SslA.

Furthermore, the CN-terminal SslA derivative with preserved self-assembly potential and exhibiting the p4 symmetry can be further engineered for the construction of recombinant, functional SslA fusion proteins that combine the self-assembly properties with a broad spectrum of specific functions (*e.g.* ligands, antibodies, antigens and enzymes) which would open up new possibilities for their application in bio- and nanotechnology.

For the design of the S-layer fusion proteins, the crystallization behaviour of the wild type S-layer protein is most important because functional domains have to be inserted at favorable positions in the polypeptide chain. Therefore, some factors that influence the *in vitro* recrystallization process were studied in detail in this section for the CN-terminal SslA truncation derivative. It became clear that in solution, the initial monomer concentration plays an important role and depending on the density of molecules in the protein solution, the self-assembly products have the shape of small patches which are unable to extend due to a fast monomer depletion or tubes that have formed as a result of the fewer nuclei, grown into protein layers which have folded into cylinders. On a silicon wafer, the morphology of the grown sheets changes according to the protein concentration, pH and time allowed for recrystallization.

Finally, the recombinant SslA protein can be regarded as a new building block for

## THE RECOMBINANT S-LAYER OF *S. UREA* ATCC 13881

various bio- and nanotechnologically relevant applications. In contrast to the *in vivo* assembled authentic SslA, this recombinant variant offers more competing possibilities and attractive features that can be used for broadening the application potential of S-layers.

# CHAPTER 4

## 4 THE SSLA-STREPTAVIDIN FUSION PROTEIN

An important line of development is directed towards the genetic manipulation of S-layers. The possibility to change the natural properties of S-layers by mutagenesis opens a new horizon for the tuning of their structural and functional features by genetic engineering. Incorporation of peptide segments corresponding to specific functional domains of other proteins while maintaining the self-assembly capability should lead to completely new structures with broad application potential.

Since one of the most relevant areas of nanobiotechnology concerns technological utilization of self-assembly systems, it appeared useful to advance the S-layer technology by construction of a recombinant functional SslA fusion protein. The aim of the construction of an SslA fusion protein was to combine the self-assembly properties of the S-layer moiety with the specific function of another protein moiety.

Streptavidin binds the small molecule biotin with femtomolar affinity and this tight and specific non-covalent interaction has caused the streptavidin-biotin system to be widely used for biomolecule labelling, purification, immobilization and patterning. Hence, this protein was chosen for constructing a chimeric SslA protein, which is the focus of this chapter.

In the following, after cloning and expression, the SslA-streptavidin chimeric protein is characterized with respect to its self-assembling properties in solution and on a silicon substrate. Furthermore, the accessibility of the streptavidin domain in the fusion protein lattice is investigated with biotinylated quantum dots.

## 4.1 DESIGN OF THE SSLA-STREPTAVIDIN FUSION PROTEIN

Molecular self-assembly systems that exploit the molecular scale manufacturing precision of biological systems are prime candidates for controlled “bottom-up” production of defined nanostructures [163, 164, 165].

To this respect, S-layers represent a unique self-assembly system as they form highly ordered arrays with different symmetries [166, 58, 165]. However, their technological utilization can be extended by the design of functional recombinant S-layer fusion proteins. By genetic modifications, S-layers can be functionalized with a broad spectrum of specific functions (*e.g.* ligands, antibodies, enzymes antigens) providing an unsurpassed precision in spatial control and alignment of functions encoded in proteins [167, 168, 169, 170]. Moreover, nanobiotechnology can employ these fusion proteins as building blocks for precise nanoscale engineering.

Functional S-layer fusion proteins comprising heavy chain camel antibodies [171, 170], IgG binding domains and the major birch pollen allergen Bet v16 [168] have already been constructed, recrystallized and used for binding of biologically active molecules, development of novel types of antiallergic vaccines [83] or exploited as a new type of sensing layer in label free detection systems such as SPR and QCMD [170, 171]. All these applications are biotechnologically relevant.

In this work a functional domain of streptavidin termed core-streptavidin was fused to the central part of SslA (**SslA<sub>341-925</sub>CN**) by genetic engineering. So far, construction of an S-layer fusion protein from a truncated S-layer version and streptavidin has not yet been reported in the literature. The aim of the construction of this S-layer fusion protein was to combine the self-assembly properties of the SslA protein with the specific ligand *i.e.* biotin binding function of streptavidin. Since the central part retains the intrinsic ability of this S-layer to self-assemble in solution and on a Si wafer into lattices of identical symmetry, it was considered for construction of the chimeric protein.

Streptavidin binds the small molecule biotin with femtomolar affinity and this non-covalent interaction is the strongest in nature.

## THE SSLA-STREPTAVIDIN FUSION PROTEIN

---

It was shown already that the protein part consisting of residues 16-133 is enough for biotin binding [172]. For fusion, this minimal sized form of streptavidin, termed “core-streptavidin”, that still retained the full biotin-binding activity, was used.

In the design of this fusion protein, an important prerequisite was the preserved self-assembly potential of the S-layer part. In the previous chapter it became clear that SslA<sub>341-925</sub>CN is able to self-assemble *in vitro* in solution and on Si surfaces into monolayers exhibiting the p4 lattice structure. Because in this lattice structure, one morphological unit consists of four monomers, a protein moiety fused to SslA<sub>341-925</sub>CN, provided that it does not interfere with lattice formation, will be presented with the same spacing *i.e.* four streptavidin molecules per lattice unit.

Moreover the insertion of the functional domain has to be done at favourable positions in the polypeptide chain so that the whole fusion protein preserves the self-assembling ability and presents the additional function of the fused protein domain. Until now, no structural model at atomic resolution of SslA is available. The position for a functional fusion was selected based on the results of previous studies showing that usually the C-terminus of S-layers can be modified without affecting the protein properties and function [173] and on the fact that SslA despite the lack of its C-terminal part has a preserved self-assembly potential. In this context, core-streptavidin was fused to the C-terminus of the SslA<sub>341-925</sub>CN.

The construct was named SslA<sub>341-925</sub>CN-cstrp and the strategy for obtaining is shown in Figure 4-1:



## THE SSLA-STREPTAVIDIN FUSION PROTEIN

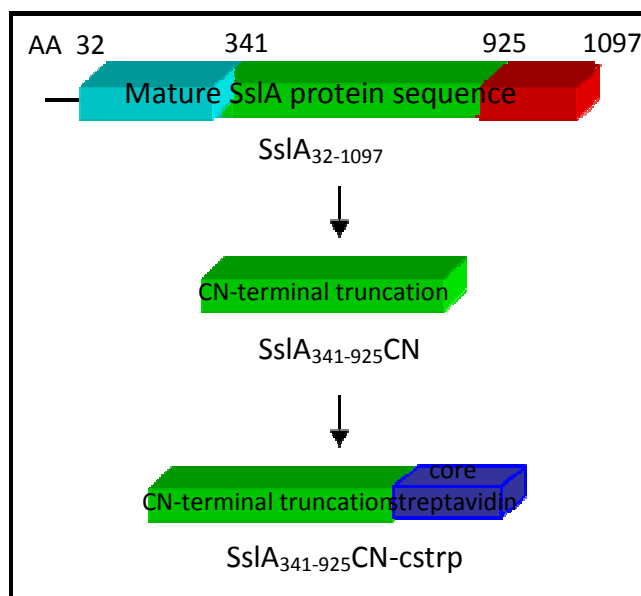


**Figure 4-1 Strategy to yield SslA<sub>341-925</sub> CN-cstrp fusion protein**

Fusion of streptavidin to a truncated SslA version - in this case to SslA<sub>341-925</sub>CN - constitutes an advantage over the fusion to the whole (mature) SslA sequence because it is shorter and in this sense, the chance that the fusion protein will be correctly folded is higher.

The DNA fragment encoding this S-layer fusion protein was created by overlap extension PCR. At first the gene encoding core-streptavidin was amplified by PCR from the pET11 plasmid using primers B and D (see Appendix). Second, the gene encoding the SslA<sub>341-925</sub>CN was amplified using primers A and C (see Appendix). The two amplified DNA fragments were purified, then mixed in a third PCR reaction for obtaining the fusion protein using primers A and D. The chimeric gene was finally cloned into the pET46 Ek/Lic (Novagen) vector using the Ek/Lic cloning strategy. The recombinant plasmid pET46Ek/Lic-SslA<sub>341-925</sub>CN-cstrp was transformed into *E. coli* Nova Blue Giga Singles (Novagen) competent cells as a non-expression host. The successful cloning was confirmed by the restriction analysis of the insert and sequencing.

The gene encoding SslA<sub>341-925</sub>CN-cstrp fusion protein consists of 2160 bps which translates into an S-layer protein of 719 amino acids with a molecular weight of 76.5 kDa and pI of 5.36. The final protein structure contains additionally an N-terminal His<sub>6</sub> tag and the Lic arm.

## 4.2 CHIMERIC GENE EXPRESSION, ISOLATION AND PURIFICATION

For heterologous expression of the chimeric gene, pET46Ek/Lic-SsIA<sub>341-925</sub>CN-cstrp plasmids from positive clones were transformed into *E. coli* Rosetta Blue (DE3) cells as expression host. Recombinant gene expression was induced with IPTG (1 mM final concentration) and carried out at 30 °C for 5 hours. Culture samples were harvested before and 1, 3 and 5 hours after induction and subjected to SDS-PAGE analysis. In comparison to *E. coli* Rosetta Blue (DE3) cells harvested before the addition of IPTG (Figure 4-2 0h), an additional high molecular mass protein band is observed which corresponds to the chimeric SsIA<sub>341-925</sub>CN-cstrp protein (Figure 4-2 1h). This additional protein band has an apparent molecular weight of 76 kDa which corresponds to the theoretical molecular mass calculated for this S-layer fusion protein. The intensity of this protein band didn't increase with time of expression *i.e.* after 3 or 5 hours of induction (Figure 4-2 3h and 5h).

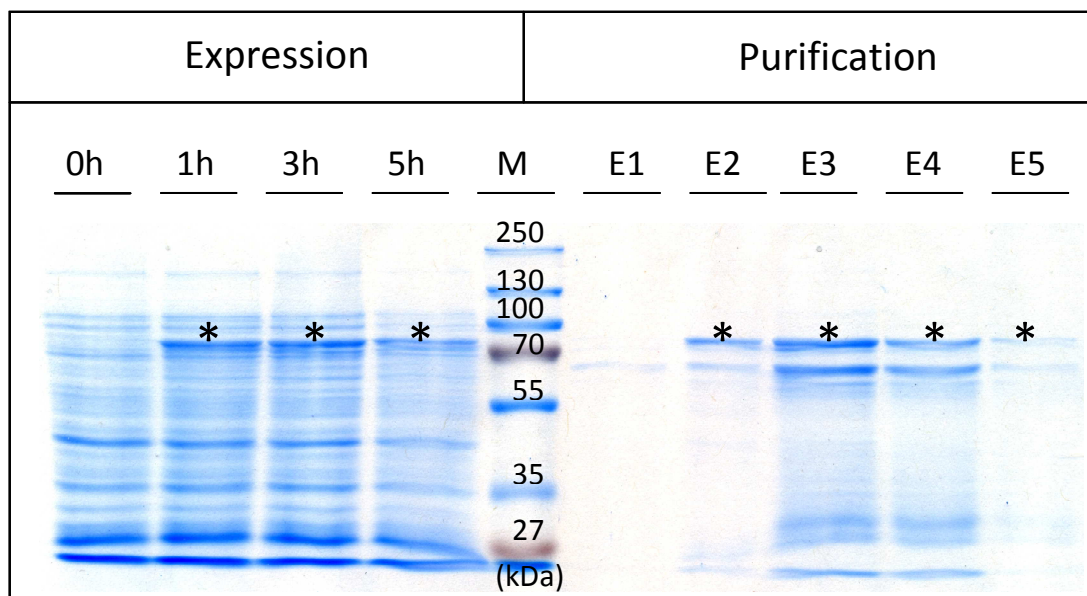


**Figure 4-2 Heterologous expression of SsIA<sub>341-925</sub>CN-cstrp in *E. coli* and purification**

The Coomassie stained protein gel shows expression in Rosetta Blue (DE3) whole cell lysates after 0, 1, 3, and 5 hours of induction with 1 mM IPTG. E1-E5 mark the elution fractions of the Ni<sup>2+</sup> affinity chromatography. M-protein ladder (Page Ruler™ Plus Prestained). 20 µg recombinant protein was loaded on the gel and its position is marked with star.

## THE SSLA-STREPTAVIDIN FUSION PROTEIN

---

The chimeric protein could be isolated from the soluble fraction of lysed *E. coli* cells. In the literature it was reported that streptavidin fused to the C-terminal of the S-layer protein of *Geobacillus stearothermophilus* PV72/p2 (SbsB) accumulated in the soluble fraction [174] as well.

After isolation, the chimeric protein was subjected to Ni<sup>2+</sup> affinity chromatography. This purification procedure was chosen because the protein is expressed with an N-terminally encoded His<sub>6</sub> tag. Fractions containing the purified protein were pooled, dialysed against distilled water for 12 hours at 4 °C and analysed by SDS-PAGE. Results of purification are shown in Figure 4-2. The chimeric protein eluted at the expected molecular mass (76 kDa) indicating that is mainly monomeric (Figure 4-2 E2-E5). In addition to the band corresponding to the fusion protein, another band can be observed as well after purification. Similar results have been reported by Posseckardt J [175].

The purification procedure yielded about 20 mg pure protein from 3 L cell culture. In comparison to the recombinant SslA (mature form), this amount is lower.

For further experiments *i.e. in vitro* recrystallization, the protein from the last elution fraction was used since this was the most pure one.

In conclusion, the SslA-corestreptavidin fusion protein could be successfully produced in *E. coli* and purified. These are important prerequisites for self-assembly experiments which are discussed in the next section.

### 4.3 SELF-ASSEMBLY OF THE CHIMERIC S-LAYER PROTEIN

After expression and purification, the self-assembly capability of the chimeric protein was tested. To this end, *in vitro* recrystallization experiments were performed in suspension and on a silicon substrate. Methods for visualization of the self-assembly products involved transmission electron microscopy (TEM) and atomic force microscopy (AFM).

#### 4.3.1 *IN VITRO* RECRYSTALLIZATION IN SOLUTION

To investigate the self-assembly properties of isolated SslA<sub>341-925</sub>CN-cstrp, the purified S-layer fusion protein was monomerized with 5M GuHCl (at a protein concentration of 1 mg/ml). The chemical was subsequently removed by dialysis against distilled water for 3 hours at 4 °C. After dialysis, the protein solution was centrifuged at 14000 g for 10 minutes and the supernatant containing the fusion protein monomers was diluted to 0.1 mg/ml with 0.1 mM CaCl<sub>2</sub> and 0.5 mM Tris/HCl buffer pH 9 until a total volume of 10 ml. 5 ml of this mixture was pipetted into a cell culture well and the fusion protein allowed to recrystallize for 48 hours. After recrystallization, protein samples were taken out and prepared for TEM imaging. The self-assembly structures formed during the *in vitro* recrystallization are shown in Figure 4-3:

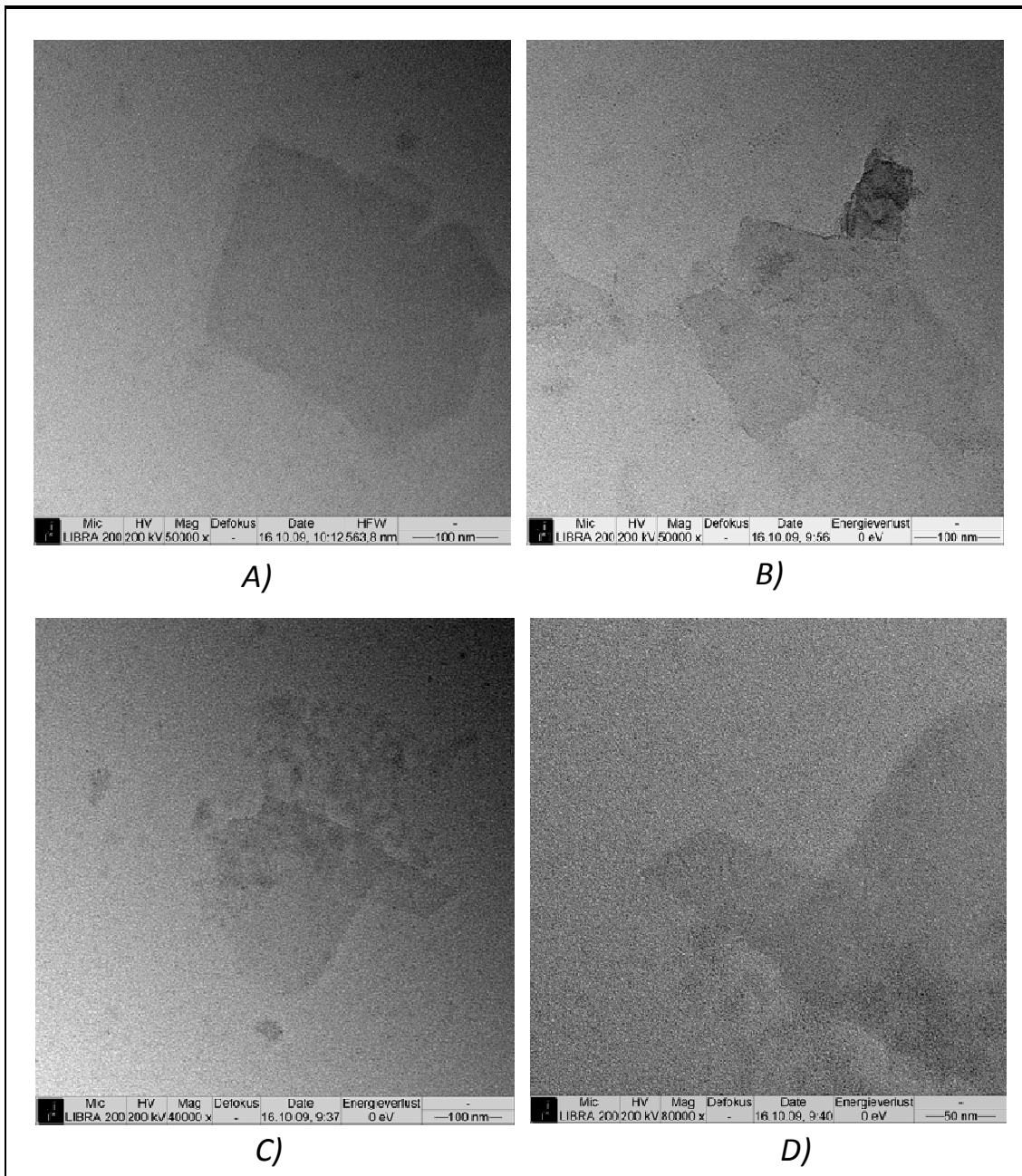


**Figure 4-3** *In vitro* recrystallization of SslA<sub>341-925</sub>CN-cstrp in solution

A), B), C) and D) TEM micrographs showing the self-assembly structures obtained

As it can be observed from Figure 4-3, the S-layer fusion protein comprising the CN-terminally truncated derivative of SslA and core-streptavidin was able to self-assemble in suspension into crystalline chimeric S-layer sheets. Square shaped coherent monolayers were formed, which have a size of approximately 200-250 nm, however multilayered structure can also be recognized (Figure 4-3 A). The square like edges of

the protein layer resembles to the structure and shape of the authentic S-layer form. The structure of the coherent monolayer(s) generated on the silicon substrate is not monocrystalline over the entire surface but consists of randomly aligned crystalline domains. In this context, the structure can be addressed as being polycrystalline and it is formed by patches that grow individually on the silicon wafer until reaching neighbour edges, than grow into each other as it can be observed in Figure 4-3 B. The small patches are by themselves monocrystalline and typically in the range of 100 nm. The lattice parameters or the p4 symmetry for the individual layers could not be determined with Fast Fourier Transformation of electron micrographs although the S-layer part without the fusion partner self-assembled into lattices exhibiting the square symmetry (see Chapter 3, Section 3.2.3). When core-streptavidin was fused to the S-layer protein SbpA of *Bacillus sphaericus*, the chimeric protein had maintained the ability to recrystallize into the square lattice structure on plain gold chips [173]. The reason for why in case of SslA<sub>341-925</sub>CN-cstrp lattice symmetry could not be identified could be that the lattice symmetry has been disturbed due to the fusion of the core-streptavidin domain in the S-layer structure.

Folding of protein layers into tube like structures is very common among S-layers. The native S-layer protein of *Sporosarcina ureae* ATCC 13881, but also its recombinant form, was able to fold into tubes. When recrystallization proceeds in solution, it is very likely that the growing patches acquire a certain curvature and fold until patch edges meet each other. Even with deletion of a certain number of amino acids, tube formation was preserved e.g. in case of SslA<sub>32-925</sub>C and SslA<sub>341-1097</sub>N. Both derivatives form tubular structures. However, folding was not observed anymore for the SslA<sub>341-925</sub>CN. The reason could be the destroyed asymmetry of this derivative by deletion of both, N- and C-terminal parts. Folding is driven by asymmetric surface structures of the S-layer i.e. different outer and inner surface. Cutting results a higher symmetry and no difference in surface energies that could cause the cylindrical curvature to appear. As a consequence, folding does not occur.

In case of the SslA<sub>341-925</sub>CN-cstrp chimeric protein, folding of the protein layer is again present as shown in Figure 4-3 C and D. With the fusion of the streptavidin domain to

SsIA<sub>341-925</sub>CN, the amino acid sequence is extended to a number of 719 amino acids. Therefore it can be supposed that a minimum number of amino acids in the protein sequence (in case of this S-layer a minimum of 719 amino acids) is a requirement for tube formation. But most certainly, not only the molecular structure of the protein, but also the recrystallization conditions affecting surface charges in the protein structure, could have an impact on this phenomenon.

Since the microscopy grids were rendered hydrophilic, the recrystallized fusion protein could orient with its hydrophilic, charged face towards the substrate and exposes its hydrophobic side. In case of double layered structures, the constituent layers are facing each other with their hydrophobic part.

The fusion of core-streptavidin protein domain to SsIA<sub>341-925</sub>CN did not compromise the self-assembly properties of the S-layer. Therefore the core-streptavidin domain might be located either above or under the plane of the whole fusion protein structure.

### 4.3.2 *IN VITRO* RECRYSTALLIZATION ON SILICON WAFER

For *in vitro* recrystallization of the SsIA<sub>341-925</sub>CN-cstrp on the silicon substrate, 0.5 mg of fusion protein was at first dissolved in 5M GuHCl than 1/5 of the monomer solution was dialysed against 10 mM Tris/HCl buffer pH 3 for 2 hours at 4 °C in the presence of an APTES functionalized Si substrate. After dialysis, the substrates incubated with the protein solution were washed with distilled water, dried on air and subsequently imaged by means of AFM. The topographical images of the SsIA<sub>341-925</sub>CN-cstrp protein layer recrystallized on silicon are shown in Figure 4-4.

As demonstrated in Figure 4-4 A and C, the fusion protein was able to self-assemble into crystalline S-layer sheets on the Si wafer. There are not only monolayers present on the substrate but also double layer formation can be observed. The monolayers on the silicon wafer have a size between 500 and 700 μm, while the double layers are relatively smaller in size. Indeed, the whole self-assembly structure extends to more than 1 μm in length. The height of one layer is approximately 3.5 nm (Figure 4-4 B).

The widely spread white dots on these protein layers represent distinct nucleation

## THE SSLA-STREPTAVIDIN FUSION PROTEIN

points on the underlying protein layers. They are clearly visible on the 3D image of the structures depicted in Figure 4-4 D as well. Nucleation is the first step of the protein recrystallization in which monomers join into small clusters. After acquiring a certain size, these clusters grow into protein layers. In this case they might give rise to another protein layer on the already existing chimeric protein sheets.

The p4 lattice symmetry and the lattice parameters of the chimeric protein could not be identified with Fast Fourier Transformation analysis of the AFM micrographs. The reason could be the following: the pores of the native SslA protein are 2 nm wide while the wild type streptavidin molecule has a height of 2 nm and a diameter of 11 nm. For fusion only part of this protein i.e. core-streptavidin was used, but this molecule is still large enough to cover the pores of SslA-corestreptavidin fusion protein. As a consequence, the lattice periodicity cannot be observed.

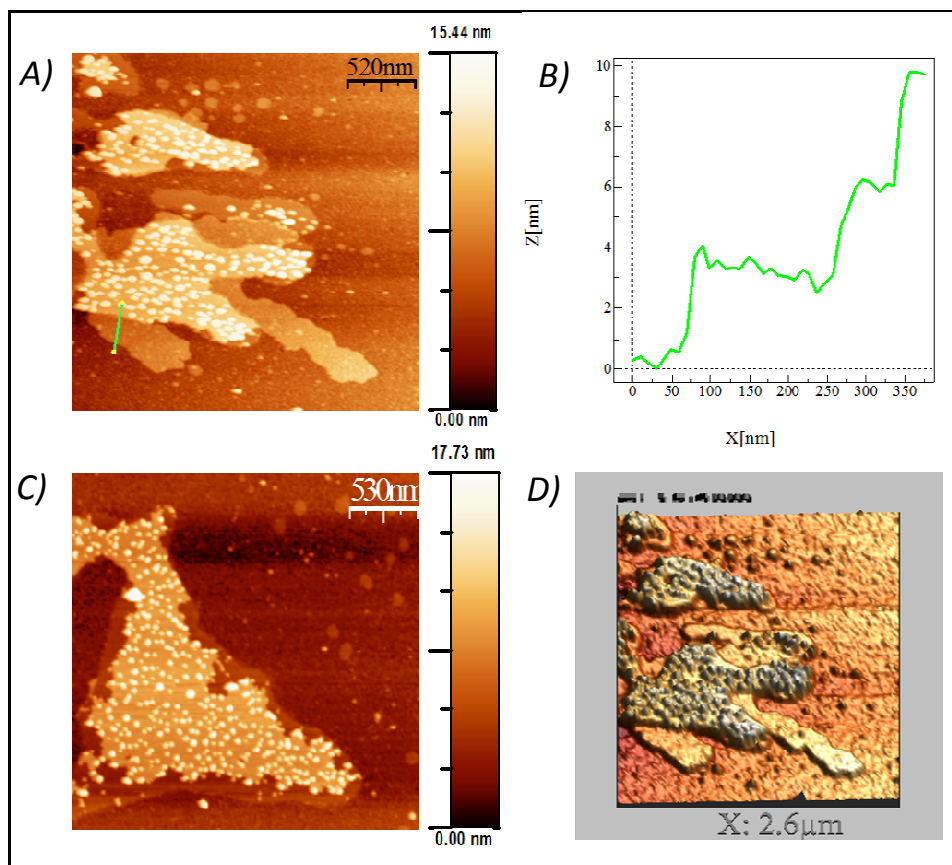


**Figure 4-4** *In vitro* recrystallization of SslA<sub>341-925</sub>CN-cstrp on a Si wafer

(A), (C) The chimeric protein was recrystallized *in vitro* at pH 3 in the presence of an APTES functionalized Si substrate (B) Height profile and (D) 3D reconstruction based on image A.



However, the *in vitro* recrystallization experiment on the silicon demonstrates once again that fusion of a functional protein domain does not interfere with the self-assembling properties of the engineered recombinant fusion protein composed of the central part of SslA and core-streptavidin. Whether the streptavidin domain in the chimeric protein lattice is exposed and sterically accessible for binding of biotinylated targets, is the subject of the next section.

### 4.4 DETERMINATION OF BIOTIN BINDING ABILITY

The SslA<sub>341-925</sub>CN-cstrp fusion protein was constructed from the CN-terminally truncated version of the S-layer of *Sporosarcina ureae* ATCC 13881 and the minimal sized streptavidin domain that still retains full biotin-binding activity. Since this latter protein domain was descended from wild type streptavidin it was assumed to show the typical high affinity for biotin. However, it remained to be investigated whether the biotin binding sites remain exposed and sterically available after the fusion or they are blocked by the S-layer partner. To test this, biotinylated quantum dots were used in a gel shift assay and as a marker that can be visualized by TEM. With the gel shift assay the binding to the chimeric protein monomers was tested, while in a second method it was analysed whether the core-streptavidin domains are exposed on the recrystallized S-layer fusion protein template. For various technological applications this latter one has a greater importance.

#### 4.4.1 INTERACTION OF BIOTINYLATED QUANTUM DOTS AND SslA<sub>341-925</sub>CN-CSTRP MONOMERS

The binding of biotinylated quantum dots to the SslA<sub>341-925</sub>CN-cstrp monomers was confirmed by electrophoretic mobility shift assay (EMSA). This method is based on the difference in migration pattern of biotinylated quantum dots bound to the fusion protein and unconjugated quantum dots. It is frequently used in molecular biology for indicating if more than one molecule is involved in the binding complex.

## THE SSLA-STREPTAVIDIN FUSION PROTEIN

---

The quantum dot-biotin conjugate is made of a core nanometer-scale crystal of CdSe semiconductor material which has been coated with an additional semiconductor shell (ZnS) to improve the optical properties of the material. This core shell material is further coated with a polymer shell that allows the materials to be conjugated to biological molecules and to retain their optical properties. This polymer shell has been directly coupled to biotin through a carbodiimide - mediated coupling reaction which yields a material with a high loading of biotin on the surface (typically 5-7 biotin molecules/Qdot conjugate [176]) and high specific biological activity. The Qdot-Biotin conjugate has the size of a large macromolecule or protein (~10-12 nm).

The Qdot-Biotin conjugates have an emission maximum near 605 nm and an excitation wavelength around 400 nm.

For binding of biotinylated quantum dots to the SslA<sub>341-925</sub>CN-cstrp monomers, 1 mg of isolated and purified fusion protein was monomerized with 5M GuHCl followed by removal of the chemical by a dialysis step against distilled water for 2 hours at 4 °C. After dialysis, the protein solution was centrifuged for 10 minutes at 14 000 g and the supernatant containing the fusion protein monomers was mixed with quantum dots. Mixtures containing different amounts of the fusion protein (5, 15, and 50 µg, respectively), 20 mM quantum dots and 10 µl 20 mM KHPO<sub>4</sub> pH 6.4 were incubated for 2 hours at RT, then separated on a 1% agarose gel at 80 V for 2 hours. Results of the gel electrophoresis are shown in Figure 4-5:

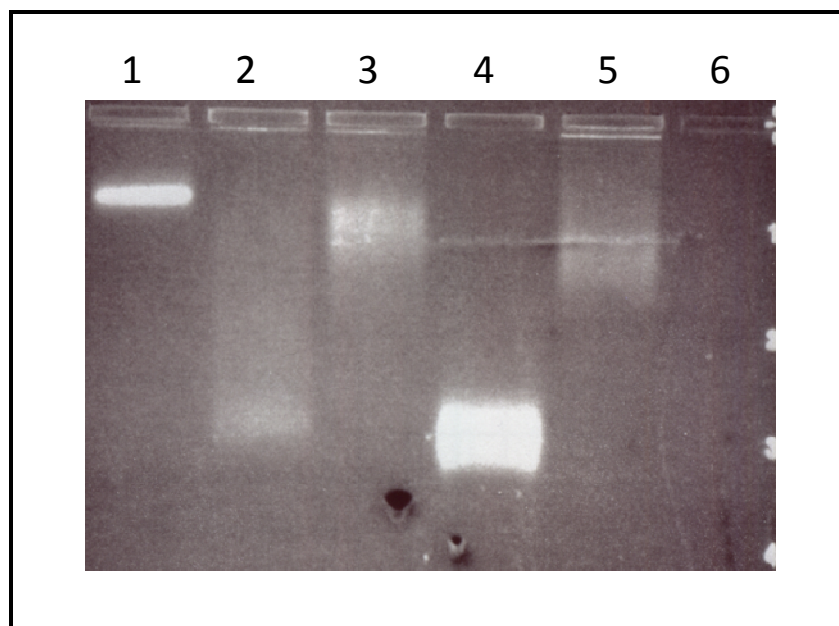


**Figure 4-5 Electrophoretic mobility shift assay (EMSA) of SsIA<sub>341-925</sub>CN-cstrp and biotinylated quantum dots.**

Numbers on top indicate:

- (1) 50 µg SsIA<sub>341-925</sub>CN-cstrp + biotinylated quantum dots
- (2) 5 µg SsIA<sub>341-925</sub>CN-cstrp + biotinylated quantum dots
- (3) 15 µg SsIA<sub>341-925</sub>CN-cstrp + biotinylated quantum dots
- (4) biotinylated quantum dots
- (5) 5 µg wild type streptavidin + biotinylated quantum dots
- (6) SsIA<sub>341-925</sub>CN-cstrp.

In the gel electrophoresis technique, a constant electric field is applied so that the charged nanoparticles migrate through the porous gel matrix with a characteristic mobility that depends on both particle size and surface net charge density. The quantum dots are negatively charged and in the gel they migrate in the direction of the anode. The migrating speed and distance made is proportional to their molecular weight. In this case the quantum dots are functionalized with biotin. Biotin is able to bind to streptavidin and this interaction is known to be strongest noncovalent interaction in nature. Upon binding of biotinylated quantum dots to the SsIA<sub>341-925</sub>CN-cstrp monomers, their migration in agarose gel will be slower than compared to the unbound quantum dots. This behaviour becomes evident when Lane 1 and 4 is

## THE SSLA-STREPTAVIDIN FUSION PROTEIN

---

compared. Lane 1 contains 50 µg of the fusion protein mixed with quantum dots and displays a visible band that is found at a smaller migration distance in comparison to Lane 4 where only quantum dots were run. The slower migration proves that biotinylated quantum dots bind to the chimeric S-layer protein.

However migration of the quantum dots is greatly influenced by the protein amount it binds. In Lane 3, 15 µg of fusion protein was incubated with the biotinylated quantum dots and migration is observed as being slower in comparison to lane 2, which contains only 5 µg of the fusion protein mixed with quantum dots. In addition, these two lanes have an appearance of a smear (spreading of the quantum dots according to how many molecules they bind). The migration pattern of these two lanes is slower in comparison to single quantum dots. This fact shows once again the successful binding of the fusion protein to the biotinylated quantum dots.

As a positive control, Streptavidin (5 µg) was also incubated with biotinylated quantum dots (Lane 5). Migration shows similarly a smear and a slower migration pattern in comparison to single QDs. The fusion protein itself cannot be visualized under UV light, therefore Lane 6 does not show any visible band (negative control).

KHPO<sub>4</sub> seems to enhance the conjugation process. This is the buffer in which wild type streptavidin is stored and it seemed to be relevant when incubating the fusion protein with the biotinylated quantum dots. When Tris/HCL pH 9 was used as a conjugation buffer, binding occurred as well, but the process is much more efficient when KHPO<sub>4</sub> is present in the reaction at a concentration of 20 mM and a pH of 6.5. Most probably the pH plays an important role as it screens the present charges and in this way favours conjugation.

GuHCl interferes with the gel electrophoresis process; therefore by the preparation of monomer solution a dialysis step was inevitable. After dialysis, a centrifugation step ensured that fusion protein monomers are mixed with the biotinylated quantum dots.

Interestingly, the quantum dot/S-layer fusion protein complexes were not too large to enter the gel. Other studies reporting about the EMSA of QD/DNA complexes [177] have evidenced that QDs completely inhibited the DNA from moving towards the positive electrode when the QDs/DNA was just at or excessive stoichiometry. The

phenomenon was accounted to the negative charges of DNA that were counteracted by the positively charged QDs or to the large size of the newly formed complexes unable to enter the gel. As shown above, this problem was not encountered during the EMSA of SslA<sub>341-925</sub>CN-cstrp and biotinylated quantum dots.

Fusion of the same core-streptavidin domain to the S-layer protein of *Bacillus stearothermophilus* ATCC 12980 (SbsC) has been described by Posseckardt J [175]. The biotin binding ability was similarly tested with EMSA of the S-layer/core-streptavidin fusion protein and biotinylated DNA; however binding could not be proved. Several reasons were suggested. For instance, the fusion protein was not at all able to bind biotinylated molecules. Or the DNA molecule (4300 bps long) was too large in comparison to the fusion protein. It has been also discussed that binding solely occurs when wild type streptavidin monomers are added to the mixture as it is known that this protein is tetrameric and the biotin binding site lies at the interface between the 4 protein subunits [178, 179].

#### 4.4.2 BINDING OF BIOTINYLATED QUANTUM DOTS ONTO THE RECRYSTALLIZED

##### SSLA<sub>341-925</sub>CN-CSTRP PROTEIN TEMPLATE

To determine whether the streptavidin moiety of the crystalline chimeric S-layer assembly is sterically accessible for binding of biotinylated targets, biotinylated quantum dots were chosen because they can be easily visualized in TEM and have uniform properties.

For the binding studies, at first chimeric protein layers were formed by *in vitro* recrystallization in solution as described in section 4.3.1 and afterwards immobilized onto plasma treated carbon-coated copper grids and allowed to adsorb for 1 hour. Biotinylated quantum dots (at a concentration of 0.02 nM in 20 mM KHPO<sub>4</sub> buffer) were allowed to adsorb for 60 minutes onto the S-layer sheets. Excess particles were washed away with several drops of TBS buffer and the samples additionally stained with 2% uranyl formiate for 20 seconds. TEM images of the patterned protein layers are shown in Figure 4-5 and reveal that the biotin functionalized quantum dots have

bound onto the surface of the S-layer chimeric protein lattices.

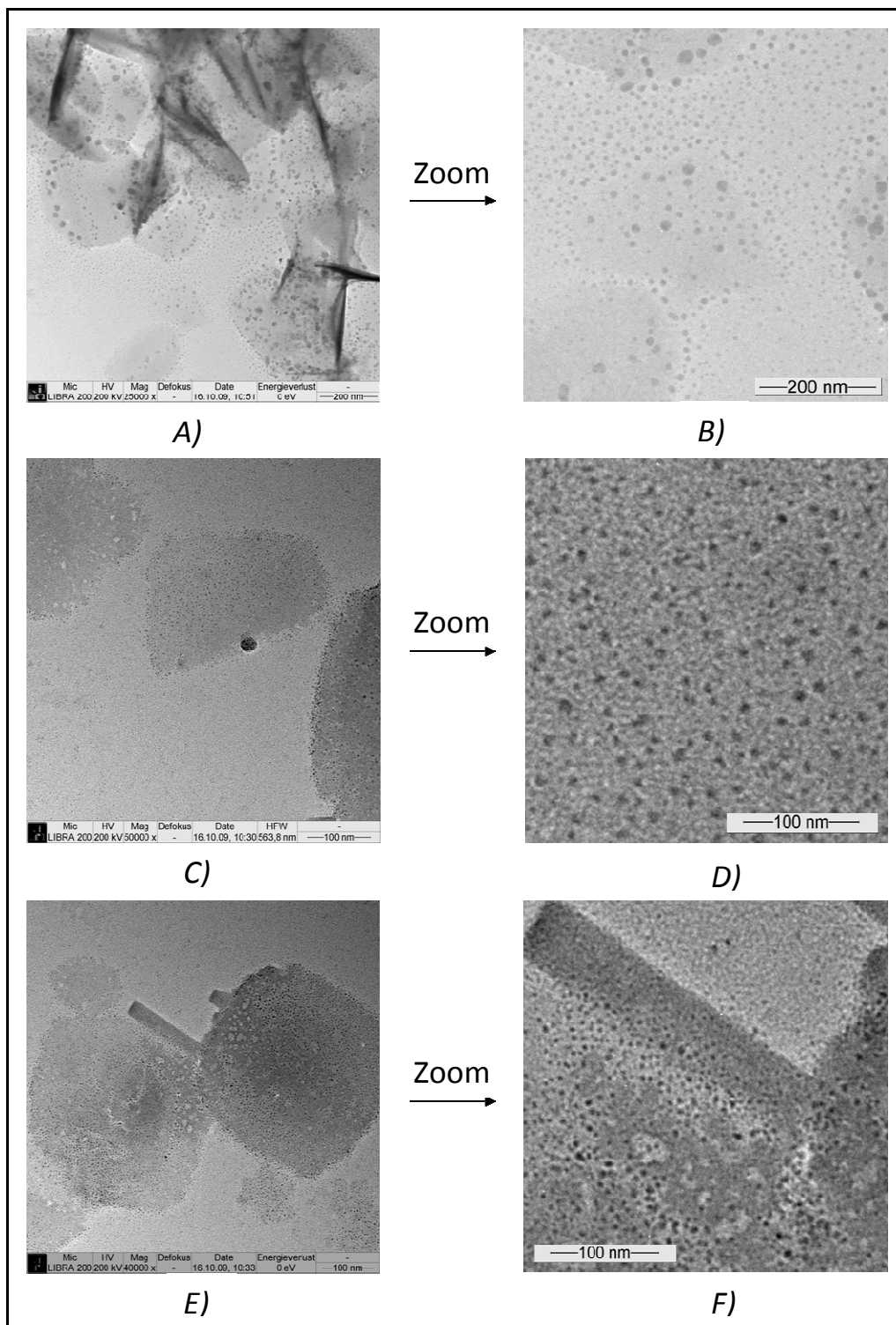


**Figure 4-6 Biotemplating of biotinylated quantum dots onto the chimeric protein template**

A), C), E) The *in vitro* recrystallized SslA<sub>341-925</sub>CN-cstrp fusion protein layers were immobilized onto plasma treated C-Cu grid followed by the adsorption of biotinylated quantum dots onto the these layers B) Zoom of image A D) Zoom of image C and F) Zoom of image E. Black dots represent biotinylated quantum dots.

## THE SSLA-STREPTAVIDIN FUSION PROTEIN

---

Black dots represent quantum dots and their size estimated from the images is in agreement with their commercial size (given by Sigma) although heterogeneity can be observed (Figure 4-6 A and B). When compared to the background, the particles are more evident and abundant on the protein template (Figure 4-6 A, C, E). This fact clearly shows that the core-streptavidin domain of the S-layer fusion is accessible in the protein lattice and that the chimeric S-layer self-assembly did not cause a steric hindrance for biotin binding.

The substrate onto which the fusion protein has been immobilized might also play a role. Due to the O<sub>2</sub> plasma treatment step, the carbon coated Cu grid surface can be regarded as being more hydrophilic, therefore the most important driving force for the protein adsorption are the long range electrostatic interactions occurring between the positively charged sites on the chimeric protein and negative charges of the substrate. As a result, the fusion protein layer adsorbs in a way that the streptavidin moiety remains exposed.

However when the protein lattice folds (Figure 4-6 E) into tube like structures, the core-streptavidin domain becomes buried and no longer accessible to the biotinylated quantum dots. Therefore no particles are bound onto these protein regions as evidenced in Figure 4-6 F. Marginal deposition is possible though, either due to the fact that the streptavidin domains are located at the edges of the protein sheets, or because during folding, tubes do not close completely, just the layer edges meet each other. It is further interesting to note that only the S-layer part of the fusion protein did not fold into tube like structures. Coupling the S-layer structure to the streptavidin domain indeed results in extension of the protein structure. This extended protein structure allows the adoption of a certain curvature when assembled into protein sheets. Besides the molecular structure of the monomers, folding is always related to the surface energies of the inner and outer surface of the protein structure due to different termination groups that are displayed by the monomers in the lattice.

The morphological unit of the SslA<sub>341-925</sub>CN-cstrp is composed of 4 monomers that bind to each other in a complex fashion giving rise to large protein layers. Every monomer in the lattice exposes one core-streptavidin binding site. Totally a number of 4 binding

site are available for interaction with the biotin moiety coupled to the quantum dot in the protein lattice. The quantum dots that were used in the binding experiments are 12 nm in diameter. Since this size is approximately the size of the lattice unit, it directly follows that only 1 quantum dot can bind per unit cell, the other 3 binding sites remain therefore empty. The binding phenomenon is further influenced by the charge of the quantum dots. It was already shown in section 4.4.1 that the quantum dots are negatively charged. As a result, a shielding effect arises that is exerted on the neighbouring particles forcing them to occupy distant positions on the fusion protein template. The magnitude of this shielding effect can be related to the Debye decay length [180], which quantitatively describes the distance from the particle over which the electrostatic potential decreases.

A chain like ordering of the quantum dots it is therefore induced as it can be observed in Figure 4-6 B and D. This ordering reflects the crystallinity and the long range structure of the chimeric protein biotemplate.

For high concentrations of salt in the solutions, the Debye length decreases and thus charged particles can approach each other more closely. In the case of the negatively charged quantum dot used here, an increased salt concentration would essentially allow the particles to be denser packed within at the available sites of the chimeric protein template.

On the other hand, the protein layers are seen as stable structures that did not distort upon addition of the charged particles. It can be speculated that this could be the result of electrostatic repulsion between neighbouring particles or of a structural reinforcement of the template by the nanoparticles.

In conclusion it can be envisaged that the precise control over the spatial arrangement of preformed nanoparticles using the fusion protein layer will open up new possibilities for the improvement of existing technologies such as nanolithography [144] and monolayer deposition [181]. This process also overcomes the inherent difficulty of fabricating close-packed monolayers of charge-stabilised aqueous colloids. Further, as the expression of only a single gene is required, the large-scale production of the fusion protein subunit is within the scope of existing biotechnological methods.



Subsequent organization of nanoparticles on fusion protein layers self-assembled onto patterned substrates could therefore result in the fabrication of biochips consisting of distinct spatial arrays of quantum dots. These arrays could have intrinsic magnetic, luminescent, metallic or semiconducting properties for the fabrication of nanoelectronic devices such as light emitting [182] and tunnel diodes [183], single electron transistors [184] and quantum cellular automata [185].

### 4.5 RELEVANCE OF THE FUSION PROTEIN AS A BIO(NANO)TEMPLATE

The bottom-up assembly of patterned arrays is an exciting and important area in nanotechnology. Such arrays are particularly attractive to serve as components in chip applications ranging from disease diagnosis to ultra-high-density data storage.

Fabrication would require the assembly or synthesis of single layer array of biological structures (flat sheets) or polymers on technologically relevant surfaces. To this end, S-layer protein adsorption on silicon substrates with predictable self-assembly patterns has emerged as a valuable tool. One particular attractive candidate is the S-layer fusion protein constructed in this work: SsIA-corestreptavidin. As shown in the previous sections, this protein, under appropriate experimental conditions, self-assembles into uniform, coherent layers on silicon wafer. This remarkable property facilitates the formation of a two-dimensional protein array with repetitive features in the nanometer range that exposes streptavidin. Due to the high affinity between streptavidin and biotin and the fact that nearly each molecule can be biotinylated, the SsIA-corestreptavidin protein template can be considered a functional biomolecular matrix for immobilizing biotinylated molecules in a controlled manner and defined spacing. For instance biotinylated-DNA, biotinylated-proteins or as shown, biotinylated-quantum dots can be attached and arranged in a defined way onto the protein template, serving therefore as a universal platform or a unique bionanotemplate for immobilizing biotinylated compounds (Figure 4-7).

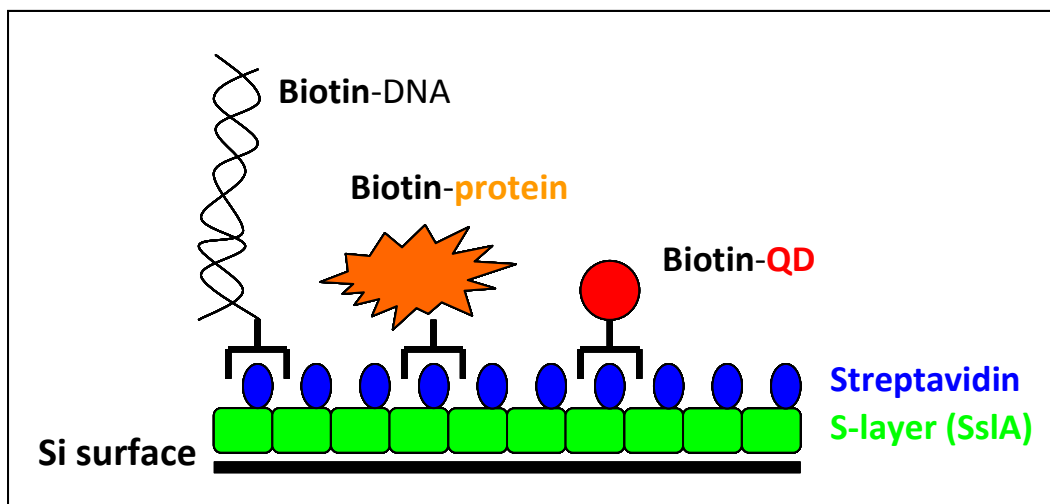


**Figure 4-7** Scheme showing the potential application of the SslA-CN-cstrp fusion protein template

Various experimental approaches involving molecules such as DNA [186], virus motor protein [187] and other organic molecules *e.g.* SAMs (self-assembled monolayers) have been explored for construction of single layer biomolecule arrays.

For instance, two-dimensional networks of DNA were synthesized by Kumara *et. al.* 2010 [186] which directed the templating of gold nanoparticles. DNA is renowned for its double helix structure and the base pairing that enables the recognition and the highly selective binding of complementary DNA strands. In comparison to SslA-corestreptavidin template, it seems rather minutious to achieve a dense coverage (diameter of a double stranded DNA is  $\sim 2$  nm) and the DNA molecules have to be tethered to the surface on order to obtain a stable configuration.

Xiao F *et. al.*, 2008 [187] have used the Phi 29 DNA-Packaging motor dodecamer of the *Bacillus subtilis* bacteriophage to produce a single layer biomolecular array. The dodecamer is part of the DNA-packaging motor complex, which *in vitro* may find interesting nanotechnological applications. In order to obtain single layered arrays, the dodecamer protein had to be genetically engineered (Strep-tag extension). When engineered, the protein formed single layers, but the assembly of these layers had to be directed by a thin lipid monolayer on mica surface. Without the support, the fragile sheet of the dodecamer could not stand alone. Contrarily to the dodecamers, SslA-corestreptavidin constitutes a more robust approach for single layer patterning. These

protein molecules assemble on Si substrates without the need of further engineering or support layer. They function as a seamless biotemplate.

As another example, the formation of SAMs provides an elegant way to form well-defined organic assemblies with a wide range of functionalities. Despite the different advantages, SAMs intrinsically form defects due to the thermodynamics of formation. Though the slow step in SAM formation often removes defects from the film, defects are included in the final SAM structure. Compared to SAMs, SsIA-corestreptavidin crystallization proceeds in a way that the resulting protein layer is coherent and continuous. This feature is relevant for a precise and accurate site-positioning and display of the biotin binding functionality especially in sensor oriented applications. In this sense, not only silicon-based sensor applications but also carbon, *i.e.* carbon nanotube (CNT) based sensor applications can be envisioned using the SsIA-corestreptavidin fusion protein template. This technology would not only offer the reward of smaller biochips with dense reaction sites, but potentially higher sensitivity and throughput.

## 4.6 CONCLUSIONS AND OUTLOOK

This chapter described the construction and characterization of the SsIA-corestreptavidin fusion protein. The biotin-streptavidin system is the strongest noncovalent biological interaction known and the strength and specificity of the interaction has led it to be one of the most widely used affinity pairs in molecular, immunological and cellular assays.

With the aim of constructing an S-layer fusion protein that combines both, the excellent self-assembling and specific ligand *i.e.* biotin binding ability, minimal sized form of streptavidin (core-streptavidin) was fused to the C-terminus of the SsIA derivative devoid of the N-terminal 341 and C-terminal 172 amino acids (SsIA<sub>341-925</sub>CN). The genetically engineered chimeric protein could be successfully produced in *E. coli*, isolated and purified via Ni affinity chromatography (due to the N-terminal His<sub>6</sub> tag). *In vitro* recrystallization experiments performed with the purified chimeric protein in

## THE SSLA-STREPTAVIDIN FUSION PROTEIN

---

solution and on a silicon wafer have demonstrated that fusion of the streptavidin domain does not interfere with the self-assembling properties of the S-layer part. The chimeric protein was able to self-assemble into mono- and multilayers with sizes ranging between 200 nm and 1  $\mu\text{m}$ . Even folding of the chimeric protein sheets could be observed, property that is uncharacteristic for its S-layer part suggesting that extension of the protein sequence might facilitate adoption of a certain curvature resulting therefore the folding of the recombinant fusion S-layer structure. But more importantly, the streptavidin domain retained its full biotin-binding ability, fact evidenced by experiments in which biotinylated quantum dots were coupled to the fusion protein monomers and adsorbed onto the *in vitro* recrystallized fusion protein template. In this way, this S-layer fusion protein can serve as a functional surface for controlled immobilization of biologically active molecules but also as a platform for the synthesis of planar arrays of quantum dots, process that represents a crucial aspect in the fabrication of ultra-small transistors and of materials possessing novel magnetic and optical properties. Furthermore, the presence of a His<sub>6</sub> tag might facilitate the deposition or growth of Ni cluster arrays that would have a great application potential for catalysis and for development of Ni-binding filter materials.

The S-layer part (SsIA<sub>341-925</sub>CN) of the SsIA-corestreptavidin fusion protein forms lattices that exhibit the p4 symmetry. In case of the p4 symmetry, 4 monomers are building up one lattice unit; therefore a protein moiety that is fused to SsIA<sub>341-925</sub>CN will be presented with the same spacing. Since the fusion protein kept its ability to self-assemble, it follows that the fused streptavidin domain is distributed in a number of 4 molecules per unit cell. However, certain applications might require less or a precise control over the density of biotin binding sites on the fusion protein template. In order to fulfil this requirement, the idea of hybrid S-layers has arisen. Hybrid S-layers composed of the recombinant SsIA-corestreptavidin fusion protein and the wild type SsIA monomers would represent protein lattices that would provide positioning of the biotin binding sites according to the stoichiometry of the components (Figure 4-8). This idea is new and intriguing because such assemblies could meet important applications

## THE SSLA-STREPTAVIDIN FUSION PROTEIN

---

not only in the biosensor field *e.g.* interface in biosensor elements to arrange molecules with precision, but also as building blocks in construction of novel nanoelectronic circuits.

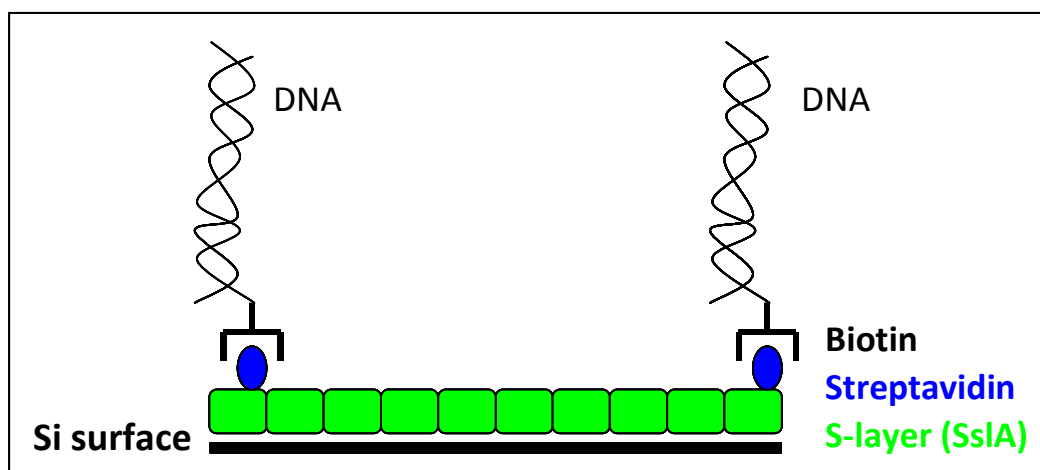


**Figure 4-8 Schematic representation of the hybrid S-layer structure**

A case where coupling of biotinylated DNA needs to be done at a certain distance.

First attempts to produce hybrid S-layer structures have been encouraging. Experiments were performed by mixing wild type SslA monomers obtained by monomerization of the isolated SslA patches with purified SslA-corestreptavidin molecules. Mixing occurred in a 1:1 ratio. After the *in vitro* cocrystallization, biotinylated quantum dots were adsorbed onto the formed structures in order to analyze the distribution pattern of the two proteins in the hybrid S-layer structure. Fluorescence microscopy imaging has revealed that there is a mixing of the wild type and recombinant fusion S-layer monomers.

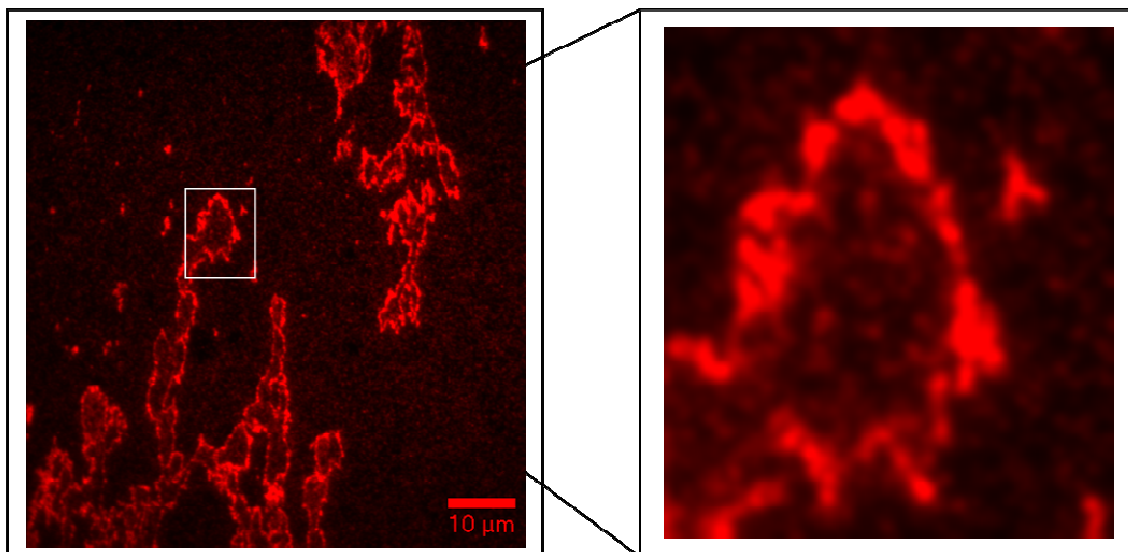


**Figure 4-9 Hybrid S-layer structures**

Chimeric and wild type S-layer monomers were cocrystallized. Afterwards biotinylated quantum dots were adsorbed onto the resulting protein lattice.

The resulting structures (Figure 4-9) have a well-defined shape as a consequence of a high-degree ordering of the quantum dots. The density of the quantum dots seems to be more accentuated laterally. However a precise distribution pattern and arrangement of the particles on the S-layer template cannot be estimated from these images. It remains to be investigated to which extent the mixing will give rise to specific, desired hybrid S-layer structures. At first, conditions for assembling coherent hybrid lattices should be investigated. Gold nanoparticles in the size of 1-3 nm could constitute an alternative to the quantum dots. Finally, a higher resolution method would be necessary for pattern elucidation.

## SUMMARY

Increasing the integration density of electron device components will necessitate the use of new nanofabrication paradigms that complement and extend existing technologies. One potential approach to overcome the current limitations of electron-beam lithography may involve the use of hybrid systems, in which existing lithographic techniques are coupled with “bottom up” approaches such as supramolecular self-assembly. In this respect, biological systems offer some unique possibilities as they combine both self-organization and spatial patterning at the nanometer length scale. In particular, Surface Layer Proteins (S-layers) can facilitate high order organization and specific orientation of inorganic structures as they are two-dimensional porous crystalline membranes with regular structure at the nanometer scale.

In this framework, the aim of the present work was the characterization of the S-layer of *Sporosarcina ureae* ATCC 13881 (SslA) with respect to its self-assembling properties and modification that would allow it to be employed as a patterning element and a new building block for nanobiotechnology.

*In vitro* recrystallization experiments have shown that wild type SslA self-assembles into monolayers, multilayers or tubes. Factors such as initial monomer concentration,  $\text{Ca}^{2+}$  ions, pH of the recrystallization buffer and the presence of a silicon substrate have a strong influence on the recrystallization process. SslA monolayers proved to be an excellent biotemplate for ordered assembly of gold nanoparticle arrays. The recombinant SslA after expression and purification formed micrometer sized, crystalline monolayers exhibiting the same lattice structure as the wild type protein (p4 symmetry). This remarkable property of self-assembling has been preserved even when SslA was truncated. The deletion of both, N- and C-terminal SslA domains does not hinder self-assembly; the resulting protein is able to form extended monolayers that exhibit the p4 lattice symmetry. The central SslA-domain is self sufficient for the self-assembly. The possibility to change the natural properties of S-layers by genetic engineering techniques opens a new horizon for the tuning of their structural and

functional features. The SslA-streptavidin fusion protein combines the remarkable property of self-assembling with the ligand *i.e.* biotin binding function. On silicon wafers, this chimeric protein recrystallized into coherent protein layers and exposes streptavidin, fact demonstrated by binding studies using biotinylated quantum dots. In this way, it can serve as a functional surface for controlled immobilization of biologically active molecules but also as a platform for the synthesis of planar arrays of quantum dots. Furthermore, the results open up exciting possibilities for construction of hybrid S-layers, structures that may ultimately promote the fabrication of miniaturized, nanosized electronic devices.



## BIBLIOGRAPHY

- [1] G. E. Moore, 1975, Progress in digital electronics, IEDM Technical Digest 75:11-13
- [2] <http://www.intel.com/technology/mooreslaw/>
- [3] B. A. Grzybowski, C. E. Wilmer, J. Kim, K. P. Browne, K. J. M. Bishop, 2009, Self-assembly: from crystals to cells, *Soft Matter* 5:1110–1128
- [4] D. Whang, S. Jin, Y. Wu, C. M. Lieber, 2003, Large-Scale Hierarchical Organization of Nanowire Arrays for Integrated Nanosystems, *Nano Lett.*, 3:1255–1259
- [5] J. C. Love, L. A. Estroff, J. K. Kriebel, R. G. Nuzzo, G. M. Whitesides, 2005, Self-Assembled Monolayers of Thiolates on Metals as a Form of Nanotechnology, *Chem. Rev.*, 105:1103–1170
- [6] C. D. Bain, E. B. Troughton, Y. T. Tao, J. Evall, G. M. Whitesides, R. G. Nuzzo, 1989, Formation of monolayer films by the spontaneous assembly of organic thiols from solution onto gold, *J. Am. Chem. Soc.*, 111:321–335
- [7] D. Witt, R. Klajn, P. Barski, B. A. Grzybowski, 2004, Applications, properties, and synthesis of  $\omega$ -functionalized *n*-alkanethiols and disulfides – the building blocks of self-assembled monolayers, *Curr. Org. Chem.*, 8:1763–1797
- [8] J. D. Hartgerink, E. Beniash, S. I. Stupp, 2001, Self-Assembly and Mineralization of Peptide Amphiphile Nanofibers, *Science*, 294:1684–1688
- [9] J. D. Hartgerink, E. Beniash, S. I. Stupp, 2002, Peptide-Amphiphile Nanofibers: A versatile scaffold for the preparation of self-assembling materials, *Proc. Natl. Acad. Sci. USA*, 99:5133–5138
- [10] C. A. Mirkin, R. L. Letsinger, R. C. Mucic, J. J. Storhoff, 1996, A DNA-based method for rationally assembling nanoparticles into macroscopic materials, *Nature*, 382:607–609
- [11] M. Li, H. Schnablegger, S. Mann, 1999, Coupled synthesis and self-assembly of nanoparticles to give structures with controlled organization, *Nature*, 402:393–395
- [12] S. J. Park, A. A. Lazarides, C. A. Mirkin, R. L. Letsinger, 2001, Directed Assembly of Periodic Materials from Protein and Oligonucleotide-Modified Nanoparticle Building Blocks, *Angew. Chem. Int. Ed.*, 40:2909–2912

- [13] A. M. Kalsin, M. Fialkowski, M. Paszewski, S. K. Smoukov, K. J. M. Bishop and B. A. Grzybowski, 2006, Electrostatic Self-Assembly of Binary Nanoparticle Crystals with a Diamond-Like Lattice, *Science*, 312:420–424.
- [14] S. S. Fan, M. G. Chapline, N. R. Franklin, T. W. Tomblor, A. M. Cassell, H. J. Dai, 1999, Self-Oriented Regular Arrays of Carbon Nanotubes and Their Field Emission Properties, *Science*, 283:512–514.
- [15] M. Yan, H. T. Zhang, E. J. Widjaja, R. P. H. Chang, 2003, Self-assembly of well-aligned gallium-doped zinc oxide nanorods, *J. Appl. Phys.*, 94:5240–5246
- [16] G. R. Desiraju, 1995, Supramolecular synthons in crystal engineering – a new organic synthesis, *Angew. Chem. Int. Ed.*, 34:2311–2327
- [17] B. Moulton, M. J. Zaworotko, 2001, From Molecules to Crystal Engineering: Supramolecular Isomerism and Polymorphism in Network Solids, *Chem. Rev.*, 101:1629–1658
- [18] J. Aizenberg, D. A. Muller, J. L. Grazul and D. R. Hamann, 2003, Direct Fabrication of Large Micropatterned Single Crystals, *Science*, 299:1205–1208
- [19] A. J. Blake, N. R. Champness, P. Hubberstey, W. S. Li, M. A. Withersby, M. Schroder, 1999, Inorganic crystal engineering using self-assembly of tailored building blocks, *Coord. Chem. Rev.*, 183:117–138
- [20] J. M. Lehn, 1990, Perspectives in supramolecular chemistry - from molecular recognition towards molecular information-processing and self-organization, *Angew. Chem. Int. Ed.*, 29:1304–1319
- [21] D. Philp and J. F. Stoddart, 1996, Self-assembly in natural and unnatural systems, *Angew. Chem. Int. Ed.*, 35:1155–1196
- [22] A. McPherson, 1999, *Crystallization of Biological Macromolecules*, Cold Spring Harbor Laboratory Press, New York
- [23] C. P. Govardhan, 1999, Cross-linking of enzymes for improved stability and performance, *Current Opinion Biotech.* 10:331-335
- [24] A. M. Kierzek, P. Zielenkiewicz, 2001, Models of protein crystal growth, *Biophysical Chemistry* 91:1-20
- [25] A. Ducruix, R. Giege, 1992, *Crystallization of Nucleic Acids and Proteins. A Practical*

Approach, IRL Press Oxford University Press, Oxford

- [26] S. D. Durbin, G. Feher, 1996, Protein crystallization, *Annu. Rev. Phys. Chem.* 47:171-204
- [27] Z. Kam, G. Feher, 1984, Nucleation and growth of protein crystals: general principles and assays, *Methods Enzymol.* 114:77-112.
- [28] D. Kashchiev and G. M. Rosmalen, 2003, Nucleation in solutions revisited, *Cryst. Res. Technol*, 38:555-574
- [29] Y. Jia, X. Liu, 2006, From surface self-assembly to Crystallization: prediction of protein Crystallization conditions, *J. Phys. Chem. B* 110:6949-4955
- [30] J. Zhang, X.Y. Liu, 2003, Effect of Protein-Protein Interactions on Protein Aggregation Kinetics, *J. Chem. Phys.* 119:10972-10977
- [31] A. A. Chernov, 1997, Protein versus conventional crystals: creation of defects, *J. Cryst. Growth*, 174:354-361
- [32] C. R. Woese, O. Kandler, M.L. Wheelis, 1990, Towards a natural system of organisms: Proposal for the domains Archaea, Bacteria, and Eucarya, *Proc. Natl. Acad. Sci. USA*, 87:4576-4579
- [33] O. Kandler, 1998, in *Thermophiles. The keys to Molecular Evolution and the Origin of Life?* (Eds. J. Wiegel, M. W.W. Adams), Taylor&Francis, London, pp 19-31
- [34] A. L. Houwink, 1953, A macromolecular mono-layer in the cell wall of *Spirillum* spec. *Biochimica et Biophysica Acta*, Vol 10, pp 360-366
- [35] D. Pum, P. Messner, U. B. Sleytr, 1991, Role of the S layer in morphogenesis and cell division of the archaebacterium *Methanococcus sinense*, *J. Bacteriol.*, 21:6865-6873
- [36] U. B. Sleytr, 1997, Basic and applied S-layer research: an overview, *FEMS Microbiol. Rev.* 20:5-12
- [37] M. Sara, U. B. Sleytr, 1996, Biotechnology and biomimetic with crystalline bacterial cell surface layers (S-layers), *Micron* 27:141-156
- [38] U. B. Sleytr, M. Sara, 1997, Bacterial S-layer proteins: structure-function relationship and their biotechnological applications, *Trends Biotechnol.* 15:20-26
- [39] U. B. Sleytr, P. Messner, D. Pum, M. Sara, 1999, Crystalline Bacterial Cell Surface

Layers: From Supramolecular Cell Structure to Biomimetics and Nanotechnology  
*Angew. Chem. Int. Ed.* 38:1034-105

[40] U. B. Sleytr, E. Györvary, D. Pum, 2003, Crystallization of S-layer protein lattices on surfaces and interfaces, *Progress in Organic Coatings*, 47:279–287

[41] D. Pum, A. Neubauer, E. Györvary, M. Sara, U. B. Sleytr, 1999, S-layer proteins as basic building blocks in a biomolecular construction kit, Seventh Foresight Conference on Molecular Nanotechnology, Santa Clara, CA.

[42] R. Wahl, 2003, Reguläre bakterielle Zellhüllenproteine als biomolekulares Template, Dissertation TU Dresden

[43] P. Messner, U. B. Sleytr, 1992, Crystalline bacterial cell surface layers in: A. H. Rose (Ed.), *Advances in Microbial Physiology*, Academic Press, London, pp. 213-275.

[44] U. B. Sleytr, P. Messner, 1989, Self-assembly of crystalline bacterial cell surface layers (S-layers) in: H. Plattner (Ed.), *Electron Microscopy of subcellular Dynamics*, CRC Press, Boca Raton, FL., pp. 13-31

[45] D. Pum, U. B. Sleytr, 1996, Molecular nanotechnology and biomimetics with S-layers, in: U. B. Sleytr, P. Messner, D. Pum, M. Sara (Eds.), *Crystalline Bacterial Cell Surface Layer Proteins (S-layers)*, Academic Press, R.G. Landes Company, Austin, TX, pp 175-209

[46] T. J. Beveridge, 1994, Bacterial S-layers, *Curr. Opin. Struct. Biol.* 4:204-212

[47] U. B. Sleytr, E.M. Egelseer, N. Ilk, D. Pum, B. Schuster, 2007, S-Layers as Basic Building Block for a Molecular Construction Kit, *FEBS Journal*, 274:323–334

[48] U. B. Sleytr, T.J. Beveridge, 1999, Bacterial S-layers, *Trends Microbiol.* 7:253–260.

[49] U. B. Sleytr, 1978, Regular arrays of macromolecules on bacterial cell walls: structure, chemistry, assembly and function, *Int. Rev. Cytol.* 53:1–64

[50] M. Sára, U. B. Sleytr, 1987, Charge distribution on the S-layer of *Bacillus stearothermophilus* NRS 1536/3c and the importance of charged groups for morphogenesis and function, *J. Bacteriol.* 169:2804–2809

[51] U. B. Sleytr, 1975, Heterologous reattachment of regular arrays of glycoproteins on bacterial surfaces, *Nature* 257:400–402

[52] H. Engelhardt, J. Peters, 1998, Structural research on surface layers: a focus on

stability, surface layer homology domains and surface layer-cell wall interactions, *J. Struct. Biol.* 124:276-302.

[53] J. L. Toca-Herrera, S. Moreno-Flores, J. Friedmann, D. Pum, U. B. Sleytr, 2005, Chemical and thermal denaturation of crystalline bacterial S-layer proteins: An atomic force microscopy study, *Microsc. Res. Tech.* 65:226-234

[54] U. B. Sleytr, P. Messner, 1983, Crystalline surface layers on bacteria, *Annu. Rev. Microbiol.* 37:311-39

[55] M. Sára, U.B. Sleytr, 2000, S-layer proteins, *J. Bacteriol.* 182:859– 868

[56] H. J. Boot, P.H. Pouwels, 1996, Expression, secretion and antigenic variation of bacterial S-layer proteins, *Mol. Microbiol.* 21:1117-112

[57] P. Messner, 1996, Chemical composition and biosynthesis of S-layers, *In* U. B. Sleytr, P. Messner, D. Pum, and M. Sara (ed.), *Crystalline bacterial cell surface layer proteins (S-layers)*. Academic Press, Landes Company, Austin, Tex. pp 35-76.

[58] M. Sára, U.B. Sleytr, 2000, S-layer proteins, *J. Bacteriol.* 182:859-868.

[59] C. Schäffer, P. Messner, 2001, Glycobiology of surface layer proteins, *Biochemistry* 83:591–599.

[60] P. Messner, C. Schäffer, Prokaryotic glycoproteins, in: W. Herz, H.Falk, G.W. Kirby, R.E. Moore, C. Tamm (Eds.), *Progress in the Chemistry of Organic Natural Products*, vol. 85, Springer, Wien, pp. 51–124.

[61] I. Etienne-Toumelin, J.-C. Sirard, E. Dufлот, M. Mock, A. Fouet, 1995, Characterization of the *Bacillus anthracis* S-layer: cloning and sequencing of the structural gene. *J. Bacteriol.* 177:614–620.

[62] N. Ilk, P. Kosma, M. Puchberger, E. M. Egelseer, H. F. Mayer, U. B. Sleytr, M. Sara, 1999, Structural and functional analyses of the secondary cell wall polymer of *Bacillus sphaericus* CCM 2177 serving as an S-layer-specific anchor, *J. Bacteriol.* 181:7643-7646

[63] B. Kuen, A. Koch, E. Asenbauer, M. Sara, W. Lubitz, 1997, Molecular characterization of the second S-layer gene *sbsB* of *Bacillus stearothermophilus* PV72 expressed by oxidative stress, *J. Bacteriol.* 179:1664–1670

[64] E. Leibovitz, M. Lemaire, I. Miras, S. Salamitou, P. Beguin, H. Ohayon, P. Gounon, M. Matuschek, K. Sahm, H. Bahl, 1997, Occurrence and function of a common domain

- in S-layer and other exocellular proteins, FEMS Microbiol. Rev. 20:127–133
- [65] M. Lemaire, , I. Miras, P. Gounon and P. Beguin, 1998, Identification of a region responsible for binding to the cell wall within the S-layer protein of *Clostridium thermocellum*, Microbiology 144:211–217
- [66] M. Sara C. Dekitsch, H. F. Mayer, E. M. Egelseer, U. B. Sleytr, 1998, Influence of the Secondary Cell Wall Polymer on the Reassembly, Recrystallization, and Stability Properties of the S-Layer Protein from *Bacillus stearothermophilus* PV72/p2 J. Bacteriol. 180:4146–4153
- [67] G. I. Vidgren, R. Palva, K. Pakkanen, Lounatmaa, A. Palva, 1992, S-layer protein gene of *Lactobacillus brevis*: cloning by polymerase chain reaction and determination of nucleotide sequence, J. Bacteriol. 174:7419– 7427
- [68] U. B. Sleytr, P. Messner, 1983, Crystalline surface layers on bacteria, Annu. Rev. Microbiol. 37:311-39
- [69] U. B. Sleytr, P. Messner, D. Pum, M. Sara, 1999, Crystalline Bacterial Cell Surface Layers: From Supramolecular Cell Structure to Biomimetics and Nanotechnology, Angew. Chem. Int. Ed. 38:1034-1054
- [70] M. Jarosch, E. M. Egelseer, D. Mattanovich, U. B. Sleytr, M. Sara, 2000, The S-layer gene *sbsC* of *Bacillus stearothermophilus* ATCC 12980: molecular characterization and heterologous expression in *Escherichia coli*, Microbiology, 146: 273-281
- [71] T. Adachi, H. Yamagata, N. Tsukagoshi, S. Udaka, 1989, Multiple and tandemly arranged promoters of the cell wall protein operon in *Bacillus brevis*, J. Bacteriol. 171:1010–1016.
- [72] M. Sara, B. Kuen, H. Mayer, F. Mandl, K. C. Schuster, U. B. Sleytr, 1996, Dynamics in oxygen-induced changes in S-layer protein synthesis from *Bacillus stearothermophilus* PV72 and its S-layer-deficient variant T5 in continuous culture and studies of the cell wall composition, J. Bacteriol. 178:2108-2117
- [73] J. A. Fisher, J. Smith, N. Agabian, 1988, Transcriptional analysis of the major surface array gene of *Caulobacter crescentus*, J. Bacteriol. 170:4706-4713
- [74] S. Chu, T.J. Trust, 1993, An *Aeromonas salmonicida* gene which influences A-protein expression in *Escherichia coli* encodes a protein containing an ATP-binding

- cassette and maps beside the surface array protein gene, J. Bacteriol. 175:3105-3114
- [75] H. J. Boot, C. P. Kolen, F.J. Andreadaki, R. J. Leer, P. H. Pouwels, 1996, The *Lactobacillus acidophilus* S-layer protein gene expression site comprises two consensus 166 promoter sequences, one of which directs transcription of stable mRNA, J. Bacteriol. 178:5388–5394
- [76] G. Seltmann, O. Holst, 2002, The bacterial cell wall, Springer, Heidelberg, Germany pp 219-261
- [77] Z. Pei, M. J. Blaser, 1990, Pathogenesis of *Campylobacter fetus* infection, J. Clin. Invest. 85:1036–1043
- [78] Schultze-Lam, 1992, Participation of a cyanobacterial S-Layer in fine grain mineral formation, J. Bacteriol. 174:7971-81
- [79] D. Moll, C. Hueber, B. Schlegel, D. Pum, U. B. Sleytr and M. Sara, 2002, S-layer-streptavidin fusion proteins as template for nanopatterned molecular arrays, PNAS, 99:14646-14651
- [80] C. Huber, J. Liu, E. M. Egelseer, D. Moll, W. Knoll, U. B. Sleytr, M. Sara, 2006, Heterotetramers formed by an S-layer-Streptavidin fusion protein and core-streptavidin as a nanoarrayed template for biochip development, Small, 2:142-50
- [81] J. Tang, A. Ebner, N. Ilk, H. Lichtblau, C. Hueber, R. Zhu, D. Pum, M. Leitner, V. Pastushenko, H.J. Gruber, U. B. Sleytr, P. Hinterdorfer, 2008, High affinity tags fused to S-layer proteins probed by Atomic Force Microscopy, Langmuir, 24: 1324-1329
- [82] C. Völlenkne, S. Weigert, N. Ilk, E. M. Egelseer, V. Weber, F. Loth, D. Falkenhagen, U. B. Sleytr, M. Sara, 2004, Construction of a functional S-layer fusion protein comprising immunoglobulin G-binding domain for development of specific adsorbent for extracorporeal blood purification, Applied and Environmental Microbiology, 70:1514-1521
- [83] A. Breitwieser, E. M. Egelseer, D. Moll, N. Ilk, C. Hotzy, B. Bohle, C. Ebner, U. B. Sleytr, M. Sara, 2002, A recombinant bacterial cell surface (S-layer)-major birch pollen allergen-fusion protein (rSbsC/Bet v1) maintains the ability to self-assemble into regularly structured monomolecular lattices and functionality of the allergen, Prot. Eng. 15: 243-249

- [84] K. Pollmann, S. Matys, 2007, Construction of an S-layer protein exhibiting modified self-assembling properties and enhanced metal binding capacities, *Appl. Microbiol. Biotechnol.* 75:1079-1085
- [85] A. Blecha, K. Zarschler, K. A. Sjollema, M. Veenhuis, G. Rödel, 2005, Expression and cytosolic assembly of the S-layer fusion protein mSbsC-EGFP in eukaryotic cells, *Microbial Cell Factories* 4:28
- [86] M. Sara and U. S. Sleytr, 1987, Molecular sieving through S-layers of *Bacillus stearothermophilus* strains, *J. Bacteriol.* 169:4092-4098
- [87] S. Scheicher, B. Kainz, S. Köstler, M. Suppan, A. Bizzarri, D. Pum, U. B. Sleytr, V. Ribitsch, 2009, Optical oxygen sensors based on Pt(II) porphyrin dye immobilized on S-layer protein matrices, *Biosens. Bioelectron.* 25:797–802
- [88] U. B. Sleytr, M. Sara, D. Pum, B. Schuster, 2001, Characterization and use of crystalline bacterial cell surface layers, *Prog. Surf. Sci.* 68:231-278
- [89] C. Weiner, M. Sara, G. Dasgupta, U. B. Sleytr, 1994, Affinity Cross-Flow Filtration: Purification of IgG with a Novel Protein A Affinity Matrix Prepared from Two-Dimensional Protein Crystals, *Biotechnol. Bioeng.* 44:55-65
- [90] S. Küpcü, C. Mader, M. Sara, 1995, The crystalline cell surface layer of *Thermoanaerobacter thermohydrosulfuricus* L111-69 as an immobilization matrix: influence of the morphological properties and the pore size of the matrix on activity loss of covalently bound enzymes, *Biotechnol. Appl. Biochem.* 21:275-286
- [91] S. Küpcü, K. Lohner, C. Mader, U. B. Sleytr, 1998, Microcalorimetric study on the phase behaviour of S-layer coated liposomes, *Mol. Membr. Biol.* 15:69-74
- [92] S. Küpcü, M. Sara, U. B. Sleytr, 1995, Liposomes coated with crystalline bacterial cells surface protein (S-layer) as immobilization structures for macromolecules *Biochim. Biophys. Acta*, 1235:263-269
- [93] B. Noonan, T. J. Trust, 1997, The synthesis, secretion and role in virulence of the paracrystalline surface protein layers of *Aeromonas salmonicida* and *Aeromonas hydrophila*, *FEMS Microbiol. Lett.* 154:1-7
- [94] J. C. Thornton, R. A. Garduno, S. G. Newman, W. W. Kay, 1991, Surface-disorganized, attenuated mutants of *Aeromonas salmonicida* as furunculosis live



vaccines, *Microb. Pathog.* 11:88-99

[95] B. Jahn-Schmid, P. Messner, F. M. Unger, U. B. Sleytr, O. Scheiner, D. Kraft, 1996, Toward selective elicitation of T<sub>H</sub>1-controlled vaccination responses: vaccine applications of bacterial surface layer proteins, *J. Biotechnol.* 44:225-231

[96] U. B. Sleytr, H. Bayley, M. Sara, A. Breitwieser, S. Küpcü, C. Mader, S. Weigert, F. M. Unger, P. Messner, B. Jahn-Schmid, B. Schuster, D. Pum, K. Douglas, N. A. Clark, J. T. Moore, T. A. Winningham, S. Levy, I. Frithsen, J. Pankovc, P. Beagle, H. P. Gillis, D. A. Choutov, K. P. Martin, 1997, Applications of S-layers, *FEMS Microbiol. Rev.*, 20:151-175

[97] D. Pum, G. Stangl, C. Sponer, W. Fallmann, U. B. Sleytr, 1996, Deep UV patterning of monolayers of crystalline S layer protein on silicon surfaces, *Colloids Surf. B* 8:157-162

[98] J. M. Calvert, 1993, Lithographic Patterning of Self-Assembled Films, *J. Vac. Sci. Technol. B*, 11:2155-2163

[99] A. Kirchner, 2005, Synthese von Edelmetallclustern auf S-Layern und deren katalytische Eigenschaften, Dissertation, TU Dresden

[100] M. Mertig, R. Wahl, M. Lehmann, P. Simon, W. Pompe, 2001, Formation and manipulation of regular metallic nanoparticle arrays on bacterial surface layers: and advanced TEM study, *Eur. Phys. J. D* 16:317-320

[101] U. Queitsch, E. Mohn, F. Schäffel, L. Schultz, B. Rellinghaus, A. Blüher, M. Mertig 2007, Regular arrangement of nanoparticles from the gas phase on bacterial surface-proteins layers, *Appl Phys Lett* 90:113114

[102] S. S. Mark, M. Bergkvist, P. Bhatnagar, C. Welch, A. L. Goodyear, X. Yang, E. R. Angert, C. A. Batt, 2007, Thin film processing using S-layer proteins: Biotemplated assembly of colloidal gold etch mask for fabrication of silicon nanopillar arrays, *Colloids and Surfaces B: Biointerfaces* 57:161-173

[103] M. Goldman, D. F. Wilson, 1977, Growth of *Sporosarcina ureae* in defined media, *FEMS Lett.* 2:113-115

[104] R. E. MacDonald, S. W. MacDonald, 1962, The physiology and natural relationships of the motile, sporeforming *Sarcinae*, *J. Microbiol.* 8:795-818

- [105] T. J. Beveridge, 1979, Surface Arrays on the Wall of *Sporosarcina ureae*, J. Bacteriol. 139:1039-1048
- [106] H. Engelhardt, W. O. Saxton, W. Baumeister, 1986, Three-Dimensional Structure of the Tetragonal Surface Layer of *Sporosarcina ureae*, J. Bacteriol. 168:309-317
- [107] H. Engelhardt, 1991, Electron microscopy of microbial cell wall proteins. Surface topography, three-dimensional reconstruction, and strategies for two-dimensional crystallization, Fungal Cell Wall and Immune Response (Eds: J. P. Latge and D. Boucias), Springer-Verlag, Berlin, Heidelberg, pp 11-25
- [108] M. Stewart, T. J. Beveridge, 1980, Structure of the Regular Surface Layer of *Sporosarcina ureae*, J. Bacteriol. 142:302-309
- [109] P. Ryzhkov, K. Ostermann, G. Rödel, 2007, Isolation, gene structure and comparative analysis of the S-layer gene *sslA* of *Sporosarcina ureae* ATCC 13881, Genetica 131:255–265
- [110] P. Ryzhkov, 2007, Bioengineering of S-layers: molecular characterization of the novel S-layer gene *sslA* of *Sporosarcina ureae* ATCC 13881 and nanotechnology application of SslA protein derivatives, Dissertation, TU Dresden
- [111] M. Mertig, R. Kirsch, W. Pompe, H. Engelhardt, 1999, Fabrication of highly oriented nanocluster arrays by biomolecular templating, Eur. Phys. J. D 9:45-48
- [112] D. D. Archibald, S. Mann, 1993, Template mineralization of self-assembled anisotropic lipid microstructures, Nature 364:430-3
- [113] E. Evans, H. Bowman, A. Leung, D. Needham, D. Tirrell, 1996, Biomembrane templates for nanoscale conduits and networks, Science 273:933-935
- [114] A. P. Alivisatos, K. P. Johnsson, X. Peng, T. E. Wilson, C. J. Loweth, M. P. Bruchez, P. G. Schultz, 1996, Organization of 'nanocrystal molecules' using DNA Nature 382:609-11
- [115] Yamashita I, 2001, Fabrication of two-dimensional array of nano-particles using ferritin molecule, Thin Solid Films 393:12-18
- [116] F. Patolsky, Y. Weizmann, I. Willner, 2004, Actin-based metallic nanowires as bio-nanotransporters, Nat. Mater. 3:692-695
- [117] U. Kreibig, M. Vollmer, 1995, Optical properties of Metal Clusters, Springer

Verlag, Berlin

- [118] N. Ma, G. Tikhomitov, S. O. Kelley, 2010, Nucleic Acid-Passivated Semiconductor Nanocrystals: Biomolecular Templating of Form and Function, *Accounts of Chemical Research* 43:173-180
- [119] A. P. Alivisatos, 1996, Semiconductor Clusters, Nanocrystals, and Quantum Dots, *Science*, 271:933-937
- [120] D. J. Mowbray, M. S. Skolnick, 2005, New Physics and Devices Based on Self-Assembled Semiconductor Quantum Dots, *J. Phys. D: Appl. Phys*, 38:2059-2076
- [121] R. Gill, M. Zayats, I. Willner, 2008, Semiconductor Quantum Dots for Bioanalysis, *Angew. Chem. Int. Ed*, 47:7602-7625
- [122] W. C. W. Chan, S. Nie, 1998, Quantum Dot Bioconjugates for Ultrasensitive Nonisotopic Detection, *Science* 281:2016-2018
- [123] Y. Masumoto, 2002, *Semiconductor Quantum Dots: Physics, Spectroscopy, and Applications*, Springer, Berlin, pp 457-478
- [124] J. M. Klostranec, W. C. W. Chan, 2006, Quantum Dots in Biological and Biomedical Research: Recent Progress and Present Challenges, *Adv. Mater.* 18:1953-1964
- [125] L. Chaiet, F. J. Wolf, 1964, The properties of streptavidin, a biotin-binding protein produced by Streptomyces, *Arch Biochem Biophys.* 106:1-5
- [126] E. A. Bayer, H. Ben-Hur, M. Wilchek, 1990, Isolation and properties of streptavidin, *Methods in Enzymology*, 184:80-9
- [127] A. S. Blawas, W. M. Reichert, 1998, Protein patterning, *Biomaterials* 19:595-609
- [128] L. Z. He, A. F. Dexter, A. P. Middelberg, 2006, Biomolecular engineering at interfaces, *Chem. Eng. Sci.* 61:989-1003
- [129] S. S. Behrens, S. Silke, 2008, Synthesis of inorganic nanomaterials mediated by protein assemblies, *J. Mater. Chem.* 18:3788-3798
- [130] C. Tamerler, M. Sarikaya, 2009, Molecular biomimetics: nanotechnology and bionanotechnology using genetically engineered peptides, *Phil. Trans. R. Soc. A* 367:1705-1726
- [131] S. Murray, T. J. Beveridge, 1980, Structure of the Regular Surface Layer of

*Sporosarcina ureae*, J. Bacterol. 142: 302-309

[132] U. B. Sleytr, E. Györvary, D. Pum, 2003, Crystallization of S-layer protein lattices on surfaces and interfaces, *Progress in Organic Coatings*, 47:278-287

[133] D. Pum, U. B. Sleytr, 1995, Monomolecular reassembly of a crystalline bacterial cell surface layer (S-layer) on untreated and modified silicon surfaces, *Supramol. Sci.* 2:193-197

[134] W. Chen, T. J. McCarthy, 1997, Layer-by-Layer Deposition: A Tool for Polymer Surface Modification, *Macromolecules*, 30:78-86

[135] M. Jarosch, E. M. Egelseer, C. Huber, D. Moll, D. Mattanovich, U. B. Sleytr, M. Sara, 2001, Analysis of the structure-function relationship of the S-layer protein SbsC of *Bacillus stearothermophilus* ATCC 12980 by producing truncated forms, *Microbiology* 147:1353-1363

[136] A. Blecha, 2005, Gentechnisches Design bakterieller Hüllproteine für die technische Nutzung, Dissertation, TU Dresden

[137] D. Pum, U. B. Sleytr, 1995, Anisotropic crystal growth of the S-layer of *Bacillus sphaericus* CCM 2177 at the air/water interface, *Colloids and Surfaces A: Physicochemical and engineering aspects*, 102:99-104

[138] A. W. Adamson, A. P. Gast, 1997, *Physical Chemistry of Surfaces*, 4<sup>th</sup> edition, John Wiley, New York

[139] R. J. Hunter, 2001, *Foundations of Colloid Science*, Oxford University Press, Oxford

[140] S. Satiropoulou, S. S. Mark, E. R. Angert, C. A. Batt, 2007, Nanoporous S-layer lattices. A Biological Ion Gate with Calcium Selectivity, *J. Phys. Chem. C* 111:13232-13237

[141] J. L. Toca-Herrera, S. Moreno-Flores, J. Friedmann, D. Pum, U. B. Sleytr, 2004, Chemical and thermal denaturation of Crystalline Bacterial S-layer proteins: an atomic force microscopy study, *Microscopy Research and Technique* 65:226-234

[142] J. Tang, A. Ebner, N. Ilk, H. Lichtblau, C. Huber, R. Zhu, D. Pum, M. Leitner, V. Pastushenko, H. J. Gruber, U. B. Sleytr, and P. Hinterdorfer, 2008, High affinity tags fused to S-layer proteins probed by atomic force microscopy, *Langmuir* 24:1324-1329

- [143] A. Ducruix, R. Giege, 1992, Crystallization of Nucleic Acids and Proteins. A Practical Approach, Oxford University Press, Oxford
- [144] K. Douglas, N. A. Clark, K. J. Rothschild, 1990, Biomolecular/Solid State Nanoheterostructures, Appl. Phys. Lett. 56:692-694
- [145] M. Mertig, R. Kirsch, W. Pompe, H. Engelhardt, 1999, Fabrication of highly oriented nanocluster arrays by biomolecular templating, Eur. Phys. J. 9:45-48
- [146] S. Dieluweit, D. Pum, U. B. Sleytr, 1998, Formation of a gold superlattice on an S-layer with square lattice symmetry, Supramol. Sci. 2:193-197
- [147] W. Shenton, D. Pum, U. B. Sleytr, S. Mann, 1997, Synthesis of cadmium sulphide superlattices using self-assembled bacterial S-layers, Nature 389:585-587
- [148] C. Chaiyasut, Y. Takatsu, S. Kitagawa, T. Tsuda, 2001, Estimation of the dissociation constants for functional groups on modified and unmodified silica gel supports from the relationship between electroosmotic flow velocity and pH, Electrophoresis 22:1267-1272
- [149] S. Liu, T. Zhu, R. Hu, Z. Liu, 2002, Evaporation-induced self-assembly of gold nanoparticles into a highly organized two-dimensional array, Phys. Chem. Chem. Phys. 4:6059-6062
- [150] H. Engelhardt, R. Guckenberger, R. Hegerl, W. Baumeister, 1985, High resolution shadowing of freeze-dried bacterial photosynthetic membranes: Multivariate statistical analysis and surface relief reconstruction, Ultramicroscopy 16:395-410
- [151] R. Wahl, H. Engelhardt, W. Pompe, M. Mertig, 2005, Fabrication of highly oriented nanocluster arrays by biomolecular templating, Chem. Mater. 17:1887-1894
- [152] U. Queitsch, E. Mohn, F. Schäffel, L. Schultz, B. Rellinghaus, A. Blüher, M. Mertig, 2007, Regular arrangement of nanoparticles from the gas-phase on bacterial surface-protein layers, Applied Physics Letters 90:113114-113117
- [153] R. J. Beiland, T. J. Trust, 1987, Cloning of the gene for the surface array protein of *Aeromonas salmonicida* and evidence linking loss of expression with genetic deletion, J. Bacteriol. 169:4086-4091
- [154] B. Kuen, M. Sara, W. Lubitz, 1995, Heterologous expression and self-assembly of the S-layer protein SbsA of *Bacillus stearothermophilus* in *Escherichia coli*, Mol.

Microbiol. 19:495-503

[155] V. Vadillo-Rodríguez, H.J. Busscher, H.C. van der Mei, J. de Vries, W. Norde, 2005, Role of *Lactobacillus* cell surface hydrophobicity as probed by AFM in adhesion to surfaces at low and high ionic strength, Coll. Surf. B: Biointerf. 41:33-41

[156] W. H. Bingle, J. Smit, 1994, Alkaline phosphatase and a cellulase reporter protein are not exported from the cytoplasm when fused to large N-terminal portions of the *Caulobacter crescentus* surface (S)-layer protein, Can J Microbiol. 40:777-782.

[157] U. B. Sleytr, H. Bayley, M. Sara, A. Breitwieser, S. Küpcü, C. Mader, S. Weigert, F. M. Unger, P. Messner, B. Jahn-Schmid, B. Schuster, D. Pum, K. Douglas, N. A. Clark, J. T. Moore, T. A. Winningham, S. Levy, I. Frithsen, J. Pankovc, P. Beagle, H. P. Gillis, D. A. Choutov, K. P. Martin, 1997, Applications of S-layers, FEMS Microbiol. Rev., 20:151-175

[158] A. Neubauer, E. Györvary, D. Pum, M. Sara, U. B. Sleytr, 2000, Investigation of the orientation of supramolecular protein structures (S-layers) on silicon, gold and lipid films by scanning force microscopy, PTB Bericht F 39:118-123

[159] M. Jarosch, E. M. Egelseer, C. Huber, D. Moll, D. Mattanovich, U. B. Sleytr and M. Sara, 2001, Analysis of the structure-function relationship of the S-layer protein SbsC of *Bacillus stearothermophilus* ATCC 12980 by producing truncated forms, Microbiology 147:1353-1363

[160] H. J. Boot, C. P. A.M. Kolen, J. M. van Noort, P. H. Pouwels, 1993, S-layer protein of *Lactobacillus acidophilus* ATCC 4356: purification, expression in *Escherichia coli*, and nucleotide sequence of the corresponding gene, J. Bacteriol. 175:6089-6096

[161] C. Huber, N. Ilk, D. Rünzler, E. M. Egelseer, S. Weigert, U. B. Sleytr, M. Sára, 2005, The three S-layer-like homology motifs of the S-layer protein SbpA of *Bacillus sphaericus* CCM 2177 are not sufficient for binding to the pyruvylated secondary cell wall polymer, Molecular Microbiology 55:197-205

[162] J. R. Larson, M. J. Coon, T. D. Porter, 2001, Purification and properties of a shortened form of cytochrome P-450 2E1: Deletion of the NH<sub>2</sub>-terminal membrane-insertion signal peptide does not alter the catalytic activities, PNAS, 81:9141-9145

[163] D. S. Goodsell, 2004, In Bionanotechnology: Lessons from Nature, Ed. J.W. Sons,

Wiley-Liss, Hoboken

- [164] G. M. Whitesides, J. P. Mathias, C. T. Seto, 1991, Molecular self-assembly and nanochemistry: A chemistry strategy for the synthesis of nanostructures, *Science* 254: 1312-1319
- [165] U. B. Sleytr, M. Sara, D. Pum, B. Schuster, 2005, Crystalline bacterial cell surface layers (S-layers): a versatile self-assembly system. In *Supramolecular Polymers*, 2<sup>nd</sup> Edition, Ed: A. Cifferi, CRC Press, Boca Raton, pp 583-616
- [166] D. Pum, A. Neubauer, E. Györvary, M. Sara, U. B. Sleytr, 2000, S-layer proteins as basic building blocks in a biomolecular construction kit, *Nanotechnology* 11:100-107
- [167] U. B. Sleytr, C. Huber, N. Ilk, D. Pum, B. Schuster, E. M. Egelseer, 2007, S-layers as a tool kit for nanobiotechnological applications, *FEMS Microbiology Letters*, 267:131-144
- [168] N. Ilk, C. Völlenkne, E. M. Egelseer, A. Breitwieser, U. B. Sleytr, M. Sara, 2002, Molecular characterization of the S-layer gene, *sbpA*, of *Bacillus sphaericus* CCM 2177 and production of a functional S-layer fusion protein with the ability to recrystallize in a defined orientation while presenting the fused allergen, *Appl. Environ. Microbiol.* 68:3251-3260
- [169] D. Moll, C. Huber, B. Schlegel, D. Pum, U. B. Sleytr, M. Sara, 2002, S-layer-streptavidin fusion proteins as template for nanopatterned molecular arrays, *Proc. Natl. Acad. Sci. USA.* 99:14646-14651
- [170] M. Pleschberger, D. Saerens, S. Weigert, U. B. Sleytr, S. Muyldermans, M. Sara, E. M. Egelseer, 2004, An S-layer heavy chain camel antibody fusion protein for generation of a nanopatterned sensing layer to detect the prostate-specific antigen by surface plasmon resonance technology, *Bioconjug. Chem.* 15:664-671
- [171] M. Pleschberger, A. Neubauer, E. M. Egelseer, S. Weigert, B. Lindner, U. B. Sleytr, S. Muyldermans, M. Sara, 2003, Generation of a functional monomolecular protein lattice consisting of an S-layer fusion protein comprising the variable domain of a camel heavy chain antibody, *Bioconjugate. Chem.* 14:440-448
- [172] A. Pähler, W.A. Hendrickson, M. A. Ganowicz Kolks, C. E. Argarana and C. R. Cantor, 1987, Characterization and Crystallization of core streptavidin, *J. Biol. Chem.*

262:13933-13937

[173] C. Huber, J. Liu, E. M. Egelseer, D. Moll, W. Knoll, U. B. Sleytr, M. Sara, 2006, Heterotetramers formed by an S-layer-streptavidin fusion protein and core-streptavidin as a nanoarrayed template for biochip development, *Small* 2:142-50

[174] D. Moll, C. Huber, B. Schegel, D. Pum, U. B. Sleytr, M. Sara 2002 S-layer-streptavidin fusion proteins as template for nanopatterned molecular arrays, *PNAS*, 99:14646-14651

[175] J. Posseckardt, 2005, Heterologe Expression und Charakterisierung des S-Layer-Fusionsproteins sbsC-Streptavidin, Diplomarbeit, TU Dresden

[176] <http://probes.invitrogen.com/media/pis/mp19003.pdf>

[177] D. Li , G. Li, W. Guo, P. Li, E. Wang, J. Wang, 2008, Glutathione-mediated release of functional plasmid DNA from positively charged quantum dots, *Biomaterials* 29:2776–2782

[178] T. Sano, C. R. Cantor, 1995, Intersubunit contacts between tryptophan 120 with biotin are essential for both strong biotin binding and biotin-induced tighter subunit association of streptavidin, *Proc. Natl. Acad. Sci.* 92:3180-3184

[179] A. Chilkoti, P.H. Tan, P.S. Stayton, 1995, Site directed mutagenesis studies of high-affinity streptavidin-biotin complex: contributions of thryptophan residues 79, 108, and 120, *Procl. Natl. Acad. Sci USA* 92:1754-1758

[180] M. M. Kohonen, M. E. Karaman, R. M. Pashley, 2000, Debye Length in Multivalent Electrolyte Solutions, *Langmuir*, 16:5749-5753

[181] R. L. Whetten, J. T. Khoury, M. M. Alvarez, S. Murthy, I. Vezmar, Z. L. Wang, P.W. Stephens, C. L. Cleveland, W. D. Luedtke, U. Landman, 1996, Nanocrystal gold molecules, *Adv. Mater.* 8: 428-433

[182] V. L. Colvin, M. C. Schamp, A. P. Alivasatos, 1994, Light-emitting diodes made from cadmium selenide nanocrystals and a semiconducting polymer, *Nature* 370:354-357

[183] S. H. Kim, G. Markovich, S. Rezvani, S. H. Choi, K. L. Wang, J. R. Heath, 1999, Tunnel Diodes Fabricated from CdSe Nanocrystal Monolayers, *Appl. Phys. Lett.*, 74:317-320



- [184] D. L. Klein, R. Roth, A. K. L. Lim, A. P. Alivisatos, 1997, A single-electron transistor made from a cadmium selenide nanocrystal, *Nature* 389:699-701
- [185] C. Lent, W. Tougaw, W. Porod, G. Bernstein, 1993, Quantum cellular automata, *Nanotechn.* 4:49-57
- [186] M. T. Kumara, D. Nykypanchuk, W. B. Sherman, 2008, Assembly Pathway Analysis of DNA Nanostructures and the Construction of Parallel Motifs, *Nanoletters* 8:1971-1977
- [187] F. Xiao, J. Sun, O. Coban, P. Schoen, J. C. Wang, R. H. Cheng, P. Guo, 2009, Fabrication of Massive Sheets of Single Layer Patterned Arrays Using Lipid Directed Reengineered Phi29 Motor Dodecamer, *ACS Nano* 3:100-107
- [188][http://www.merck-chemicals.de/life-science-research/vector-table-novagen-pet-vector-table/c\\_HdSb.s1O77QAAAEhPqsLdcab](http://www.merck-chemicals.de/life-science-research/vector-table-novagen-pet-vector-table/c_HdSb.s1O77QAAAEhPqsLdcab)
- [189] A. Blüher, 2008, S-Schichtproteine als molecular Bausteine zur Functionalisierung mikroelektronischer Sensorstrukturen, Dissertation, TU Dresden

---

## APPENDIX

### A.1 MATERIALS

#### FINE CHEMICALS

Agarose	BioZym
Agar	Formedium
Acetone	AppliChem
Ampicillin	Roth
Acrylamide / Bisacrylamide (30%)	AppliChem
AEBSF	AppliChem
APS	Merck
BSA	New England Biolabs
Bromophenol blue	Serva
Benchmark Protein –Ladder	Invitrogen
Chloramphenicol	Roth
Calcium chloride (CaCl <sub>2</sub> )	Merck
Coomassie Brilliant blue G250	Sigma
Dithiothreitol (DTT)	Roth
dNTPs	New England Biolabs
Ethanol	AppliChem
Ethidium bromide (EB)	Sigma-Aldrich
EDTA	Roth
Guanidine hydrochloride (GuHCl)	Roth
Isopropanol	AppliChem
Imidazol	AppliChem
IPTG	AppliChem
Magnesium sulphate (MgSO <sub>4</sub> )	Roth
Methanol	Roth

---

Nickel Suphate (NiSO <sub>4</sub> )	Roth
Potassium chloride (KCl)	Roth
Potassium dihydrogenphosphate (KH <sub>2</sub> PO <sub>4</sub> )	Roth
Peptone / Tryptone	Roth
Sodium chloride (NaCl)	AppliChem
Sodium dodecyl sulphate (SDS)	AppliChem
Dried milk powder	AppliChem
Sodium carbonate (Na <sub>2</sub> CO <sub>3</sub> )	Roth
TEMED	Roth
Tris base	AppliChem
Triton X-100	Sigma
Tween 20	Merck
Yeast extract	Formedium
β-mercaptoethanol	Roth
ENZYMES	
Restriction enzymes	Invitrogen, New England BioLabs
Taq DNA polymerase	England BioLabs
Pfusion DNA polymerase	New England BioLabs
T4 DNA Polymerase	Novagen
Deoxyribonuclease (DNase) I	Roth
Ribonuclease (RNase) A	Roth, Boehringer
Proteinase K	Roth
Lysozim	New England BioLabs
KIT SYTEMS	
Dc-Protein Assay	BIORAD
ECL <sup>TM</sup> -System	GE Healthcare
Nucleospin <sup>®</sup> Plasmid kit	Macherey-Nagel
Invisorb Fragment Clean Up Kit 250	Invitek
pET - 46 Ek/Lic Vector kit	Novagen

pET – 51b(+) Ek/Lic Vector kit Novagen

#### COMMERCIAL BUFFERS AND STOCKS

10xT4DNA polymerase buffer Novagen  
 DTT stock [100 mM] Novagen  
 EDTA stock [25 mM] Novagen  
 Nuclease free water Novagen  
 Restriction enzyme buffers New England Biolabs

#### RECOMBINANT PLASMIDS

Recombinant plasmids used in this study are summarized in Table 1:

**Table 1: Summary of the used and created recombinant plasmids**

Recombinant plasmid	Genetic markers	Vector	Insert	Reference
pET-23b+1t	Amp <sup>R</sup>	pET-23b+	SslA <sub>341-925</sub> CN	Ryzkov 2007
pET-23b+3t	Amp <sup>R</sup>	pET-23b+	SslA <sub>32-925</sub> C	Ryzkov 2007
pET-51 Ek/Lic_2t	Amp <sup>R</sup>	pET-51 Ek/Lic	SslA <sub>341-1097</sub> N	This work
pET-46 Ek/Lic_4t	Amp <sup>R</sup>	pET-46 Ek/Lic	SslA <sub>32-1097</sub>	This work
pET-46 Ek/Lic_1t_cstrp	Amp <sup>R</sup>	pET-46 Ek/Lic	SslA <sub>341-925</sub> CN-cstrp	This work

#### OLIGONUCLEOTIDES

The melting temperature (T<sub>m</sub>) of oligonucleotides was calculated using Vector NTI. The annealing temperature (T<sub>a</sub>) was calculated using the formula:

$$T_a = T_m + /- 3^{\circ} \text{C}$$

Primers used in this study are summarized in Table 2:

**Table 2: Summary of primers used in this work**

No.	Name	Sequence (5'-3')	Direction
1	Primer A	CGC GGC <b>CAT ATG</b> GGC GTT AAA AAA GCA GGA AT	Forward
2	Primer B	ATG CAT TAG TTA TTA GTT CGG GCA TCA CCG GCA CCT GGT A	Reverse
3	Primer C	GTA CCA GGT GCC GGT GAT GCC CGA ACT AAT AAC TAA TGC ATT TGC AGT TG	Reverse
4	Primer D	CAC TAG <b>CTC GAG</b> CAC CTT GGT GAA GGT GTC GTG G	Forward
5	Pfor p1t_cstrp_Lic	<b>GAC GAC GAC AAG ATG</b> ACT GGC GTT AAA AAA GCA	Forward
6	Prevp1t_cstrp_Lic	<b>GAG GAG AAG CCC GGT TTA</b> CAC CTT GGT GAA GGT	Reverse
7	Pfor341Licp1strpII	<b>GAC GAC GAC AAG ATG</b> ACT GGC GTT AAA AAA GCA GG	Forward
8	Prev925strpII_p1	<b>GAG GAG AAG CCC GGT TTA</b> CGA ACT AAT AAC TAA TGC ATT TGC	Reverse
9	Pfor_261_gesaura	ATA TAT <b>AGG ATC CGC</b> CAT ACC GTG CTA TTA GAC TAT CAT C	Forward
10	Prev_3858_gesaura	ATA TAT <b>AGG ATC CGA</b> GGA TTA GGC TAT TGT GAT TTG ACT G	Reverse
11	Pfor_p46_p4	<b>GAC GAC GAC AAG ATG</b> GCT GAA TTC ACA GAT GTA AAA GAC AA	Forward
12	Prev_p46_p4	<b>GAG GAG AAG CCC GGT TTA</b> AGA AGT TAC TTT TAT AAC AGG TGT ATT TAG TCA	Reverse
13	Pfor341Lic_p2	<b>GAC GAC GAC AAG ATG</b> ACT GGC GTT AAA AAA GCA GGA	Forward
14	Prevmatp4Lic_p2	<b>GAG GAG AAG CCC GGT</b> AGA AGT TAC TTT TAT AAC AGG TGT ATT TAG TCA	Reverse

## STRAINS

*E. coli* strains used in this study are summarized in Table 3.

**Table 3: Summary of strains used in this work**

Strain	Genotype	Source
<i>S. ureae</i> ATCC 13881	Wild type	MBZ
<i>E. coli</i> Rosetta Blue (DE3)	endA1, hsdR17(rK- mK+), supE44, thi-1, recA1, gyrA96, relA1, lac, (DE3), [F':::Tn10 proA+B+lacIq ZΔM15], pRARE2, (CamR, TetR)	Novagen
<i>E. coli</i> BL21 (DE3)	F-, ompT, hsdSB(rB-mB-), dcm, gal, (DE3)	Novagen
Novablue	endA1, hsdR17(rK12- mK12+), supE44, thi-1, recA1, gyrA96, relA1, lac[F'[proA+B+lacIq ZΔM15:Tn10], (TetR)	Novagen

## A.2. METHODS

### GROWTH OF *E. COLI* CELLS

*E. coli* cells were grown in liquid at 37 °C or at 30 °C under continuous agitation at 140 rpm. For selection of bacterial transformants, ampicillin was added to media (final concentration 110 µg/ml). For bacterial gene expression in *E. coli* expression strains, cultures were grown until an OD<sub>600</sub> of 0.4 afterwards induced with IPTG (1 mM final concentration).

LB (Luria-Bertani) medium:	1.0 % (w/v) Peptone / Tryptone
	0.5 % (w/v) Yeast extract
	0.5 % (w/v) NaCl
	110 mg/L Ampicillin (for LB-amp medium)
	1.5 % (w/v) Agarose (for solid LB medium)

### GROWTH OF *S. UREAE* CELLS

*S. ureae* ATCC 13881 cells were grown at 30 °C in *S. ureae* growth medium I, while continuously agitating at 200 rpm until OD<sub>600</sub> of 1.5, which is within the logarithmic growth phase.

<i>S. ureae</i> growth medium I:	17.01 g Na <sub>3</sub> PO <sub>4</sub> x 12 H <sub>2</sub> O
	1.28 g Glucose
	1.0 g Yeast extract
	10 g Peptone 5.28 g (NH <sub>4</sub> ) <sub>2</sub> SO <sub>4</sub>

### DETERMINATION OF THE OD<sub>600</sub> OF BACTERIAL CULTURES

1 ml of the harvested cell culture was pipetted into the spectrophotometer cuvette and its optical absorbance was measured at a wavelength of 600 nm with the Ultrospec 3000 spectrophotometer.

### EXPRESSION KINETIC STUDIES

Cell colonies were picked up from the LB-amp plates and cultured O.N. in 5 ml of liquid LB medium containing the appropriate antibiotic. Next day, 500 µl of these cultures were inoculated into 25 ml of LB-amp and expression cultures were grown until they

reached an OD<sub>600</sub> of 0.4. Expression was induced by adding IPTG (final concentration of 1 mM) to the cultures. For expression kinetics studies, 2 ml samples from these cultures were taken before, 1, 3 and 6 hours after induction with IPTG. OD<sub>600</sub> of these samples was measurements followed by their preparation for SDS-PAGE analysis.

### A.2.1 DNA Techniques

#### ISOLATION OF GENOMIC DNA FROM *S. UREAE* ATCC 13881

4 ml of *S. ureae* cell culture was harvested at 4000 x g for 10 minutes at RT and the cell pellet was dissolved in 100 µl TB buffer containing lyzozim. To this suspension 200 µl LT buffer and 20 µg/µl Proteinase K was added. The whole mixture was vortexed and incubated for 20 minutes at 37 °C, than for 5 minutes at 70 °C followed by the addition of 600 µl G buffer. After vortexing and centrifugation at 13000 rpm for 10 minutes, the supernatant was transferred to a DNA binding column and washed at first with 600 µl than with 400 µl buffer W. Genomic DNA was eluted from the column with 100 µl TB buffer.

TB buffer:	10 mM Tris/HCl pH 8.5
LT buffer:	10 mM Tris/HCl pH 8
	1 mM EDTA
	1% SDS
G buffer:	6 M GuHCl
W buffer:	60% isopropanol
	100 mM NaCl

#### POLYMERASE CHAIN REACTION

DNA fragments were amplified by 30 cycles reaction in total volumes of 50 µl. The standard reaction mixture contained:

1-100 ng template DNA

150 pM forward and reverse primers

500-800 µM dNTPs mix

PCR buffer (1x)

1 mM MgSO<sub>4</sub>

2.5 U polymerase (Phusion or Taq)

For creation of modified DNA fragments overlap extension PCR was applied as described by Pogulis *et. al.* in 1996.

PCR buffer:        750 mM Tris/HCl pH 9  
                          0.1 % Tween 20  
                          200 mM (NH<sub>4</sub>)<sub>2</sub>SO<sub>4</sub>

#### AGAROSE GEL ELECTROPHORESIS AND DNA EXTRACTION FROM GEL

DNA fragments were separated by gel electrophoresis in horizontal, 1% (w/v) agarose gels in TBE buffer at 80-120 V. For visualization of the DNA fragments, 0.1 µg/ml of ethidium bromide was added to the gel. Length of DNA fragments was estimated with regard to the standard ladder (obtained after treatment of λ phage DNA with EcoRI and BamHI enzymes). Following separation, the fragments of interest were excised from the gel under UV light and extracted using the Invisorb Fragment Clean Up Kit 250 (Novagen) according to the manual provided by the manufacturer.

TBE buffer (10x):    89 mM Borate  
                          89 mM Tris  
                          2 mM EDTA (pH 8.0)  
TBS-T buffer: 1x TBS buffer  
                          0.1 % (v/v) Tween 20

#### T4 DNA POLYMERASE TREATMENT OF INSERT DNA

In order to generate compatible overhangs on the insert DNA, the following reaction was prepared in a total volume of 20 µl:

0.2 pmol purified PCR product in up to 14.6 µl TlowE buffer

10x T4 DNA Polymerase buffer

25 mM dATP

100 mM DTT

2.5 U/ µl T4 DNA Polymerase



The reaction mixture was incubated for 30 minutes at 22 °C. The enzyme was inactivated by incubation at 75 °C for 20 minutes.

TlowE buffer:        10 mM Tris/HCl  
                             0.1 mM EDTA pH 8

#### ANNEALING OF DNA FRAGMENTS AND VECTOR

For the annealing reaction, 0.02 pmol T4 DNA polymerase treated DNA fragment was mixed with 1 µl vector DNA (0.1 µg/µl) and incubated at 22 °C for 5 minutes. To this mixture 25 mM EDTA in a total volume of 4 µl was added and incubated again at 22 °C for 5 minutes.

#### TRANSFORMATION OF *E. COLI* CELLS

##### ***Preparation of E. coli competent cells***

An *E. coli* overnight culture was diluted to 1:100 by fresh LB medium. When the culture reached an OD<sub>600</sub> of 0.6, it was chilled on ice for 30 minutes and cells were harvested by centrifugation at 4000 xg for 15 minutes at 4 °C. Pelleted cells were washed twice with 40 ml icecold, sterile 10% glycerol (v/v) and once in icecold sterile distilled water. After centrifugation at 4000 xg for 10 minutes at 4 °C, cells were resuspended in 2 ml 10% glycerol, aliquoted (40 µl), frozen and stored at -80 °C.

##### ***Electroporation***

4 µl of the ligation mixture was dialysed on a dialysis membrane (Millipore) against sterile distilled water for 10-15 minutes, than gently mixed with 40 µl of *E. coli* electrocompetent cells and transferred to the prechilled electroporation cuvette (2 mm gap). Electroporation was done at 25 µV, 200 Ω and 2.5 kV. Immediately after the pulse, the transformation mixture was diluted with 1 ml of SOC (super optimal broth, catabolite) medium and incubated for 1 hour at 37 °C under shaking at 300 rpm. After incubation, the transformation mixture was centrifuged at 4000 x g for 10 minutes at RT. Cells were resuspended in 100 µl fresh LB medium and plated onto LB plates containing the appropriate antibiotics (*e.g.* ampicillin, tetracyclin or chloramphenicol) in order to screen for transformed cells. Plates were incubated at 37 °C overnight.

SOC medium:	2 % (w/v) Peptone / Tryptone
	0.5 % (w/v) Yeast extract
	2.5 mM KCl
	10 mM NaCl
	10 mM MgCl <sub>2</sub> x 6H <sub>2</sub> O
	10 mM MgSO <sub>4</sub> x 7H <sub>2</sub> O
	20 mM Glucose/Dextrose

### ***Transformation by heat shock***

Nova Blue Giga Singles electrocompetent cells were provided by the manufacturer in the pET Ek/Lic Vector kit (Novagen). After thawing these cells on ice for 2 minutes, 1 µl of annealing reaction was added directly to the cells, mixed and incubated on ice for 5 minutes. Afterwards the whole mixture was heated in a 42 °C water bath for 30 seconds, then placed on ice for 2 minutes. Cells were resuspended in 250 µl of SOC medium and incubated at 37 °C under continuous shaking at 250 rpm for 1 hour. To select transformants, a portion of the transformation was plated on LB plates containing ampiciline. Plates were incubated overnight at 37 °C.

### ISOLATION OF PLASMID DNA FROM *E. COLI* CELLS

Plasmid DNA from the transformed *E. coli* cells were prepared by the alkaline lysis method as described by Birnboim and Doly (1979) using 2-5 ml of an overnight culture. To obtain plasmid DNA of higher purity required for sequencing reaction, Nucleospin Plasmid Quick Pure kit (Macherey-Nagel) was used according to the manual of the manufacturer.

### DNA SEQUENCING

DNA sequencing was done by sending the DNA samples to MWG-Biotech AG Company with the appropriate primers.

## A.2.2 Protein techniques

### PROTEIN CONCENTRATION ASSAY

Protein concentrations were determined using a Lowry based Dc protein assay system (Bio-Rad) according to the manual provided by the manufacturer.

### SEPARATION OF PROTEINS BY SDS-PAGE

Separation of proteins by SDS-PAGE was performed as described by Laemmli (1970). A typical gel consisted of 10% separating gel and 4% stacking gel. Gels with separated proteins were stained or subjected to electro-transfer procedure and then stained with Coomassie staining solution for 30 minutes at RT and washed with destaining solution until the protein band become visible.

Stacking gel (5 %):	1 M Tris/HCl pH 6.8 30 % (w/v) Acrylamide 0.8% (w/v) Bisacrylamide 10 % (w/v) SDS 10 % (w/v) APS TEMED dH <sub>2</sub> O
Separating gel (10 %):	1.5 M Tris/HCl pH 8.8 30 % (w/v) Acrylamide 0.8 % Bisacrylamide 10 % (w/v) SDS 10 % (w/v) APS TEMED dH <sub>2</sub> O
Running buffer:	25 mM Tris-base 192 mM Glycine 0.1% (w/v) SDS
Protein loading buffer (6x):	300 mM Tris/HCl (pH 6.8) 30 % (w/v) Glycerol

---

	10 % (w/v) SDS
	0.1% (w/v) Bromophenol blue
	600 mM DTT (freshly added)
Coomassie blue stain:	45 % (v/v) Methanol
	17 % (v/v) Acetic acid
	0.1% (w/v) Coomassie brilliant blue G250
Destaining solution:	30 % (v/v) Methanol
	7 % (v/v) Acetic acid

## WESTERN BLOT

Separation of proteins by SDS-PAGE was followed by their electro-transfer to a nitrocellulose membrane in Transfer buffer by means of semi-dry technique. Membranes were blocked in TBS-T buffer containing 5% (w/v) fat free skimmed milk for 1 h at RT. Blocked membranes were incubated with the respective mono- or polyclonal antibodies for 1 h at RT. After intensive washing, antibodies bound to the protein of interest were detected with horse radish peroxidase (HRP) conjugated secondary antibodies (raised against the immunoglobulins of host organism that generated the primary antibodies) by incubation for 1h at RT. Membranes were washed in TBS-t and detected proteins were visualized with the ECL<sup>plus</sup> chemiluminescence- based system according to the manufacturer's manual.

## ISOLATION OF THE RECOMBINANT S-LAYER FROM *E. COLI* CELLS

### ***Cell lysis by sonication***

The harvested *E. coli* cell culture was centrifuged at 10000 g for 10 minutes and the pellet resuspended in 20 ml Buffer B with 10 mg Lysozyme and 1 mM AEBSF. After an incubation step of 2 hours at 30 °C under continuous shaking at 300 rpm, the cell suspension was chilled on ice for 15 min. After addition of Triton X-100 in a final concentration of 0.5 % (v/v), the tube containing the cell suspension was placed into a beaker filled with salted ice and positioned inside of the Sonopuls UW 2070 ultrasonic homogenizer. Sonication was performed with 30 pulses of 10 sec with intervals of 20 sec between pulses, with tip immersion of approximately 0.5 cm, paying attention that

minimal amount of foam is formed and cell suspension stays cool during this procedure. Following sonication, DNase I and Rnase A was added to the mixture (to hydrolyze the nucleic acids) and incubated for 15 minutes at 30 °C under continuous shaking followed by a centrifugation step at 13000 xg for 10 min to separate the insoluble cell fraction. The supernatant was applied to a Ni affinity chromatography purification column containing Ni<sup>2+</sup> ions on a resin.

#### PROTEIN PURIFICATION BY Ni<sup>2+</sup> AFFINITY CHROMATOGRAPHY

The high affinity of polyhistidine peptides to Ni ions allows selective immobilization of His tagged proteins onto a Ni containing resin. An NTA-agarose filled column was charged with Ni<sup>2+</sup> ions from a NiSO<sub>4</sub> solution. The unbound Ni<sup>2+</sup> was washed with Buffer B. The cell fraction containing the His tagged S-layer proteins (supernatant), was incubated with the Ni-NTA-agarose. Purification under native conditions involved washing of the column at first twice with Buffer B, than twice with Buffer W1, W2 and W3 respectively. Elution of the bound S-layer proteins was done by washing the column with Elution buffer and collection of 5 fractions of 5 ml each. The protein fractions were immediately dialyzed against ultrapure water at 4 °C overnight.

Buffer B:	20 mM Tris/HCl pH 7.9 0.5 M NaCl 5 mM imidazol
Buffer W1:	20 mM Tris/HCl pH 7.9 0.5 M NaCl 20 mM imidazol
Buffer W2:	20 mM Tris/HCl pH 7.9 0.5 M NaCl 40 mM imidazol
Buffer W3:	20 mM Tris/HCl pH 7.9 0.5 M NaCl 60mM imidazol

---

Elution buffer: 20 mM Tris/HCl pH 7.9  
0.5 M NaCl  
1 M imidazol

#### PREPARATION OF DIALYSIS TUBING

Dialysis tubings were cut to the length of 10 to 20 cm and boiled for 10 minutes in the tubing preparation buffer I. Subsequently, tubings were washed several times with distilled water, immersed into the tubing preparation buffer II and boiled for another 10 minutes. After boiling, they were rinsed with distilled water and stored in 25 % (v/v) isopropanol at 4 °C.

Buffer I: 2 % (w/v) Na<sub>2</sub>CO<sub>3</sub>  
1 mM EDTA (pH 8.0)  
Buffer II: 1 mM EDTA (pH 8.0)

#### DIALYSIS

##### ***General protocol***

The dialysis tubings were immersed into distilled water or dialysis buffer I. Dialysis was performed at 4 °C for a certain time interval. Removal of GuHCl was facilitated by a rotating magnet.

Dialysis buffer I: 0.5 mM Tris/HCl pH 7  
10 mM CaCl<sub>2</sub>

#### *IN VITRO* RECRYSTALLIZATION IN SOLUTION

X mg protein was at first monomerized with 1 ml 5M GuHCl for 2 hours at 37 °C. The chemical was subsequently removed by dialysis against ddH<sub>2</sub>O or dialysis buffer I solution at 4 °C usually for 24 hours. Samples from the dialysed solution were adsorbed for 1 hour onto cleaned silicon substrates and analysed.

### *IN VITRO* RECRYSTALLIZATION ON A SILICON SUBSTRATE

Similarly, X mg of S-layer protein was monomerized with 1 ml of 5M GuHCl for 2 hours at 37 °C. After monomerization, the protein solution was dialysed against 10 mM Tris/HCl buffer pH 3 at 4 °C in the presence of APTES functionalized silicon substrate. After 2 hours, the substrates were taken out, washed in distilled water and dried on air.

### VERIFICATION OF BIOTIN BINDING

#### ***Band shift assay in agarose gel***

1 mg of purified S-layer protein was monomerized with 1 ml 5 M GuHCl for 2 hours and dialysed against pure water at 4 °C for another 2 hours. Monomers were separated by a centrifugation step at 14 000 rpm for 10 minutes and incubated with the quantum dots (20 nM). The mixture was runned on a 1% agarose gel at 80V for 2 hours followed by visualization under UV light.

#### ***Quantum dot assay***

1 mg of purified S-layer protein was monomerized with 1 ml 5 M GuHCl for 2 hours and dialysed against pure water at 4 °C for 3 hours. Monomers were separated by a centrifugation step at 14 000 rpm for 10 minutes and diluted to a concentration of 0.1 mg/ml with 0.1 mM CaCl<sub>2</sub> and 0.5 mM Tris HCl pH 9. Next day, the recrystallized the S-layer sheets (10 µl solution) were adsorbed onto plasma treated C-Cu grids for 1 hour. Afterwards the grids were washed in a drop of water and incubated with Quantum dot-biotin solution (at a concentration of 0.02 nM in 20 mM KHPO<sub>4</sub>) for 1 hour at RT. After rinsing twice with TBS buffer, the samples were stained with 2% uranyl formiate for 20 seconds and afterwards investigated with the transmission electron microscope.

TBS buffer:            0.2 M Tris/HCl pH 7.4  
                             1.37 M NaCl

### A.3. Characterization techniques

#### SCANNING ELECTRON MICROSCOPY (SEM)

##### ***Preparation of SEM samples***

After dialysis, a droplet of 7  $\mu$ l of the protein solution was placed onto the cleaned silicon surface and let to adsorb for 1 hour. Then the silicon substrate was gently washed with ddH<sub>2</sub>O. Before drying out, 7  $\mu$ l of 2.5% uranyl acetate was applied to the silica surface. After 20 seconds, the fluid was soaked with filter paper and the sample let drying on air.

Scanning electron micrographs were obtained with the low voltage SEM Zeiss Gemini 982 device.

#### TRANSMISSION ELECTRON MICROSCOPY (TEM)

##### ***Preparation of TEM samples***

Formvar/carbon films on copper grids (PLANO) were plasma treated for 10 seconds (O<sub>2</sub> SPI Plasma Prep II) in order to make them hydrophilic. Directly thereafter, 10  $\mu$ l of fusion protein solution were applied onto the grid and left for adsorption for 1 hour. Afterwards, the grid was washed with distilled water and the protein stained with 7  $\mu$ l of 2% uranyl formiate. After staining the whole grid was blotted with filter paper and dried on air.

Transmission electron micrographs were obtained on a Zeiss LIBRA200FEG using 200 kV acceleration voltage.

#### ATOMIC FORCE MICROSCOPY (AFM)

##### ***Preparation of AFM samples***

After dialysis, a droplet of the protein solution was sat on the cleaned (and functionalized) silicon substrates and let to adsorb for a certain time period. Or the silicon substrates were directly added into the dialysis bag. In this latter case, the self-assembly structures have adsorbed during the dialysis procedure. After adsorption, the substrates were washed with ddH<sub>2</sub>O and dried with nitrogen.



Silicon 130  $\mu\text{m}$  long tips were used for imaging. The images were analyzed with the help of the software WsxM [Nanotech Electronica S.L.]. The measurements were performed tapping mode in air using the Extended Multimode AFM with Nanoscope IIIa controller system Digital Instruments, Inc Veeco Metrology.

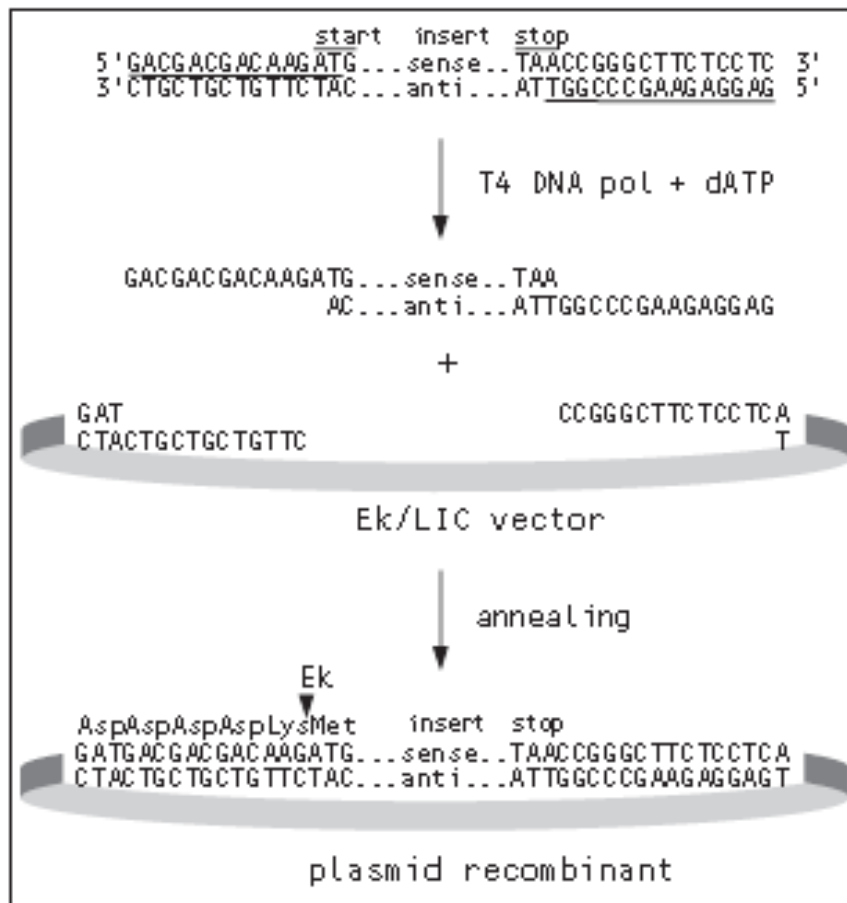
### DYNAMIC LIGHT SCATTERING (DLS)

#### ***Preparation of DLS samples***

9640  $\mu\text{g}$  of native SslA was monomerized with 1 ml 5M GuHCl for 2 hours at 37  $^{\circ}\text{C}$ , followed by a dialysis step against ddwater for 2 hours. The dialysate was centrifuged at 14000 xg for 10 minutes. The supernatant was added into the spectrophotometric cuvette along with 30 mM  $\text{CaCl}_2$  in a final volume of 1 ml. DLS measurements were performed for 4 hours (number of measurements: 60, number of runs: 10, run duration: 18 sec). The device used for the DLS measurements was the Zetaseizer Nano ZS instrument (Malvern Instruments).

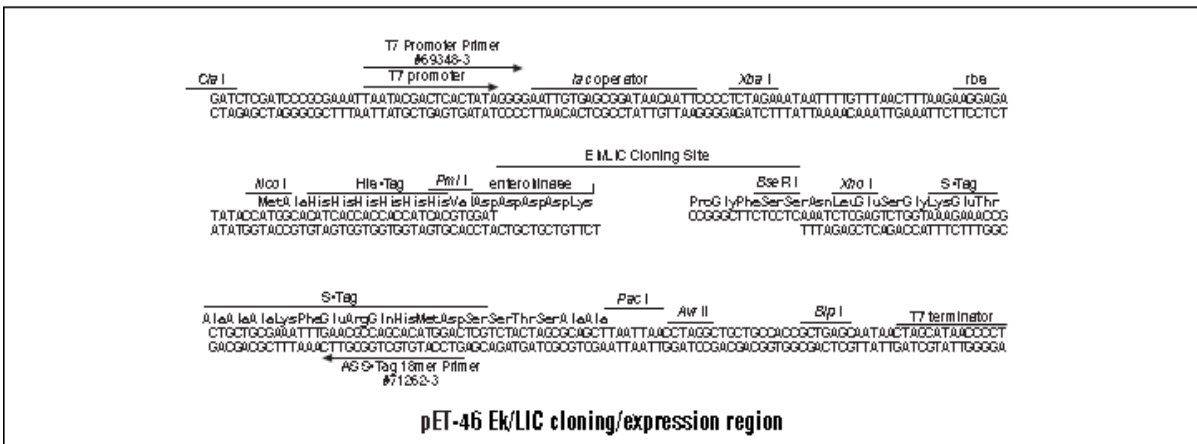
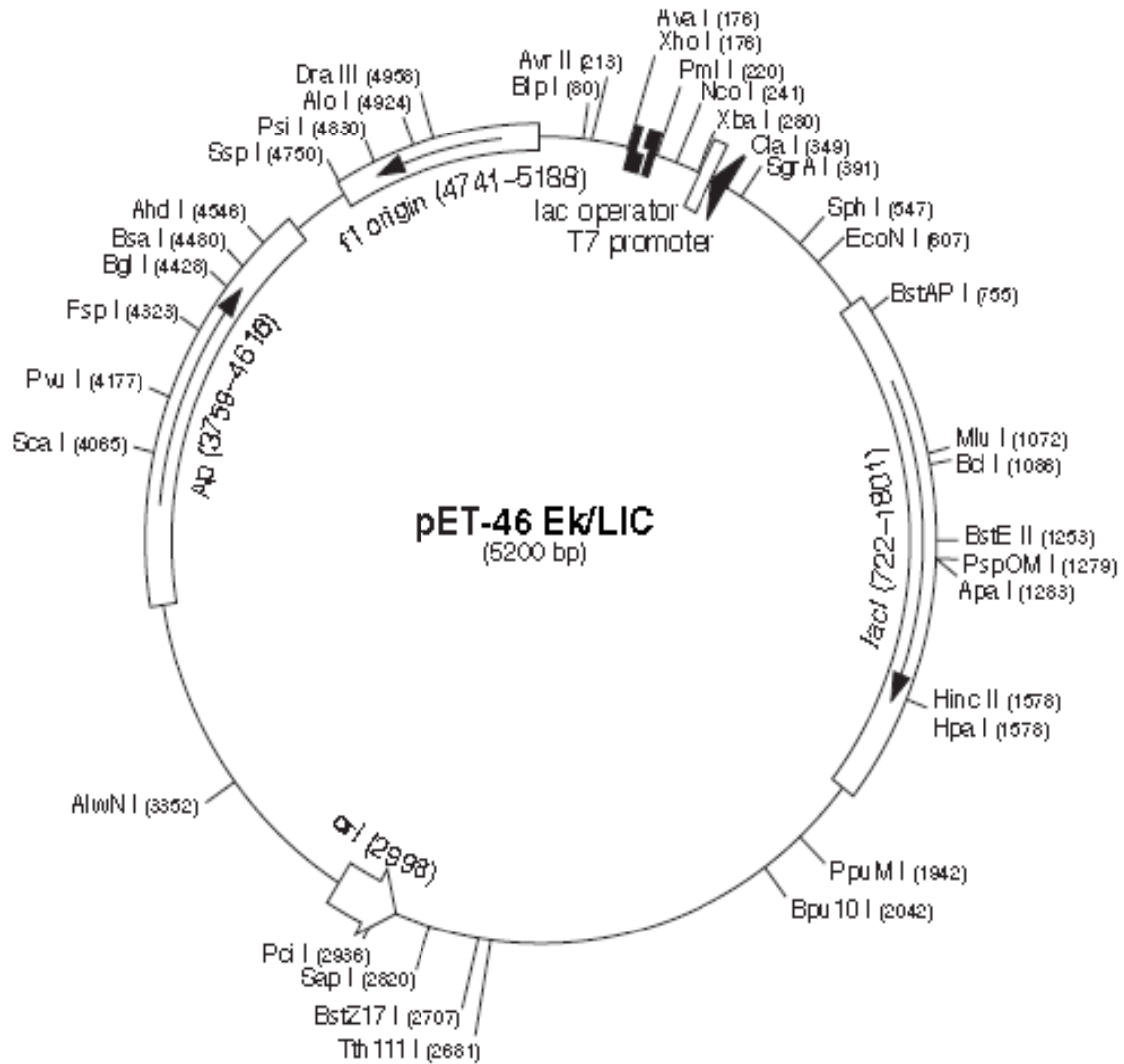
## THE EK/LIC CLONING STRATEGY

The Ek/Lic cloning strategy belongs to the directional cloning methods and takes advantage of the 3'→5' exonuclease activity of T<sub>4</sub> DNA polymerase to create very specific 12- to 15- nucleotide single stranded overhangs, so called "Lic arms" in the vector and insert (e.g. 5'- GAC GAC GAC AAG ATX for the sense primer and 5'- GAG GAG AAG CCC GGT for the antisense primer), so that the vast majority of annealed constructs consists of the desired molecules. The annealed LIC vector and insert are transformed directly into competent *E. coli* cells and covalent bonds are formed at the vector-insert junctions within the cell to yield the circular plasmid.

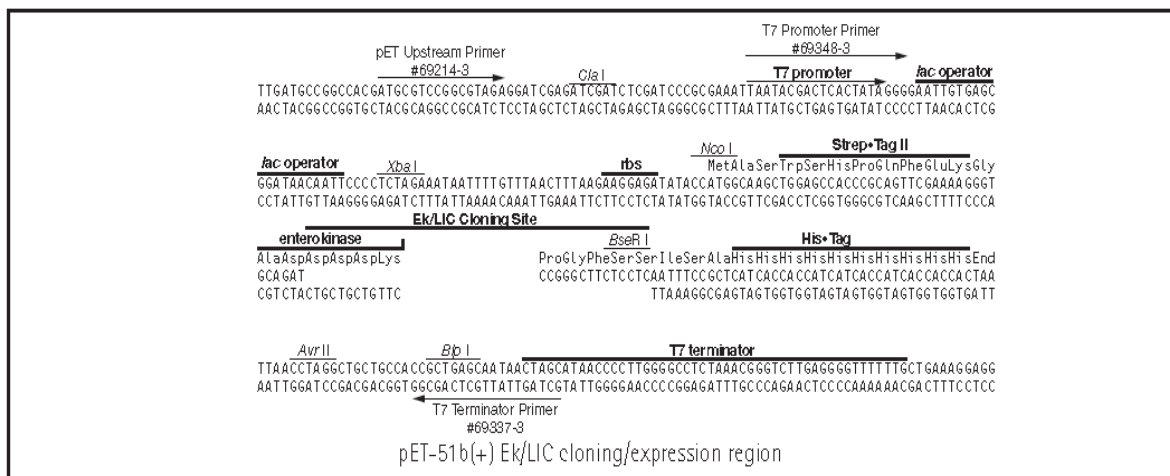
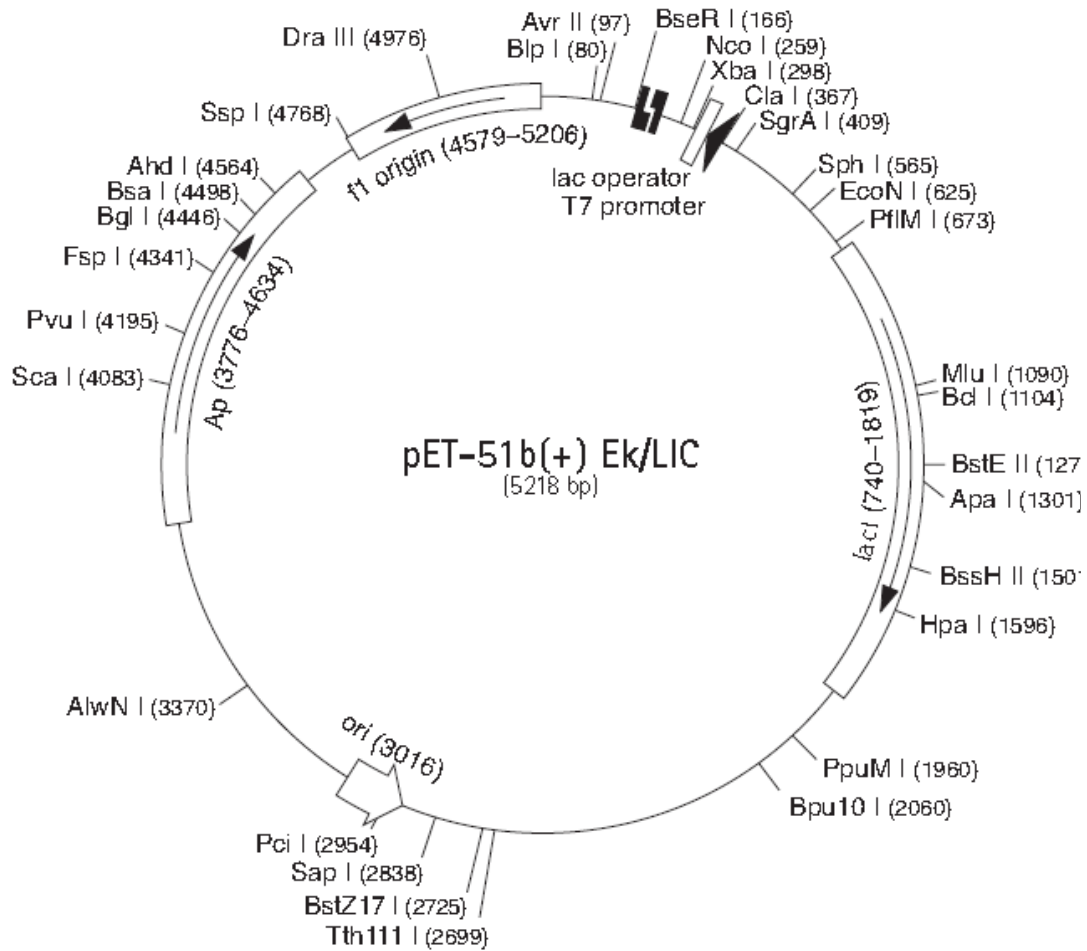


EK/LIC CLONING VECTORS

Map of the pET46 Ek/Lic (adapted from [188]) and the respective MCS sequences:



Map of the pET51b(+) Ek/Lic vector (adapted from [188]) and the respective MCS sequences:



**Amino acid sequence of the recombinant SslA protein (mature form):**

MAHHHHHHVD DDDKMAEFTD VKDNNSHKAA IDALSDAGVI  
 SGYPDGTTFQP NKTLTRSDVV KLMGKWLVSSE GYKVPTDYKT  
 KPRFSDLKTT SNDELLKMSA LVYDNGVDFVG KPDGSLDANG  
 DITRENMAIV LVRAFDRVYD VDLVSYVKAQ EFKKDVTDLG  
 KAKAEARPAI DVLDFFDITN PAAPEFNPKS TTTRGQFASF  
 LYKTTKVDFFD EVGGGIVAPG VASVKGINAT TVEVTMKDKV  
 SNIDSLKFTI DGLTVSNAAV KQTDDKTIVL TTATQKGGEK  
 YTVKLDGKEI GSFTGIEAVV PTTLKITNAS VQGKTGQQAI  
 LSADTGVKKA GIPVTFNVKA DTLNNTNKDQ VFEVMTNEDG  
 IATFSYTQYS AGKDEVTAYP TGAPTVRDQG FVFWGVDTIL  
 NIEDVTVGNT IANGANKTYK ITYKDAKTGK VEANKTFNVS  
 LAENINVTSD KLSNATVNGV KVSQLVNDKA PKTATVTTDS  
 KGEATFTVSG TNTTATPVVF GLNPSNGKTA ATYESNLLQA  
 KASTVTFSAQ QAEYAIELTR DGGDIAAKDV SNGRKYNVVV  
 KNKEGNIAKN EIINVAFNED LDRVISTNTQ AYFIKVNDDK  
 TQTKLGKQVS VKTDSEGKAS FVIGSDVEND YATPIAWIDV  
 NTPNAVEGRL DQGEPLTIGS ISYFKDAYLD GAALKVYKGN  
 KETSSFQONE TATFKASLVN QSNKTMPTS IKTVSYTIFN  
 TGANNVIVDG QTISPNRSFT VTHGAANADL DVKTVDGMSS  
 SVRVLATGTA IDTDGKDYAF TAKEATATFT SVTSVVKEYT  
 GAVGAVNKKT IQFVDKDAIT IKDGAKFFGG NGSEIIGIDA  
 FITELESYNN GVIVTYLEDA DGKQTFKVVR EDTNGQLVNA  
 AKLTEAEITR AKTDSVVVTK ATANALVISS NPDVIVEGVT  
 YAYDANATDA DLKLYKNAAD LAEKITNDES HDVTAKIGGA  
 GNLNLTGDAE GENFTYKIGA ASAVTTANGV KASQAVKQQI  
 TFTFTEAVKA NIDDSVNVGP TGAAVAGTVT DVAGTNVVVT  
 LETALNLGSE INVFDVKGTA VKTKVSEKNV D

**Amino acid sequence of the SslA-streptavidin fusion protein:**

MAHHHHHHVD DDDKMTGVKK AGIPVTFNVK ADTLNTTNKD  
QVFEVMTNED GIATFSYTQY SAGKDEVTAY PTGAPTVRDQ  
GFVFWGVDTI LNIEDVTVGN TIANGANKTY KITYKDAKTG  
KVEANKTFNV SLAENINVTS DKLSNATVNG VKVSQLVNDK  
APKTATVTTD SKGEATFTVS GTNTTATPVV FGLNPSNGKT  
AATYESNLLQ AKASTVTFSA QQA EYAI E L T RDGGDIAAKD  
VSNRKYNVV VKNKEGNI AK NEI I N V A F N E DLDRVISTNT  
QAYFIKVND D KTQTKLGKQV SVKTDSEGKA SFVIGSDVEN  
DYATPIAWID VNTPNAVEGR LDQGEPLTIG SISYFKDAYL  
DGAALKVYKG NKETSSFQGN ETATFKASLV NQSNKTMPNT  
SIKTVSYTIF NTGANNVIVD GQTISPNSRF TVTHGAANAD  
LDVKTVDGMS SSVRVLATGT AIDTDGKDYA FTAKEATATF  
TSVTSVVKEY TGAVGAVNKK TIQFVDKDAI TIKDGAKFFG  
GNGSEIIGID AFITELESYN NGVIVTYLED ADGKQTFKVV  
REDTNGQLVN AAKLTEAEIT RAKTDSVVVT KATANALVIS  
SGITGTWYNQ LGSTFIVTAG ADGALTGTYE SAVGNAESRY  
VLTGRYDSAP ATDGSGTALG WTVAWKNNYR NAHSAT'TWSG  
QYVGGAEARI NTQWLLTSGT TEANAWKSTL VGHDTFTKV

## PUBLICATIONS

### BOOK CHAPTER:

**M. Varga**, N. Korkmaz. "S-layer Proteins as Self-assembly Tool in Nano Bio Technology"  
In: Bio and Nanopackaging Techniques for Electronic Devices (G. Gerlach and K. Wolter, eds.), Springer, Heidelberg (accepted by the editors)

### ARTICLES:

**M. Varga**, W. Pompe and G. Rödel "Truncation derivatives of the S-layer of *Sporosarcina ureae* ATCC 13881: crystallization and kinetics"  
To be submitted (2010)

**M. Varga**, G. Rödel and W. Pompe "S-layer fusion protein as a tool for nanopatterning biotinylated molecules"  
To be submitted (2010)

### POSTERS:

**M. Varga**, A. Blüher, K. Ostermann, M. Mertig and G. Rödel "S-layer derivatives as nanotemplates: expression and structure analysis of a truncated SslA protein form of *Sporosarcina ureae* ATCC 13881"  
SBE's 4th International Conference on Bioengineering and Nanotechnology, July 22-24, 2008 Dublin, Irland

**M. Varga**, N. Korkmaz, K. Ostermann, W. Pompe and G. Rödel "Recombinant S-layer protein SslA of *Sporosarcina ureae* ATCC 13881 as a tool in nanobiotechnology"  
Max Bergmann Symposium, Nov 4-6, 2008 Dresden, Germany

**M. Varga**, K. Ostermann, W. Pompe and G. Rödel “Genetically engineered S-layer protein as a tool for nanopatterning biotinylated molecules”

ESONN 2009, Aug 23 –Sept 11, Grenoble, France

**M. Varga**, K. Günther, W. Pompe and G. Rödel “Hybrid S-layer structures for controlled nanopatterning”

TechConnect World Conference & Expo 2010, Jun 21-25, Anaheim, CA, USA

**M. Varga**, W. Pompe and G. Rödel “Self-assembly of the recombinant S-layer protein of *Sporosarcina ureae* ATCC 13881”

RTG Workshop “Bio-Nano-Tech 2010”, Sept 9, 2010, Dresden, Germany



## ACKNOWLEDGEMENTS

Finishing this work would not have been possible without the help and support of many people.

My sincere thanks go to Prof. Dr. Gerhard Rödel for giving me the opportunity to do my PhD in his group and work on a very challenging topic. I especially thank him for the freedom I enjoyed while working in his lab which helped me to grow up as an experimentalist who can plan, supervise and make intelligent decisions related to research. His support and assistance are greatly acknowledged.

Furthermore I would like to express my sincere gratitude to Prof. Dr. Wolfgang Pompe for his helpful guidance and advices throughout my PhD work. He was also my Professor in my Master studies and his enthusiasm for Nanotechnology got me into this exciting scientific field working at the interface of biology and nanotechnology. He brought me into the Research Training Group “Bio and Nanotechniques for Electronic Device Packaging”. It was a great opportunity being part of it. The interdisciplinarity of the group and the high number of lectures and seminars have broadened my view concerning various scientific research fields. Besides, I was not only part of a research training group but part of a group of great people and colleagues (and Professors) where collaborations and team building was demonstrated especially during our sailing Workshop. Yes, we held one of our compulsory Workshops while we were sailing on the Baltic Sea. Jacob, thanks a lot for the idea and most of the organization!

My special thanks go to Prof. Dr. Michael Mertig for allowing me to perform experiments in his group (BNS) and to use the microscopy facility located in the Max Bermann Center of Biomaterials. Here I would like to acknowledge the help of the BNS group members. Notably I would like to thank Anja Blüher for her excellent SEM investigations and for the fruitful discussions concerning S-layer crystallization studies. Furthermore I thank Kathrin Günther for the help and expertise in the quantum dot

## ACKNOWLEDGEMENTS

---

work. Beate Katschner provided me the *S. ureae* ATCC 13881 cells and the purified native S-layer protein. Many thanks for that. Furthermore I thank Christiane Erler for excellent TEM imaging and Juliane Posseckardt for the critical reading of the first draft.

In addition, I would like to thank all my colleagues in the Genetics group for providing a good working atmosphere. Karolina Ihle was an excellent colleague from whom I learned many experimental skills. Her suggestions and guidance were extremely instrumental in the first part of my work. She is also a great friend! My special thanks go to Kirsten Kottmeier, Corina Oswald and Suzi Kurz for the support and help while I was writing up. Many thanks to all office girls (Anett Gross, Suzi Lauffer, Simone Thierfelder, Anja Tauche and Corina Oswald) with whom I've enjoyed the most often very colourful working days.

I also thank Alexander Türke and Rober Luxenhofer for the assistance with DLS measurements.

Last but not least, my special thanks go to my parents without whose support and help I would have never achieved this degree. Their devotions and blessings have been a strengthening factor of my life.

# Statement of authorship - Selbständigkeitserklärung

Hiermit versichere ich, dass ich die vorliegende Arbeit ohne unzulässige Hilfe Dritter und ohne Benutzung anderer als der angegebenen Hilfsmittel angefertigt habe; die aus fremden Quellen direkt oder indirekt übernommenen Gedanken sind als solche kenntlich gemacht. Die Arbeit wurde bisher weder im In- noch im Ausland in gleicher oder ähnlicher Form einer anderen Prüfungsbehörde vorgelegt.

Die Dissertation wurde von Prof. Dr. Gerhard Rödel am Institut für Genetik der TU Dresden betreut und von October 2006 bis October 2010 verfasst.

Meine Person betreffend erkläre ich hiermit, dass keine früheren erfolglosen Promotionsverfahren stattgefunden haben.

Die Promotionsordnung der Fakultät für Mathematik und Naturwissenschaften, Technische Universität Dresden wird anerkannt.

Dresden, October 2010

---

MELINDA VARGA